Aus dem Bereich: Neurologie

Der Medizinischen Fakultät

der Universität des Saarlandes, Homburg/Saar

Early neurodegenerative changes in a rat model of multiple sclerosis

Dissertation zur Erlangung des Grades eines Doktors der Naturwissenschaften

der Medizinischen Fakultät

der UNIVERSITÄT DES SAARLANDES

2012

vorgelegt von: Dorit Hoffmann

geb. am: 14.08.1982 in Bremen

1 Abstract/Zusammenfassung

In recent years neurodegeneration in MS has become a focus of research since it is thought to be the main determinant of irreversible neurological disabilities in patients. The relationship between inflammation and neurodegeneration is not fully understood. An animal model of MS, myelin oligodendrocyte glycoprotein (MOG) - induced experimental autoimmune encephalomyelitis (EAE) was used to examine the temporal relationship between early neurodegeneration, optic neuritis and changes in the retina and optic nerve. Fluorogold-labeling of retinal ganglion cells (RGCs), histopathological staining and immunohistochemistry with antibodies identifying T-cells and microglia/macrophages in the optic nerve confirmed previous results, that degeneration of RGCs can be observed prior to the onset of clinical symptoms and optic neuritis, which is characterized by demyelination, axonal loss and infiltration with inflammatory cells. There is, however, significant activation of resident microglia in the optic nerve and retina prior to onset of optic neuritis, correlating with the onset of RGC degeneration. This indicates that activated microglia could be involved in early death of RGCs and might cause subtle axonal changes prior to onset of clinical symptoms and optic neuritis.

The mechanisms of axonal damage and RGC degeneration are not well understood but are likely to involve calcium influx and subsequent activation of the calcium-activated protease calpain. Experiments using manganese-enhanced MRI were performed, showing increased calcium influx in the optic nerve and retina during the induction phase, prior to onset of optic neuritis and calcium influx in the retina correlated with onset of RGC degeneration. Blocking experiments showed involvement of NMDA receptors in manganese enhancement in the retina during the induction phase of the disease.

Calpain activity was examined by performing western blots with an antibody specific to one of the calpain-mediated spectrin breakdown products (145 kDa, BDP_N). Increased amount of BPD_N in the optic nerve was observed during the induction phase, correlating with calcium influx and in the retina it correlated with onset of calcium influx and onset of RGC degeneration. Treatment of MOG-immunised animals with the calpain inhibitor calpeptin increased the number of surviving RGCs both during the induction phase and after onset of optic neuritis and also decreased

demyelination, infiltration with inflammatory cells and axonal disturbances (indicated by APP accumulation) in the optic nerve after onset of clinical symptoms.

Taken together these data indicate that microglial activation might be involved in early degeneration of RGCs and that calcium influx and calpain activation correlates with the onset of RGC degeneration in the retina. Inhibition of calpain activity with calpeptin suggests that calpain activation plays a role in infiltration with inflammatory cells and in degeneration of RGCs since both have been shown to be reduced with calpeptin treatment.

In den letzten Jahren ist die Neurodegeneration bei Multipler Sklerose in den Fokus der Forschung gerückt, da man davon ausgeht, dass sie die hauptsächliche Ursache für irreversible neurologische Störungen bei Patienten ist. Der Zusammenhang zwischen Entzündung und Neurodegeneration ist nicht vollständig untersucht. Im Folgenden wurde ein Tiermodell der Multiplen Sklerose, MOG-induzierte Experimentelle Autoimmune Enzephalomyelitis (EAE), genutzt um den zeitlichen Zusammenhang zwischen früher Neurodegeneration, Optikusneuritis und Veränderungen in der Retina und im Sehnerv zu untersuchen.

Das markieren von retinalen Ganglienzellen (RGC) mit Fluorogold, histopathologische und immunohistochemische Untersuchungen zur Identifizierung von T-Zellen und Mikroglia/Makrophagen im Sehnerv bestätigte frühere Ergebnisse, dass die Degeneration von retinalen Ganglienzellen bereits vor Eintreten der klinischen Symptome und vor Beginn der Optikusneuritis welche durch Demyelinisierung, Axonverlust und Infiltration mit inflammatorischen Zellen gekennzeichnet ist, zu beobachten ist.

Es zeigte sich schon vor Beginn der Optikusneuritis eine signifikante Aktivierung von Mikroglia im optischen Nerv und der Retina, welche mit dem Beginn der Degeneration der retinalen Ganglienzellen korrelierte. Dies deutet darauf hin, dass aktivierte Mikroglia in der frühen Degeneration der retinalen Ganglienzellen eine Rolle spielen könnten und möglicherweise auch subtile axonale Veränderungen verursachen.

Die Mechanismen die zur Degeneration von retinalen Ganglienzellen und axonalen Schäden führen sind noch nicht vollständig untersucht aber es ist anzunehmen, dass Calciumeinstrom und die nachfolgende Aktivierung der calcium-abhängigen Protease Calpain eine Rolle spielen. MRT Aufnahmen mit manganhaltigem Kontrastmittel deuten auf einen erhöhten Calciumeinstrom in der Retina und im Sehnerv hin der bereits vor Beginn der Optikusneuritis einsetzte. Der Calciumeinstrom in der Retina korrelierte dabei zeitlich mit dem Beginn der Degeneration der retinalen Ganglienzellen und Experimente mit einem NMDA Rezeptor Blocker deuten darauf hin, dass diese eine Rolle bei der Kontrastverstärkung in der Retina spielen könnten. Um die Calpain Aktivität zu bestimmen wurden Western Blots mit einem Antikörper durchgeführt der spezifisch ist für eines der Spaltprodukte von Spectrin, welches nur entsteht wenn Spectrin durch Calpain gespalten wird.

Eine erhöhte Konzentration des Spaltprodukts konnte im Sehnerv vor Beginn der Optikusneuritis festgestellt werden und korrelierte mit der beobachteten Kontrastverstärkung nach Manganinjektion. In der Retina war ebenfalls eine Erhöhung der Konzentration des Spaltprodukts zu finden, welche zeitlich mit der Kontrastverstärkung und dem Einsetzen der Degeneration von retinalen Ganglienzellen korrelierte.

Die Behandlung der MOG-immunisierten Tiere mit dem Calpain-Inhibitor Calpeptin führte zu einer erhöhten Überlebensrate der retinalen Ganglienzellen vor Beginn der Optikusneuritis und auch im späteren Verlauf. Bei behandelten Tieren mit Optikusneuritis zeigte sich im Vergleich zu unbehandelten Tieren eine Reduktion der Demyelinisierung, weniger Infiltration mit inflammatorischen Zellen und eine reduzierte Störung des axonalen Transports (erkennbar durch reduzierte Akkumulation von APP positiven Axonen).

Zusammenfassend deuten diese Daten darauf hin, dass Aktivierung von Mikroglia eine Rolle in der frühen Degeneration von retinalen Ganglienzellen spielen könnte und das Calciumeinstrom und Aktivierung der Protease Calpain in der Retina mit der Degeneration von retinalen Ganglienzellen korrelierten. Die Ergebnisse der Behandlungsstudie mit Calpeptin deuten darauf hin, dass Calpain Aktivität die Infiltration mit inflammatorischen Zellen beeinflusst und eine Rolle bei der Degeneration von retinalen Ganglienzellen spielt, da Beides in behandelten Tieren reduziert ist.

2 Introduction

2.1 Multiple sclerosis

Multiple sclerosis (MS) is an inflammatory, demyelinating autoimmune disease of the central nervous system (CNS). The age of onset is usually between twenty and forty years and it is the most common non-traumatic cause for neurological disability in young adults. MS is a complex genetic disease, meaning that genome aleic variations, postgenomic modification and environmental factors play a role in developing MS (Oksenberg and Hauser, 2008).

2.1.1 Genetics of Multiple Sclerosis

The genetic component of MS is amongst other things suggested by a higher incidence in some ethnic groups. People from northern European origin are at a higher risk than people from Africa and Asia. Environmental factors cannot explain these differences because resistant ethnic groups that reside in high-risk areas still show lower incidence for MS. For example Japanese living in North America have a lower incidence than the people of European descent in the same area (Detels *et al.*, 1977). The familial aggregation of MS also points to the role of a genetic component and it cannot be explained by a shared environment since adopted family members have the same susceptibility as the general population (Ebers *et al.*, 1995). The risk of developing MS is approximately 0.1 % (Sadovnick and Ebers, 1993) in the general population but rises to 1-3 % if mother, father or a sibling is affected. The risk is even higher when a twin is affected. The concordance in monozygotic twins is much higher (20-40%) than in dizygotic twins (2-5 %) (Sadovnick *et al.*, 1993), thus providing additional evidence for a genetic etiology of MS. On the other hand the discordance in monozygotic twins (after all only 20 – 40 % of the twins develop MS as well) also points to the role environmental factors play in disease development.

The Major histocompatibility complex (MHC) is thought to play a major role in genetic susceptibility and disease course. The MHC is a region on chromosome 6 that can be found in most vertebrates and whose genes play an important role in the immune

system. The best known genes in this region encode for antigen presenting proteins. In humans the genes in this subset are called human leukocyte antigen (HLA) genes. The encoded proteins are expressed on the cell surface and present antigens to T-cells. The HLA genes are divided into two classes: HLA-I and HLA-II. The major genes of the HLA-I class are HLA-A, B and C, they encode for proteins which are all part of different surface receptors which present peptides from inside the cell to T-cells. These surface receptors can be found on all cells. The proteins encoded by the genes of the HLA-II class can be found only on the surface of a few cell types, including macrophages, dendritic cells and B-cells which all belong to the professional antigen-presenting cells (APCs). The genes in this class are: HLA-DPA1, HLA-DPB1, HLA-DQA1, HLA-DQB1 HLA-DRA and HLA-DRB. For each gene of both the HLA-I and II class numerous alleles and thus protein variations are known. 2,496 alleles are known for HLA-I and for HLA-II 1032 alleles are known (IMGT/HLA Database, 2009). A strong association with the HLA-DRB1 locus and the DR2 haplotype (*DRB1*1501*, *DQB1*0602*) have been confirmed in a study of multicase MS families in the USA (Barcellos *et al.*, 2002). Other genes outside the HLA region have also been associated with MS, for example certain alleles of the interleukin-2 receptor α gene (*IL2RA*) and the interleukin-7 receptor α gene (*IL7RA*) (The International Multiple Sclerosis Genetics Consortium, 2007).

2.1.2 Infectious agents in Multiple Sclerosis

Apart from an inherited suceptibility for MS, environmental factors also play a role in developing MS. People of northern European origin who live outside of Europe/America have a much lower prevalence than those with a similar genetic background who live in high risk areas (Compston and Coles, 2002). It is known that viral infections can cause neurological diseases. In Subacute Sclerosing Panencephalitis (SSPE), a chronic inflammatory disease of white and gray matter, measles virus can be found in brain samples from patients (Payne *et al.*, 1969). Progressive Multifocal Leukoencephalopathy (PML), a demyelinating disease, is caused by an infection with the JC virus, which can be found in oligodendrocytes of patients (Padgett *et al.*, 1971). Evidence for an infectious nature of MS is the high concentration of IgG in the brain and cerebrospinal fluid (CSF) of more than 90 % of

MS patients. This IgG manifests as oligoclonal IgG bands (OGBs) and can be found in many other CNS diseases, for example SSPE and PML (Vandvik *et al.*, 1976; Weber *et al.*, 1997). The IgG in these diseases is directed against the virus which causes the disease but so far the antigenic target of the OGBs in MS remains elusive. The bacterium *Chlamydophila pneumonia* and the herpesviruses human herpesvirus 6 and Epstein-Barr virus (EBV) have been implicated to have a role in MS. For the first two no significant association was found (Tsai and Gilden, 2001; Liedtke *et al.*, 1995; Mirandola *et al.*, 1999) and while seroepidemiology studies show association between MS and EBV infection this might be due to a predisposition for both MS and certain viral infections (Niller *et al.*, 2008) and thus does not prove a causative role for this virus. Further studies on the the specifity of the OGBs could help to identify the causative antigen.

2.1.3 Different forms of Multiple Sclerosis

MS can be separated into two groups: relapsing-remitting and chronic-progressive. Relapsing-remitting multiple sclerosis (RRMS) is the most common form of disease at onset, approximately 85 % of patients first present with this form and overall this subtype accounts for 55 % of MS cases (Committee on Multiple Sclerosis, 2001). In RRMS the reoccurrence of symptoms which last at least 24 hours, is followed by a period of remission in which the symptoms improve (Figure 2.1 A1) or disappear (Figure 2.1 A2). These remissions usually last between 4 and 8 weeks, and two attacks must be separated by at least 30 days before the time in between is considered as remission. In the beginning, the relapses are often followed by a complete recovery, however later on in the disease some deficits persist and eventually develop into the secondary progressive form of the disease (see SPMS) (Committee on Multiple Sclerosis, 2001).

The chronic-progressive form can be separated into 3 different subtypes: Secondary-Progressive MS (SPMS) occurs often following an initial course of RRMS which then turns into a progressive form with or without relapses (Figure 2.1 B1 and B2) Natural history studies of untreated RRMS indicate that 10 years after the onset of RRMS 50 % of the patients would develop SPMS and after 25 years 90 % would develop SPMS. It is also the most common form of chronic-progressive MS and accounts for

30 % of MS cases (Committee on Multiple Sclerosis, 2001). The Primary-Progressive (PPMS) and Progressive-Relapsing (PRMS) forms of the disease are usually associated with a later onset (45 years or older), 15 % of patients presenting first with one of these two chronic-progressive forms. PPMS progresses continuously without flare-ups of symptoms (Figure 2.1 C1), sometimes with plateaus and temporary minor improvements (Figure 2.1, C2). PRMS is the least common form of MS, only 5 % of patients first present with this form. PRMS is also progressive from the start but shows flare-up of symptoms. Between the attacks the disease progresses further. After an attack the level of disability can return to its former state (Figure 2.1 D1) or some disability from the attack can remain (Figure 2.1 D2).

The neurological deficits in RRMS and SPMS are believed to have a different origin. In RRMS the reversible disability is caused by inflammation, oedema and demyelination and resolving of inflammation, reorganisation of sodium channels along the axon and ultimately remyelination are thought to contribute to clinical recovery after relapses (Brück, 2005). Anti-inflammatory therapies work well in RRMS emphasizing the role of inflammation at this point (Trapp and Nave, 2008). Once patients have developed SPMS the results of anti-inflammatory therapies are unsatisfactory. At this stage axonal loss causes ongoing, irreversible disability. Axonal loss occurs early in the disease but is clinically silent because the CNS can compensate the loss of neurons (Trapp *et al.*, 1999). It is estimated that in other neurodegenerative diseases such as Parkinson´s disease and Amyotrophic Lateral Sclerosis, 50 – 80 % of target neurons need to be lost before compensatory mechanisms are no longer able to prevent neurological disability (Bradley, 1987; Lloyd, 1977). A comparison between patients with PPMS and RRMS leads to interesting new concepts regarding the course of the disease. Relapses in RRMS have very little effect on accumulation of permanent disability later in the disease. Patients with PPMS have few or no relapses and the age of onset is about 10 years later than in patients with RRMS but they still reach disability milestones around the same age (Confavreux and Vukusic, 2006 ; Trapp and Nave, 2008). This data indicates that neurodegeneration might start in both patient groups around the same time but patients with RRMS are diagnosed earlier because of clinical symptoms caused by inflammatory episodes at a time when the loss of axons is still in range of compensatory mechanisms and thus clinically silent (Fig. 1.2.) (Trapp *et al.*, 1999). This emphasises the important role of neurodegeneration and also underlines the

unique opportunity of early intervention with neuroprotective therapies when only minimal axonal loss has taken place and there is chance to reduce ongoing axonal loss, irreversible disease progression and conversion from RRMS to SPMS.
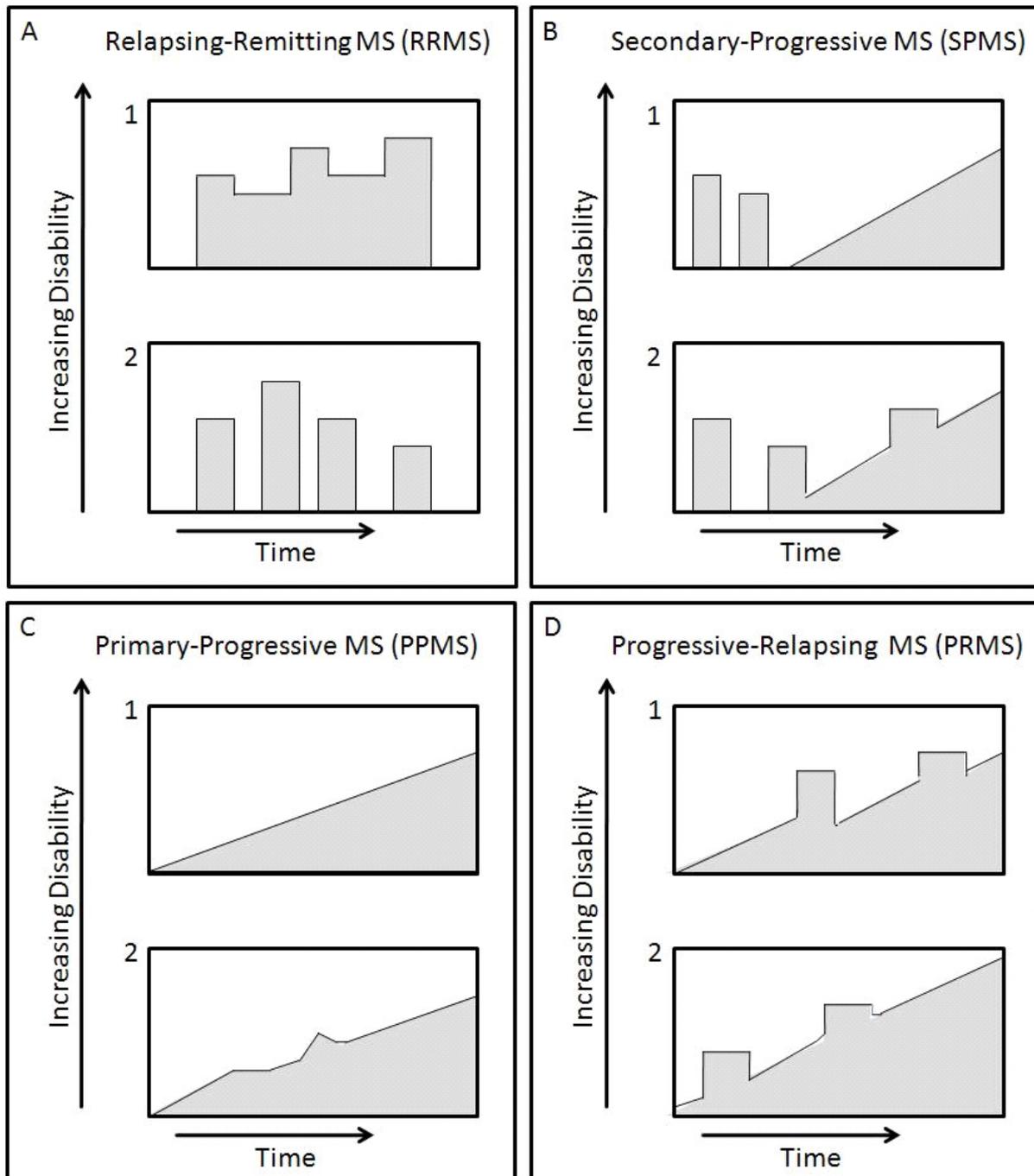
Figure 2.1 The four different forms of multiple sclerosis. Adapted from Lublin and Reingold, 1996

MS can be divided into two groups: relapsing-remitting and chronic progressive. Figure A shows Relapsing-remitting MS (RRMS), Figure B, C and D show the three forms of chronic progressive MS. RRMS is the most common form of MS and in time patients with RRMS often develop a Secondary-Progressive MS (SPMS). Primary Progressive MS (PPMS) and Progressive-Relapsing MS are more uncommon with only 15 % of patients first present with these forms.
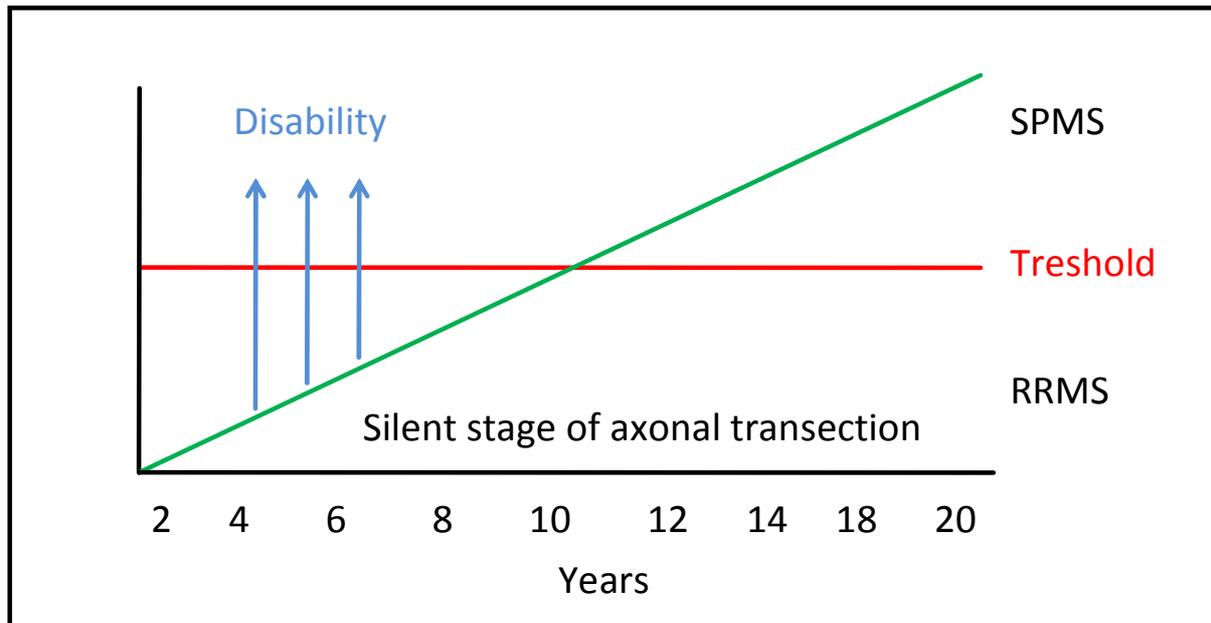
Figure 2.2 Transition from the clinical silent stage to chronic disability in MS Adapted from Trapp *et al*, 1999

There is a clinically silent phase in all neurodegenerative diseases, in this phase the CNS can still compensate for neuronal loss. However because MS has both a neurodegenerative and an inflammatory component, symptoms occur very early in the disease course and the illness can be identified before axonal loss leads to irreversible disability.

2.2 Disease pathology

Inflammation and the formation of new white matter lesions are the hallmarks of acute MS and RRMS in particular. In the progressive phase new inflammatory lesions are rare and diffuse atrophy of grey and white matter takes place, as a consequence of which anti-inflammatory therapies are less efficient in the progressive phase of the disease (Coles *et al.,* 2006). Inflammation is caused by autoreactive T-cells which cross the blood-brain barrier (BBB). Harmful autoreactive T-cells are mostly destroyed in the thymus during maturation but some of them escape and can be found in the periphery of healthy individuals as well as MS patients (Danke *et al.*, 2004). These autoreactive T-cells are suppressed by regulatory T-cells (Treg) in healthy individuals. The function of the CD4$^+$CD25^{high}CD127^{low} Tregs is not compromised in MS patients but the hyperproliferation of CD4$^+$CD25^{high}CD127^{high} Tregs might interfere with their ability to suppress autoreactive T-cells and thus leading to higher numbers of active autoreactive T-cells (Michel *et al.*, 2008). Autoeactive CD4$^+$ T-cells produce cytokines

which activate adhesion molecules on the endothelium of the BBB (ICAM-1 and VCAM-1) and express receptors (LFA-1 and VLA-4) which allow them to adhere to and transmigrate through the endothelium (Baron *et al.*, 1993; Engelhard and Ransohoff, 2005; Sospedra and Martin, 2008). The sites of injury in the CNS are called plaques. In active plaques, the BBB is disturbed which is accompanied by a leakage of serum proteins (Kirk *et al.*, 2003). The plaques are infiltrated with inflammatory cells and show increased levels of chemokines expressed by astrocytes, T-cells and microglia/macrophages (Simpson *et al*, 1998; Sørensen *et al.*, 1999; Balashov *et al*, 1999; Sindern *et al.*, 2001). Pro-inflammatory cytokines expressed by T-cells and microglia/macrophages (Cua *et al.*, 2003; Sospedra and Martin, 2008) contribute to further activation of resident cells like astrocytes and microglia, BBB opening and axonal injury (Compston and Coles, 2002), while the chemokines are responsible for the recruitment of B-cells, T-cells and monocytes from the peripheral blood. Myelin breakdown starts in the plaque and macrophages contain early myelin breakdown products pointing to their role in myelin clearance (Patrikios *et al.*, 2006). In the chronic active plaque a thin rim of active myelin breakdown is present but the core of the lesion resembles a chronic inactive lesion (Hickey, 1999). Infiltrating cells are still present and there is evidence that the BBB is still disturbed (Kirk *et al.*, 2003). Astrocytes in the demyelinated area undergo morphological changes and increase expression of glial fibrillary acidic protein (GFAP) (Hickey, 1999). The socalled reactive astrocytes (defined by their increased GFAP expression) synthesise more cytoskeletal proteins and extend pseudopodia. Ultimately they form a dense web of plasma membrane extensions and thus become a major contributor to the glial scar (Stichel and Müller, 1998).

Chronic inactive plaques are in general quiescent glial scars formed by reactive astrocytes. The numbers of infiltrating inflammatory cells is greatly diminished. Shadow plaques have a thin layer of myelin and show faint staining with Luxol Fast Blue. This is the result of partial or complete remyelination. The plaques can be distinguished from active plaques by a few characteristics: shadow plaques show a reduction of axonal density, low number of inflammatory infiltrates and no macrophages with early myelin degradation products (Patrikios *et al,.* 2006)

The mechanisms of demyelination can be divided into four patterns (Lucchinetti *et al.,* 2000): In pattern I and II, active demyelination is linked to T-cell and macrophage-dominated inflammation. In pattern I, the destructive process is most likely induced

by toxic products from macrophages. Deposition of immunoglobulins (Ig) and complement antigen C9neo can only be found in pattern II and are the major features that distinguish these two patterns. The deposition at sites of active demyelination suggests an important role for antibodies in this pattern. These two patterns of demyelination show high numbers of oligodendrocytes in the center of inactive lesions and a high incidence of remyelinated shadow plaques.

Patterns III and IV show signs of oligodendrocyte dystrophy. In pattern III, the processes of oligodendrocytes are more affected than the cell body. This is consistent with a dying back oligodendropathy which was first described in oligodendrocytes after Cuprizone administration (Ludwin and Johnson, 1981), and can also be found in MAG-deficient mice (Lassman *et al.*, 1997) which fits to the fact that in this pattern the expression of the myelin-associated-glycoprotein (MAG) is reduced. Dying-back neuropathies are characerised by the inability of the cell to maintain the metabolic processes neccesary to support the distal part of the axon. Therefore the axon starts to degenerate from the periphery and the cell body might remain intact for some time. In pattern IV, primary oligodendrocyte death in the periplaque white matter leads to secondary demyelination. The reason for the degeneration of oligodendyrocytes is unclear; it might be due to a genetic defect which renders the cells vulnerable to toxic mediators. In both patterns the inactive center shows a nearly complete loss of oligodendrocytes and remyelinated shadow plaques are absent in these patterns. Remyelinated shadow plaques usually present with less pronounced axonal injury, failure of remyelination is therefore likely to contribute to axonal injury. Several mechanisms for this failure have been discussed. After remyelination the number of oligodendrocytes in the area is higher than before (Prayoonwiwat and Rodriguez, 1993), which implies the generation of new oligodendrocytes. Post-mitotic oligodendrocytes are not able to form a new myelin sheath around the axon when transplanted into demyelinated areas (Targett *et al.*, 1996), thus it is necessary to recruit oligodendrocytes progenitor cells (OPCs) to the demyelinated area. These OPCs differentiate into pre-myelinating oligodendrocytes and then form processes which are wrapped around the demyelinated axon. A possible explanation for the failure of remyelination in later stages after repeated cycles of demyelination and remyelination is the depletion of the OPCs (Trapp *et al.*, 1998). Since the OPCs have to be recruited into the demyelinated area, failure of recruitment can also be a cause for failure of remyelination even in the presence of

sufficient numbers of OPCs in the neighbouring areas (Franklin, 2002). The fact that some chronic lesions contain sufficient numbers of OPCs but are still demyelinated led to the hypothesis that the OPCs fail to differentiate and build a myelin sheath. In tissue of MS patients, cells of the oligodendrocytes-lineage were identified but these cells were quiescent, apparently unable to differentiate into remyelinating oligodendrocytes (Wolswijk, 1998). Axons play a role in proliferation, survival and differentiation of oligodendrocytes (Bozalli and Wrabetz, 2004). A shift in surface molecules on chronically demyelinated axons might render them unreceptive to remyelination or lead to a lack of differentiation triggers for the oligodendrocytes (Chang *et al.*, 2002). It has been proposed that remyelination protects axonal integrity due to trophic support and protection against an inflammatory environment (Kornek *et al.*, 2000).

2.3   Neurodegeneration in Multiple Sclerosis

Axonal injury in MS lesions was described by Charcot at the end of the 19th century (Charcot, 1868) but the development of inflammatory models of demyelination and some success of steroids in the treatment of relapses in MS patients shifted attention towards immune-mediated demyelination (Wilkins and Scolding, 2008) and the importance of axonal pathology was ignored for many decades. Interest in axonal pathology was renewed when MRI and post-mortem studies revealed that axonal destruction starts early during the disease course (Ferguson *et al.*, 1997; Kuhlmann *et al.*, 2002; Schirmer *et al.*, 2009) and that it correlates strongly with the severity of disability in patients (De Stefano *et al.*, 1998; Bjartmar and Trapp, 2003; Schirmer *et al.*, 2011). Extensive loss of axons can be seen in acute demyelinating lesions but this lesion state usually only lasts for a few weeks. As mentioned before the brain has the ability to compensate for axonal loss to a certain degree and it is unlikely that the axonal loss in acute lesions exceeds this threshold (Dutta and Trapp, 2011), accounting for the fact that disabilities at this stage are still reversible. Chronic demyelinated lesions on the other hand can persist for years and over time slow, ongoing axonal loss is thought to make a major contribution to overall axonal loss which ultimately exceeds the brains compensatory capacity and leads to irrversible neurological disability. This would explain the transition from RRMS to SPMS and also the slow but steady accumulation of disabilities in progressive forms of MS.

Axonal loss in acute demyelinating lesions correlates with the inflammatory response (number of T-cells and macrophages) (Ferguson *et al.*,1997; Trapp *et al.*, 1998) and activated immune and glial cells release a number of substances, including proteolytic enzymes, matrix metalloproteases, nitric oxide and cytokines (Hohlfeld *et al.*,1997; Trapp and Nave, 2008) which can damage axons. Glutamate toxicity can also contribute to axonal loss, by damaging oligodendrocytes. Neurodegeneration cannot only be observed in the highly inflammatory conditions of the acute demyelinating lesion but also in normal-appearing white matter (NAWM) in the absence of demyelination (Bitsch *et al.,* 2000; Kornek *et al.,* 2000). Studies show that activated microglia are associated with formation of lesions in the NAWM (De Groot *et al.*, 2001; van der Valk & Amor, 2009) and that their activation cen be seen prior to demyelination and infiltration with T-cells (Barnett and Prineas, 2004; Gay *et al.*, 1997).

In recent years neurodegeneration in the retina of MS patients has become a focus of research. It has been shown that atrophy of the retina is associated with total brain weight (Green *et al.*, 2010), and thinning of the retinal nerve fibre layer (RNFL) correlates with white matter atrophy (Gordon-Lipkin *et al.*, 2007) suggesting that retinal pathology might reflect occurance of neurodegeneration on a more global level and may be considered as a surrogative marker for brain atrophy. Thinning of the RNFL where the unmyelinated part of the axons of the RGCs is located and macular thinning has been shown in patients with MS and optic neuritis (Trip *et al.*, 2005; Fisher *et al.*, 2006; Henderson *et al.*, 2010). In addition, in patients not affected by optic neuritis thining of the RNFL can also be observed (Fisher *et al.*, 2006; Pulicken *et al.*, 2007; Henderson *et al.*, 2008) as well as macular thinning and reduced ganglion cell layer thickness (Henderson *et al.*, 2008, Syc *et al.*, 2011). Retinal autopsy material confirmed RNFL thinning and loss of RGCs, but also revealed cell loss in the inner nuclear layer (where bipolar, horizontal and amacrine cells are located) (Green *et al.*, 2010). It has been proposed that retinal pathology could occur as a primary event, independent from optic neuritis. A subset of patients has been described in which the macula rather than the RNFL or optic nerve are affected (Saidha *et al.*, 2011), suggesting that neurons can be targeted primarily, without involvement of optic nerve pathology. The mechanism by which primary retina pathology occurs is unclear but involvement of reactive astrocytes and activated microglia is implicated by their presence in the retina (Green *et al.*, 2010).

2.4   Experimental autoimmune encephalomyelitis – an animal model of MS

Experimental autoimmune encephalomyelitis (EAE) is an animal model of multiple sclerosis that mirrors many different aspects of the disease. The origins of EAE go back to the 1920s when spinal cord inflammation was induced in rabbits by inoculation with human spinal cord (Gold *et al.*, 2006).

The benefit of this model can be seen in the fact that three of the most commonly used therapies for MS have been developed in an animal model of EAE. For example, an antibody against α4β1 integrin was found to prevent EAE in Lewis Rats (Yednock *et al.*, 1992) and was approved for MS treatment under the trademark name Natalizumab in 2004 (Steinman, 2005). After three patients developed multifocal leukoencephalopathy Natalizumab was withdrawn from the market but it has been reinstalled in 2006. Another therapy that has been successful in both the animal model and MS patients is mitoxantrone. It was shown that mitoxantrone suppressed clinical symptoms of EAE in Lewis rats (Ridge *et al.*, 1985) and it has been approved for treatment for RRMS, SPMS and PRMS in 2000 (Hartung *et al.*, 2002). Copolymer 1, better known as glatiramer acetate (GA) was originally tested as an inducing agent for EAE. It did not induce EAE but actually prevented its symptoms (Teitelbaum *et al.*, 1971). It was shown that GA reduces the relapse rate in RRMS (Johnson *et al.*, 1995) and it was approved for treatment of RRMS in 1996.

EAE can be induced in a variety of animals, mice, rats and guinea pigs are most common but EAE can also be induced in rhesus monkeys, macaques and the common marmoset (´t Hart *et al.*, 2000). The advantage of monkey models is the rather close relationship between monkeys and humans. An advantage of using mice is the possibility of creating knock-outs to determine the role of specific molecules in the disease course. However in mice there is little demyelination and also the fact that B-cell deficient knock-out mice develop EAE that is very similiar to EAE in wildtype mice questions the importance of B-cells and autoantibodies for primary demyelination in the mouse model of EAE (Hjelmström *et al.*, 1998). Since B-cells and antibodies play an important role in MS, the rat model is more suitable to examine this part of the disease since some rat models of EAE mimic this aspect very well.

The induction of EAE can be separated into three groups: spontaneous EAE, adoptive transfer EAE (AT-EAE) and actively induced EAE. There are no natural occurring models of spontaneous EAE but there are several transgenic mice strains that can spontaneously develop EAE (Wekerle, 2008). Mice that express MBP-specific T-cells receptors can develop spontaneous EAE at variable rates, depending on the hygiene level of the breeding facility (Goverman et al., 1993).

In AT-EAE myelin-specific T-cells are obtained from immunised animals and injected into healthy recipients which then develop symptoms of EAE. In the first succesful attempt of transferring EAE from one rat to another, lymph cells from immunised animals caused EAE in the recipients between day 11 and 19 after injection (Paterson, 1960). The role of T-cells in the induction of the disease became clear when the adoptive transfer of MBP-specific T-cells induced EAE in naive animals (Ben-Nun et al., 1981). It has to be noted that AT-EAE in rats is not a complete model of MS. It is an inflammatory disease with a monophasic course and only very little demyelination. Although T-cells play a key role in the breakdown of the blood-brain-barrier and pathogenesis of EAE, this alone is insufficient to trigger extensive demyelination and chronic disease activity in rats, which are characteristic hallmarks for the human disease (Gold et al., 2006). This makes AT-EAE a suitable model to examine the pathogenesis of T-cell mediated inflammation in the CNS but in order to also examine B-cell and antibody response and subsequent demyelination, another model is more suitable: In actively induced EAE the animals are injected with either myelin basic protein (MBP), proteolipid protein (PLP) or MOG which are all proteins of the myelin sheath. MBP and PLP induce an encephalitogenic T-cell response in different rat strains with weak antibody response and only little demyelination (Gold et al., 2006). The induction of EAE with MOG on the other hand can also include a severe demyelinating autoantibody response depending on the rat strain used.

The RT1 haplotypes which are analogue to the MHC in humans differ between different strains of rats. Brown Norway rats have the $RT1^{n}$ type and Lewis rats the $RT1^{l}$ type. In a comparison between the two strains it was shown that Brown Norway rats, which are resistant against purely T-cell mediated autoimmune diseases but very susceptible to autoantibody-mediated disease, exhibit a more severe course.

The fact that the haplotype modulates the MOG-specific autoantibody response makes it clear that the B-cell mediated autoantibody response plays an important role in disease severity and susceptibility (Stefferl et al.; 1999). Since the MH complex

also plays a role in MS where several genes within the complex have been associated with higher susceptibility for MS this is another similarity between MS and EAE. Besides similarities in demyelination patterns between MS and MOG-induced EAE a comparative study of axonal loss in active, inactive and remyelinating lesions in MS patients and rats with MOG-induced EAE showed a strong resemblance in the axonal pathology (Kornek *et al.*, 2000), suggesting that MOG induced EAE is very suitable model to investigate pathological features of MS.

In this study the model of MOG-induced EAE in Brown Norway rats was used, focussing on optic neuritis. Around 65 % of all MS patients develop at least one episode of optic neuritis at some point and 15 to 20 % of MS cases first present with an episode of optic neuritis (Arnold, 2005). The 15 year risk to develop MS after an episode of optic neuritis lies between 25% and 72% correlating with the occurrence of white matter lesions at the same time (The Optic Neuritis Study Group, 2008). It has been previousley demonstrated that optic neuritis occurs in 80 to 90 % of MOG-immunised Brown Norway rats (Meyer *et al.*, 2001) and leads to axonal degeneration and loss of RGCs (Hobom *et al*, 2004; Diem *et al.*; 2005a). The anatomical organisation of the visual system with the cell bodies of RGCs located in the retina and their axons which comprise the optic nerve allows a separate examination of neurodegenerative events in cell bodies and axons. As mentioned above optic neuritis is a common first symptom, demonstrating an early manifestation of the disease in humans and in the Brown Norway rat model and thus giving the latter a great potential to understand early neurodegenerative changes.

2.5   Apoptotic pathways in RGCs

In MS and EAE lesions, transection and swelling of axons as well as disturbed axonal transport and changes in cytoskeletal proteins can be observed (Zhu *et al.*, 1999; Wujek *et al.*, 2002; Trapp *et al.*, 1998; Meyer *et al.*, 2001) and are thought to be responsible for secondary apoptosis of cell bodies, including that of RGCs (Diem *et al.*, 2005a). During development, apoptosis is needed to acquire the correct number of neurons since most classes of neurons produce more cells than needed during development (Bähr, 2000). After that initial period during development

neurons have to be maintained for the entire life and in the adult CNS their irreversible loss due to apoptosis contributes to clinical symptoms for example in neurodegenerative diseases and trauma. Apoptosis of neuronal cell bodies can be observed after traumatic axonal injury (Garcia-Valenzuela *et al.*; 1994; Isenmann *et al.*, 1997; Diem *et al.*, 2001) and despite strong differences concerning the trigger of the axonal injury, degeneration of RGCs shares common apoptotic pathways in axotomy models and under autoimmune inflammatory conditions. These include changes in proteins of the Bcl-2 family and the PI3K/Akt pathway and involvement of caspase 3. The Bcl-2 family contains pro-apoptotic proteins such as Bax, Bad, Bim and Bid and anti-apoptotic proteins such as Bcl-2, Bcl-X_L and Bcl-W (Korsmeyer, 1999). Overexpression of the anti-apoptotic protein Bcl-X_L inhibits release of cytochrome c from the mitochondria (Kharbanda *et al.*, 1997) and local protein delivery promotes RGC survival during EAE (Diem *et al.*, 2005b). Overexpression of anti-apoptotic Bcl-2 in mice leads to resistance of RGCs to cell death after axotomy and ischemia (Martinou *et al*, 1994; Cenni *et al.*; 1996) and resistance against MOG-induced EAE (Offen *et al.*, 2000). Pro-apoptotic members of the Bcl-2 family such as Bax promote cytochrome c release which together with Apaf1 forms the apoptosome. Pro-caspase 9 is recruited to the apoptosome and activated. Active caspase 9 then activates other caspases such as caspase 3. Bax ablation reduces axonal damage in mice with EAE (Lev *et al.*, 2004): And siRNA against Bax and Bax knockout reduces RGC death after optic nerve axotomy in mice (Lingor *et al.*, 2005; Goldenberg-Cohen *et al.*, 2011). After axotomy, a decrease in anti-apoptotic Bcl-2 and an increase in pro-apoptotic Bax can be found (Isenmann *et al.,* 1997), and the same can be observed during optic neuritis, preceding the loss of RGCs (Hobom *et al.*, 2004). Axotomy of the optic nerve leads to an increase in caspase 3 activity and DNA fragmentation, visualized with TUNEL staining (Kermer *et al.*, 1999) which can also be observed in RGC death during optic neuritis (Meyer *et al.*; 2001).

Another important mechanism in the regulation of apoptosis after axotomy and during optic neuritis is the the PI3K/Akt pathway. The phosphorylation of Akt via Phosphoinositide 3-kinase (PI3K) is reduced in RGCs after optic nerve transection (Kermer *et al.,* 2000) and also during optic neuritis (Hobom *et al.*, 2004). Phospho-Akt can phosphorylate, and thereby inhibit the pro-apoptotic proteins Bad and caspase 9 (Datta *et al.*; 1997; Cardone *et al.*; 1998) which leads to decreased levels of caspase 3 (Li *et al.*; 1997). Therapies which increase the amount of phospho-Akt,

including TNF- alpha, erythropoietin and insulin growth factor-I (IGF-I), lead to increased RGC survival after axotomy and during optic neuritis (Weishaupt *et al.*; 2004; Kermer *et al.,* 2000; Diem *et al.*, 2001; Sättler *et al.*, 2004). In addition to the apoptotic death of RGCs after onset of clinical symptoms, death of RGCs can also be observed prior to clinical symptoms in a model of MOG-induced EAE in Brown Norway rats (Hobom *et al.*, 2004) but the mechanism of this early degeneration of RGCs has not been elucidated yet.
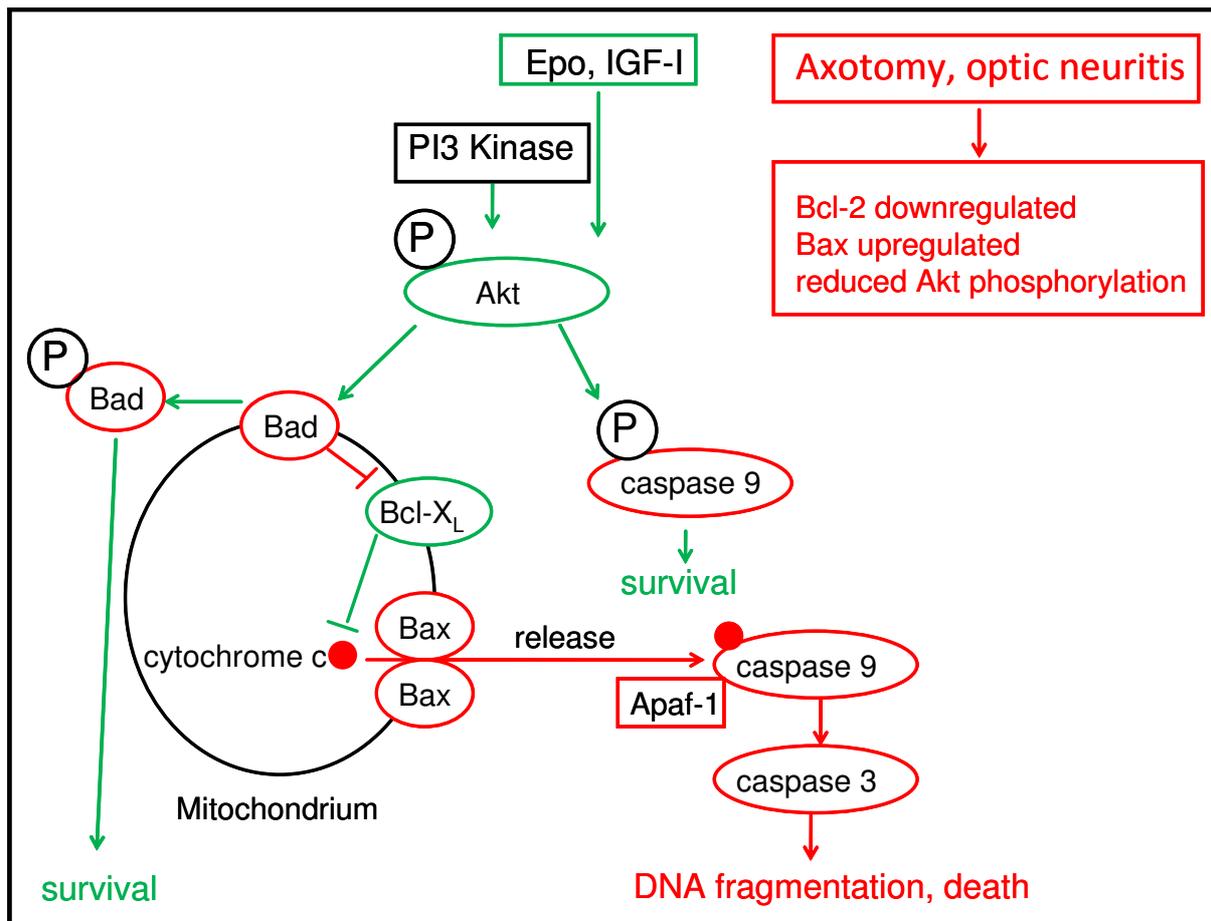
Figure 2.1 Apoptotic and survival pathways of RGCs after axotomy and during optic neuritis

Axotomy of the optic nerve as well as optic neuritis leads to death of RGCs via similar pathways. Changes in proteins of the Bcl-2 familiy can be observed, namely downregulation of anti-apoptotic Bcl-2 and upregulation of Bax. Bax is thought to build a pore through which cytochrome c can be released from the mitochondria. The formation of this pore is inhibited by the anti-apoptotic protein Bcl-2. Ablation of Bax and overexpression of Bcl-2 and Bcl-X$_L$ promotes survival of RGCs. Cytochrome c forms the apoptosome together with Apaf-1, activating caspase 9 which then activates caspase 3. Increased activity of caspase 3 can be seen both after axotomy and during optic neuritis.

Treatment studies show that phosphorylation of Akt protects RGCs in axotomy and optic neuritis. Phospho-Akt phosphorylates caspase 9 which than no longer is able to be a part of the apoptosome and also phoshporylates and thus inactivates the pro-apoptotic protein Bad.

2.6   Calcium influx in neuronal and axonal degeneration

Dysregulation of calcium homeostasis has been observed in several neurodegenerative diseases such as ALS, Parkinson´s disease and Huntington´s disease as well as in stroke and traumatic brain injury (TBI) (reviewed in Marambaud *et al*., 2009 and Wojda *et al*., 2008) and several studies show involvement of calcium

in axonal degeneration in trauma (George *et al.*, 1995), anoxia (Imaizumi *et al.,* 1999) ischemia (Stys *et al.*, 2005) and inflammatory models (Kornek *et al.*, 2001). Excessive calcium influx can be caused by several mechanisms, including sodium influx and subsequent influx of calcium through voltage dependent calcium channels (VDCCs) and the Na^+/Ca^{2+} exchanger (NCX) (Figure 2.4). In normal axons the voltage-gated sodium channels Na_v 1.2 and 1.6 are mostly restricted to the node of Ranvier. After demyelination of the axon, sodium channels are redistributed along the whole axon (Waxman *et al.*, 2004) as an attempt to re-establish conduction. The redistribution of the sodium channels along the axons leads to a higher energy/ATP demand because action potentials are now accompanied by higher sodium influx and more energy is needed to keep the resting potential and sodium concentration within the normal range. ATP-depletion as a result of increased energy demand and mitochondrial dysfunction (Dutta *et al.*, 2006) can induce failure of the sodium/potassium ATPase (Na/K-ATPase) and thus cause elevated sodium levels in the cell. The blockade of sodium channels with phenytoin proved to be neuroprotective for both RGCs and their axons in a glaucoma model (Hains and Waxman, 2005) and for spinal cord axons in a mouse model of EAE (Black *et al.* , 2006), suggesting a role for sodium influx in neurodegeneration. The influx of sodium leads to depolarisation of the membrane and activation of voltage dependent calcium channels (VDCC). In both MS patients and rats with EAE, accumulation of the pore-forming subunit of N-type voltage-gated calcium channels could be found along the axon colocalising with APP (Kornek *et al.*, 2001), suggesting a role for these channels in axonal degeneration. This hypothesis is further strengthend by the fact that treatment with the N-type calcium channel blocker conotoxin reduces axonal damage in EAE (Gadjanski *et al.*, 2009). In spinal cord axons of MS patients and EAE rats a co-localization of sodium channels with the NCX was found. The exchanger normally pumps three sodium ions into the cell in exchange for pumping out one calcium ion. Elevated sodium concentrations as well as membrane depolarisation can cause the NCX to go into reverse mode and thus lead to elevated calcium concentrations in the cell (Yu and Choi, 1997). Blockade of the NCX proved to be neuroprotective in axons following spinal cord white matter injury in rats (Li *et al.*, 2000) and attenuated calcium influx and subsequent neurodegeneration in cultured hippocampal neurons (Araujo *et al.,* 2007).

Another source for elevated intracellular calcium levels are ionotropic glutamate receptors which can be found on the cell body. Glutamate is the major excitatory neurotransmitter in the CNS (Curtis and Johnston, 1974; Fonnum, 1984). It has long been known that excessive or prolonged exposure to glutamate leads to neuronal degeneration, including degeneration of inner retinal layers such as the ganglion cell layer (Lucas and Newhouse, 1957; Olney, 1969; Sisk and Kuwabara, 1985) and that a rise in intracellular calcium concentration is a key component in glutamate-induced (excitotoxic) degeneration of neurons (Sucher *et al.*, 1997; Sattler and Tymianski, 2000). There are three classes of ionotropic glutamate receptors, named after their selective agonists: N-methyl D aspartate (NMDA), α-amino-3-hydroxy-5-methyl-4-isoxazolepropionic acid (AMPA) and kainate receptors. Binding of glutamate or the specific receptor agonists leads to opening of the pore and subsequent influx of ions such as sodium and calcium. Rodent RGCs express NMDA, AMPA and kainate receptors as was shown with electrophysiological recordings (Aizenman *et al.* 1988; Taschenberger *et al.* 1995; Karschin *et al.*, 1988) and with single cell molecular profiling with RT-PCR (Jakobs *et al.*, 2007). AMPA and kainate receptors usually have low calcium permeability (Hollmann *et al.*, 1991; Burnashev *et al.*, 1992; Sommer *et al.*, 1991). NMDA receptors on the other hand are highly permeable to calcium (Mayer and Westbrook; 1987) and exposure to NMDA causes loss of cells in the inner retina layer (Siliprandi *et al.*, 1992; Lam *et al.*, 1999) implying an important role for these receptors in glutamade-mediated toxicity. Blocking the NMDA receptor with the specific antagonist (+)-5-methyl-10,11-dihydro-5H-dibenzo[a, d]cyclohepten-5, 10-imine (MK801) reduces glutamate-induced cell death in cultured RGCs (Pang *et al.*, 2007) and also leads to reduced calcium influx in cultured RGCs (Hartwick *et al.*, 2008). Their study suggests an important role for NMDA receptors in excitotoxic degeneration of RGCs, whereas they suggest that activation of AMPA and kainate receptors results mainly in cell depolarisation, resulting in the release of the Mg^{2+} block of the NMDA receptors, therefore only making a minor contribution to calcium influx. These results suggest NMDA receptors as a suitable target for blocking experiments to examine the role of calcium influx via ionotropic glutamate receptors in the retina and as a potential method to protect RGCs against glutamate-induced neurodegeneration.
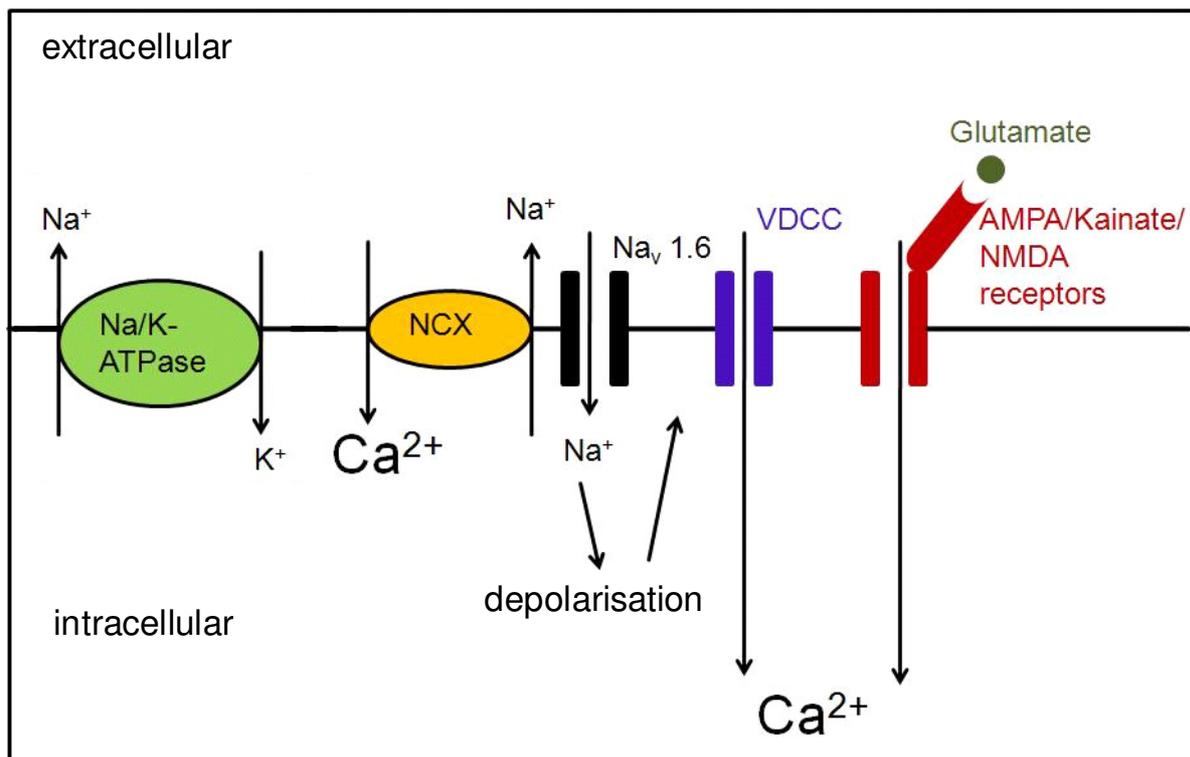
Figure 2.3 Calcium entry pathways

The redistribution of sodium channels (Na_v 1.6) along the axon (following demyelination) leads to an elevated intracellular sodium concentration. The redistribution also leads to a higher energy demand because action potentials now cause higher sodium influx and more ATP is needed to keep the resting potential and sodium concentration within normal range. ATP-depletion can induce failure of the sodium/potassium ATPase (Na/K-ATPase) and thus elevate sodium levels in the cell further. This causes depolarisation which activates VDCCs and thus leads to accumulation of calcium in the cells. The elevated sodium concentration also drives the sodium-calcium exchanger (NCX) into reverse mode which also contributes to elevated intracellular calcium concentration. Binding of glutamate to the ionotropic glutamate receptors (mainly NMDA but also AMPA/kainate) causes calcium influx.

2.7 Manganese-enhanced MRI (MEMRI)

MRI is an important tool to assess MS- or EAE-related pathological changes including inflammation, scar formation and atrophy. In patients with clinically defined MS, brain MRI imaging reveals multifocal cerebral white matter (WM) lesions in more than 95 % of patients (Inglese, 2006) and MRI features for dissemination in space and time have been incorporated within the diagnostic criteria for MS in 2001 (McDonald *et al.*, 2001).

Using contrast agents allows better visualisation of anatomical structures but it can also be used to measure disease activity. Gadolinium enhancement for example is believed to be a highly sensitive marker for disease activity. Gadolinium cannot cross

the BBB under normal circumstances and enhancement implies a disruption of the BBB (Ding *et al*., 2006), which can be found in active lesions in MS. Manganese (in the form of $MnCl_2$ or Mangafodipir Trisodium (MnDPDP)) is another contrast agent used in MRI. The paramagnetic ion reduces the spin-lattice relaxation time constants (T1) of tissues in which it has accumulated and thus causes positive contrast enhancement in T1-weighted MRI. The manganese ion (Mn^{2+}) has been used as a tracer for calcium influx, as it is well established that it can enter cells via calcium transport mechanisms such as the sodium/calcium exchanger and voltage-dependent calcium channels (VDCC) due to its similar size and ionic properties (Lin and Koretsky; 1997; Takeda, 2002). Experiments in MOG-induced EAE in Brown Norway rats have established that signal enhancement in the optic nerve can be seen after onset of clinical symptoms. The question if manganese enhancement in the optic nerve can already be seen during the induction phase of EAE has not yet been answered.

Since the death of RGCs is an early finding in MOG-induced EAE in Brown Norway rats, manganese enhanced MRI of the retina could help to elucidate the role of calcium influx in RGC degeneration. Studies show changes in manganese uptake in the rat retina after insults such as increased intraocular pressure (Berkowitz *et al*., 2008) and also an increase in manganese uptake correlating with decreased light exposure (Berkowitz *et al*. 2009).

As mentioned above the NMDA-receptor blocker MK801 is known to reduce calcium influx in RGCs *in vitro* (Hartwick *et al*., 2008). MK801 is also able to cross the BBB (Clineschmidt *et al*., 1982), which makes it suitable for examining the role of NMDA receptors in manganese enhancement and thus calcium influx at early time-points.

2.8   The calcium-activated protease calpain

Elevated intracellular calcium concentration leads to the activation of different enzymes, one of which is the cysteine protease calpain. When activated calpain cleaves cytoskeletal proteins, for example ankyrin and members of the spectrin family such as α2-spectrin and β4-spectrin (Hall *et al*., 1987; Siman *et al*., 1984, Lövfenberg and Backmann, 1999; Schafer *et al*., 2009). These cytoskeletal proteins are important for maintaining membrane integrity and to restrict difussion of transmembrane proteins (Bennet and Gillian, 1993; Czogalla and Sikorski, 2005).

Breakdown products from α2-spectrin are commonly used as indicator for caspase and calpain activity. Caspase cleaves α2-spectrin into two fragments of 150 and 120 kDa and calpain cleaves them into fragments of 150 and 145 kDa. The two best characterized members of the calpain family are µ-calpain and m-calpain which are expressed ubiquitously. They differ from each other in the amount of calcium that is needed for activation: m-calpain needs 0.2-0.8 mM whereas µ-calpain requires 2-80 µM calcium (Camins *et al.*, 2006). Under physiological conditions the calcium concentration is in the nanomolar range and only slight proteolytic modification of calpain substrates can be found. When the calcium concentration in the cells rises, more calpain is activated which leads to increased spectrin proteolysis. In hippocampal neurons stimulation of NMDA receptors leads to increased proteolysis (Seubert *et al.*, 1988), whereas inhibition of proteases reduced the concentration of spectrin breakdown products (SBDP) in hippocampal neurons and promoted their survival (Lee *et al.*, 1991). After onset of EAE, the calpain activity has been shown to rise, and might contribute to demyelination since it can cleave MBP and MOG (Schaecher *et al.*, 2001; Shields and Banik, 1999). In an animal model of TBI calpain-specific MBP breakdown products were found (Liu *et al.*, 2006), suggesting a role for calpain in demyelination *in vivo*. Calpain is known to cause neurofilament breakdown in anoxic and ischemic optic nerves in rats (Stys and Jiang, 2002), which could contribute to axonal pathology. Activation of calpain also leads to internalisation of the plasma membrane Ca^{2+} ATPase (PMCA) (Pottorf *et al.*, 2006) and cleavage of NCX (Bano *et al.*, 2005) which leads to prolonged elevated calcium levels.

Calpain is also involved in the apoptotic pathway. Calpain cleavage activates the protein phosphatase calcineurin which desphosphorylates the pro-apoptotic protein Bad. The dephosphorylated Bad forms a heterodimer with the anti-apoptotic proteins Bcl-2 and Bcl-X_L (Hara and Snyder, 2007) and inactivates them. In a model of glaucoma the inhibition of calcineurin prevented cytocrome c release and death of RGCs (Huang *et al.*, 2005). Calpain-mediated cleavage of the pro-apoptotic proteins Bid and Bax leads to cytochrome c release from mitochondria and activation of the caspase 3 dependent apoptotic pathway. In cultured NIH 3T3 cells calpain inhibition increased Akt phosphorylation and cell viability and it has been proposed that calpain activity inhibits phosphorylation of Akt by interacting with PI3K (Beltran *et al.,* 2011). Cleavage of the cyclin-dependent kinase 5 (CDK5) activator p35 by calpain leads to deregulation of CDK5 and subsequent hyperphosphorylation of tau which has been

proposed to be neurotoxic (Azuma and Shearer, 2008). In addition, it has been shown that calpain inhibitors reduce processing of p35 and death of cultured RGCs (Nath *et al.*, 2000; Verdaguer *et al.*, 2005).

Taken together these results show that calpain plays an important role in neurodegeneration in different models and via different pathways. The role of calpain in our model and the time course of calpain activation have not yet been examined and it remains to be seen how it correlates with axonal degeneration and death of RGCs.
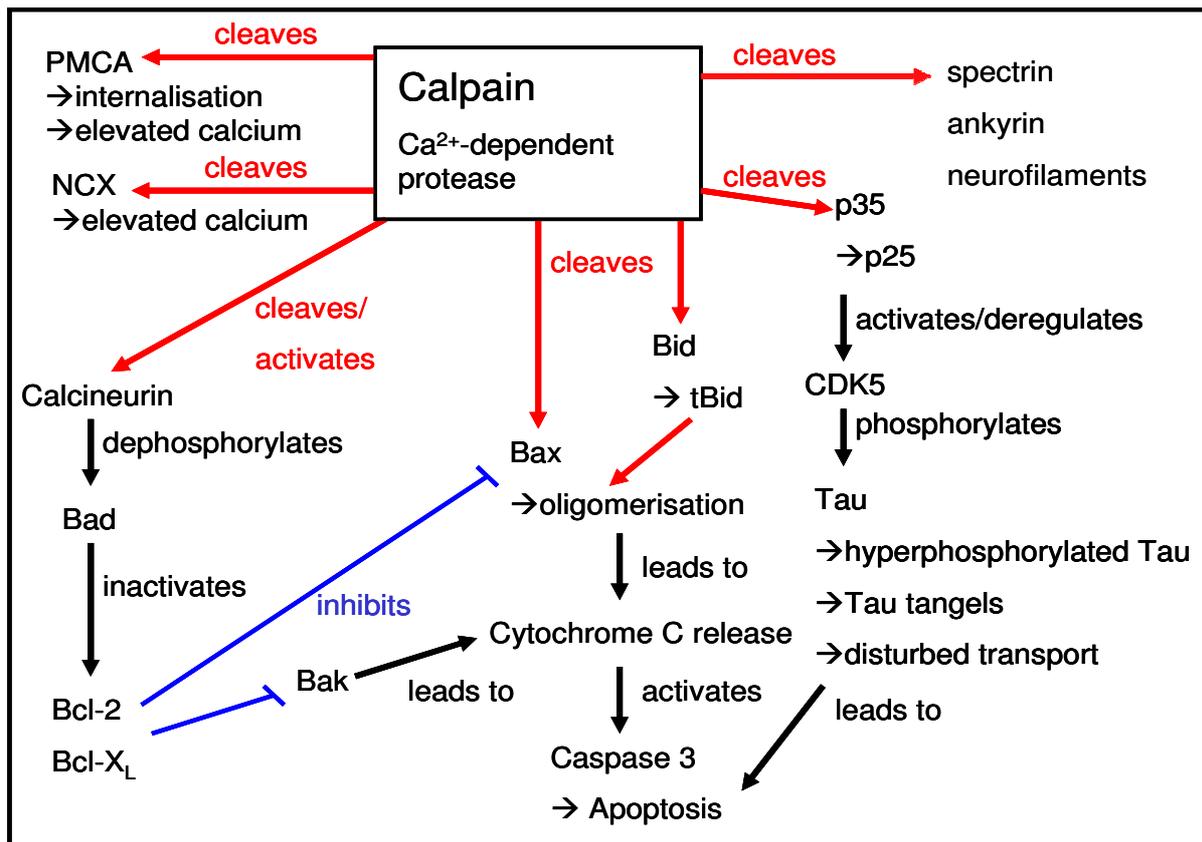
Figure 2.4 The role of calpain in apoptosis and axonal damage

Calpain can cleave cytoskeletal proteins such as neurofilaments, spectrin and ankyrin. Calpain can also cleave the plasma membrane Ca^{2+} ATPase (PMCA) and the Na^+/Ca^{2+} Exchanger (NCX) and thus contribute to prolonged elevated calcium levels. The activation of calcineurin via calpain-mediated cleavage inactivates anti-apoptotic proteins. Calpain cleavage also activates pro-apoptotic proteins which lead to cytochrome c release and subsequent caspase 3 activation and apoptosis. Calpain-mediated deregulation of the cyclin-dependet kinase 5 (CDK5) leads to hyperphosphorylation of tau which then forms tangles, causing disturbed transport. By interacting with the PI3 kinase calpain causes reduced phosphorylation of Akt, which also contributes to apoptosis.

2.9   Calpain activity as therapeutic target

As discussed above, activation of calpain plays an important role in apoptotic processes and axonal damage. Recently it was shown that calpain inhibition with calpeptin reduces CCL2 induced chemotaxis in T-cells (Butler *et al.*, 2009). Pretreatment of MBP-specific T-cells with calpeptin before adoptive transfer leads to reduced clinical symptoms and reduced inflammation, demyelination and axonal loss in the spinal cord in mice (Guyton *et al.*, 2009) and treatment with calpeptin also reduces clinical symptoms, inflammation, demyelination and axonal loss in the spinal

cord of Lewis rats with EAE (Guyton *et al*., 2010). Treatment of cultured RGCs with calpeptin reduces apoptosis after ionomycin-induced calcium influx (Das *et al*., 2006). Treatment with calpeptin could therefore prove to be beneficial in reducing severity of optic neuritis by reducing inflammatory infiltration and may decrease degeneration of RGCs by attenuation of apoptosis.

Aim of the study

The research in MS has been traditionally focused on understanding the role of inflammation. However, in recent years neurodegeneration has emerged as an important research area, due to an increasing amount of evidence that neurodegeneration is an early event in the disease, occurring from the onset and is also probably the main determinant of permanent clinical disability.

In the model used in this study early neurodegeneration can be observed in the RGCs but the relationship with the immune response is unclear since degeneration is observed prior to onset of inflammatory infiltration of the optic nerve and subsequent axonal injury. This raises the question if subtle axonal changes or changes in the retina itself could contribute to early neurodegeneration and which mechanisms are involved in the early death of RGCs. It has been shown that calcium influx and subsequent calpain activation can cause neuronal and axonal damage and increased calcium influx during the clinical phase of EAE has already been proven. The questions if calcium influx in the optic nerve already starts in the induction phase of the disease and if early calcium influx in the retina and subsequent activation of calpain could be a possible mechanism for early death of RGCs were examined in this study since they have not yet been adressed. Since neurodegeneration is now thought to be a main contributor to permenant clinical disability in patients, neuroprotective strategies have become a focus of research. This study adresses the question if inhibition of calpain activation could prove beneficial for RGC survival both during the induction and clinical phase of EAE.

3 Material and Methods

3.1 Animals

Female Brown Norway rats 8–10 weeks of age were used in all experiments. They were obtained from Charles River (Sulzfeld, Germany) and kept under environmentally-controlled conditions in the absence of pathogens. All experiments that involved animal use were performed in compliance with the relevant laws and institutional guidelines of the Saar-Pfalz Kreis.

3.2 Induction and evaluation of EAE

Whole recombinant MOG (Weissert *et al.*, 1998) was used to induce MOG-EAE. Animals were anesthetized by inhalation of 5 % isoflurane and injected intradermally in the tail with a volume of 200 µl containing 100 µg of MOG (gift from Prof. D. Merkler, Department of Pathology and Immunology, University of Geneva) in phosphate-buffered saline (PBS, Sigma, St. Louis, USA) mixed (1:1) with complete Freund´s adjuvant (Sigma) containing 200 µg of heat-inactivated *Mycobacterium tuberculosis* (Difco Microbiology, Kansas, USA). Sham controls were immunised without MOG.

Rats were scored daily for clinical signs of EAE. The following scoring system was used: grade 0.5: distal paresis of the tail; grade 1: complete tail paralysis; grade 1.5: paresis of the tail and mild hind leg paresis; grade 2.0: unilateral severe hind leg paresis; grade 2.5: bilateral severe hind limb paresis; grade 3.0: complete bilateral hind limb paralysis; grade 3.5: complete bilateral hind limb paralysis and paresis of one front limb; grade 4: complete paralysis (tetraplegia), moribund state, or death.

3.3   Retrograde labeling of RGCs

One week before immunisation, rats were anaesthetized by intraperitoneal injection (i.p.) of ketamine 10 % (0.6 ml / kg; Serumwerk, Bernburg, Germany) and xylazine 2 % (0.3 ml / kg; Riemser, Greifswald, Germany) and placed in a stereotactic frame. A mediosagittal incision was made and two holes were drilled in the skull, one above each superior colliculus (6.8 mm dorsal and 2 mm lateral from Bregma). The rats were then injected with 2 µl of the fluorescent dye Fluorogold (5 % in saline, Fluorochrome LLC, Denver, USA) into each superior colliculus using a 100 µl glass syringe (Hamilton, Reno, USA) at a speed of 0.75 µl / min.

3.4   Quantification of RGC numbers

At the end of experiments, rats received an overdose of ketamine 10 % (1 ml / kg) and xylazine 2 % (0.5 ml / kg) and were perfused via the aorta with 4% paraformaldehyde (PFA) in phosphate-buffered saline (PBS). The retinas were dissected and flat-mounted onto glass slides. They were examined with a fluorescence microscope (Nikon, Japan) using an UV filter (365/420 nm). RGC densities were quantified by two observers (second observer was Dr. Sarah Williams) by counting of labelled cells in 12 distinct areas of 62,500 μm^2 each (three areas per retinal quadrant at three different eccentricities of 1/6, 1/2 and 5/6 of the retinal radius).

3.5   Tissue preparation

Animals were perfused via the aorta with 4 % PFA in PBS. The tissue was post-fixed in PFA overnight and 12 hours prior to dissection the tissue was placed in PBS.

3.5.1 Preparation of paraffin-embedded tissue and sections

Optic nerves and spinal cord were removed and put in PBS. Tissue was then embedded in an automatic tissue processor (Leica, Wetzlar, Germany). After this, tissue was embedded in paraffin using a paraffin embedding machine (Leica). For optic nerves, embedding was performed in two different orientations to create both longitudinal and cross-sections. For spinal cords only cross-sections were created. For cross-sections, the optic nerves were cut into three pieces. After embedding in paraffin, blocks were cooled on a cooling plate and afterwards cut into 0.5 µm thick sections with a microtome (Leica) and placed on frosted slides (VWR, Darmstadt, Germany).

3.5.2 Preparation of frozen tissue and sections

For retinal sections, the cornea, vitreous body and parts of the sclera were removed. The eyes were cryoprotected in 30 % sucrose (AppliChem, Darmstadt, Germany) in PBS overnight. The tissue was placed in a base mold (Medite, Burgdorf, Germany) filled with optimum cutting temperature (OCT) compound (Medite) and then frozen by placing the base mold in isopenthane which was precooled in liquid nitrogen. Frozen tissue was kept at -80 °C, and shortly before cutting the tissue was transferred to -20 °C. Retinas were cut into 18 µm thick sections using a cryostat (Fisher Scientific, Schwerte, Germany) with a chamber temperature of -25 °C, placed on frosted slides (VWR) and then stored at -20 °C.

3.6 Histopathology

3.6.1 Luxol Fast Blue

To determine the extent of demyelination, 0.5 µm optic nerve (ON) cross- and longitudinal-sections were stained with Luxol Fast Blue (LFB). After deparaffinization in rothihistol (Roth, Karlsruhe, Germany), the sections were placed in 100 % and 96

% alcohol. Afterwards they were incubated overnight in 0.1% LFB solution in 96 % Ethanol with 0.1 % acetic acid (Solvent blue 38, Sigma, Steinheim, Germany) at 60°C. On the second day the slides were cooled to room temperature (RT) and put in 90 % alcohol. Then each slide was put individually into 0.05 % lithiumcarbonate solution (Fluka/Sigma) until the colour of the tissue changed from dark blue to turquoise. The slides were put in 70 % ethanol and then in water. Afterwards the slides were put in periodic acid (Sigma) for 10 minutes followed by 5 minutes in running tap water. The tissue was then incubated for 30 minutes in Schiff´s reagent (Sigma) and left under running tap water for 5 minutes for the blue colour to develop. A counterstain was performed with haematoxylin and then the tissue was dehydrated and mounted with Roti® - Histokitt II (Roth).

Demyelinated areas were determined as a percentage of the whole ON cross-section area. The surface area of the ON was measured using the ImageJ software (NIH Image, http://rsb.info.nih.gov/ij/)

3.6.2 Bielschowsky´s Silver Impregnation

To determine the extent of axonal loss, ON cross-sections were stained with Bielschowsky´s silver impregnation. Sections were rehydrated and then incubated in 20 % silver nitrate solution (Roth) for 20 mins. Following this, slides were then transferred to distilled water (dH$_2$O) and ammonia (VWR) was added dropwise to the silver nitrate solution until it became clear. The slides were placed in the solution and incubated for 20 mins in the dark. Afterwards the developer was added dropwise until the tissue became brown. The stain was then fixed with 2 % sodium-thiosulfate (Fluka/Sigma) for 2 mins. Finally the sections were dehydrated and mounted with Roti® - Histokitt II.

Axonal densities were determined semi-quantitatively with an eyepice graticule (Nikon, Japan). The unit area has 25 crosses and each point where an axon intersected the cross or the circle around it was counted as positive. Four unit area areas were randomly positioned within the area of the ON cross section.

3.7 Immunohistochemistry

Paraffin-embedded sections were placed overnight at 60 °C and then deparaffinized in Roti Histoclear (Roth) and hydrated in a decreasing series of alcohols. After washing in dH_2O the slides were heated in a microwave in various antigen retrieval solutions (Table 2-2) and left to cool down for 15 minutes before washing in PBS. For the tissue to be treated with diaminobenzidine (DAB, Sigma) the endogenous peroxidase activity was quenched in 3 % H_2O_2 (Fischar, Saarbrücken, Germany) for 10 minutes at RT, followed by washing in PBS. Tissue was blocked with 10 % serum / 2 % bovine serum albumin (BSA, Sigma) in PBS for 20 minutes at RT. Afterwards the primary antibody was applied (Table 3-1 for details) and the tissue was incubated overnight at 4 °C.

Frozen retina sections were thawed for 10 minutes at RT and then washed in PBS for 3x5 minutes. The tissue was blocked for one hour in 20 % serum and afterwards the primary antibody was applied (Tabelle 3-2 for details) and the tissue was incubated overnight at 4 °C.

3.7.1 Light microscopy:

Following washing in PBS, the appropriate secondary antibody was applied (Table 2-3 for details) and left on the tissue for 1h at RT, followed by a further 3 washes in PBS. Then the tissue was incubated with ABC Elite Kit (Vector, Burlingame, USA) for 1h at RT and coloured using either DAB or SG substrate (Vector) for 10 minutes at RT. The reaction was stopped by putting the slides in water (DAB) or PBS (SG) for 5 minutes.

When counterstaining was required, slides were put for 3 minutes in haematoxylin and then dipped in HCl-EtOH. Afterwards the tissue was dehydrated in increasing ethanol concentrations, placed in Roti Histoclear and then mounted with Roti® - Histokitt

3.7.2 Fluorescence microscopy

Afther the secondary antibody was applied (Table 3-3 for details) the tissue was incubated for 1h at RT in the dark, followed by 3 washes in PBS. Tissue was mounted with Vectashield containing DAPI (4', 6-diamidino-2-phenylindole) (Vector).

Table 3-1 Primary antibodies and antigen retrieval methods used for immunohistochemistry with paraffin sections

Antibody	ED1	PCNA	CD3	EMAP II
Company	Serotec, UK	Santa Cruz, USA	Dako, Denmark	Abcam, UK
Antibody subtype	mouse IgG1	mouse IgG2A	rabbit polyclonal	mouse IgG
Antigen Retrieval (15 min)	citrate buffer, pH 6.0	Antigen unmasking solution (Vector)	EDTA buffer, pH 7.4	citrate buffer, pH 6.0
Blocking serum	horse Vector	horse Vector	goat Sigma	horse Vector
Antibody concentration	1:500	1:5000	1:600	1:600

Tabelle 3-2 Primary antibodies used for immunohistochemistry with frozen retina sections

Antibody	ED1	GFAP
Company	Serotec	Sigma
Antibody subtype	mouse IgG1	rabbit polyclonal
Blocking serum	horse Vector	goat Sigma
Antibody concentration	1:400	1:400

Table 3-3 Secondary antibodies for immunohistochemistry (DAB and fluorescence)

Antibody	Horse α Mouse biotinylated	Goat α Rabbit biotinylated	Goat α Mouse Cy3	Goat α Rabbit Cy3
Company	Vector	Vector	Jackson Labs, USA	Jackson Labs, USA
Antibody subtype	anti-mouse IgG	anti-rabbit IgG	anti-mouse IgG	anti-rabbit IgG
Blocking serum	horse Vector	goat Vector	goat Sigma	goat Vector
Antibody concentration	1:200	1:200	1:400	1:400

3.7.3 Immunohistochemistry for β-amyloid precursor protein (APP)

For APP staining, a modified protocol was necessary:

Sections were deparaffinized overnight at 60°C and then rehydrated to 96 % ethanol before the endogenous peroxidase activity was quenched in 0.7 % H_2O_2 in methanol for 30 min. Afterwards the tissue were rehydrated further and then placed in distilled water for 5 min. The slides were then put in a steamer (Braun, Kronberg Germany)

with 0.2 % citrate buffer pH 6,0 (Merck) for one hour and then allowed to cool down for another hour. Afterwards the tissue was blocked with 20 % horse serum in antibody diluent (Dako, Glostrup, Denmark) for one hour at RT. Afterwards the primary antibody was applied and the tissue was incubated at 4°C overnight and then washed with PBS before adding the secondary antibody for one hour at RT. After washing the slides were then placed in Avidin solution (Sigma; 1:100) for one hour at RT and coloured with DAB substrate kit for peroxidase for 10 minutes. The reaction was stopped in distilled water. For counterstaining, tissue was incubated for 10 minutes in haematoxylin, and then dipped in HCl-EtOH (Merck). Afterwards the tissue was dehydrated in increasing ethanol concentrations, placed in Roti Histoclear (Roth) and then mounted with Roti® - Histokitt II.

3.7.4 Immunohistochemistry with two antibodies

When tissue was stained with two different antibodies in combination, following the first set of primary and secondary incubations, sections were washed in PBS, blocked a second time in 10 % serum / 2 % BSA, and followed by the second set of antibodies.

In order to control for the cross-reaction of antibodies in these double labelling experiments, the following controls were performed (Table 3-4).

The results showed that each combination gave similar results. For further staining ED1 was used with DAB and PCNA with SG because PCNA positive and negative cells was easier to distinguish with SG staining.

Table 3-4 Controls performed for double staining

Antibody	Substrate
ED1	DAB
ED1	SG
PCNA	DAB
PCNA	SG
1.ED1 2.PCNA	1.DAB 2.SG
1.ED1 2.PCNA	1.SG 2.DAB
1.PCNA 2.ED1	1.DAB 2.SG
1.PCNA 2.ED1	1.DAB 2.SG

3.8 Western Blot analysis

For western blot analysis, rats were sacrificed by inhalation with CO_2. Retinas and ONs were dissected and placed in ice cold lysis buffer (Roche, Mannheim, Germany) containing several protease inhibitors, and mechanically homogenized (Kontes, Vineland, USA). The lysates were sonicated for 5 seconds. Cell debris was pelleted at 13,000 rpm for 15 minutes at 4°C. For all western blots a minimum of three animals per time point were used. Supernatant protein concentrations were determined using a bicinchoninic acid (BCA)-based assay (Pierce, Rockford, USA). Proteins were then separated by reducing sodium-dodecyl sulfate -polyacrylamide gel electrophoresis (SDS-PAGE). Sample buffer (2x Tris Glycine SDS sample buffer, (Anamed Elektrophorese, Gross-Bieberau, Germany) was added to all samples prior to boiling at 95 °C for 10 minutes. Samples were loaded on a 10 % Tris Glycine gel (Anamed Elektrophorese), and electrophoresis was performed for 1.5 hours at 120 V in running buffer containing 25 mM Tris Base, 190 mM glycine and 0.1 % SDS in dH_2O. Afterwards proteins were transferred to a nitrocellulose membrane (Whatman, Dassel, Germany) with either the wet blot technique at 100V for one hour at RT or

with the semi-dry blot technique at 200 mA for two hours at RT (Transfer buffer: 25 mM Tris base, 192 mM glycine and 20 % MeOH). To confirm the transfer, the proteins on the membrane were stained with Ponceau (Sigma).

Membranes were blocked for 1h at RT and, depending on the antibody, in either milk (Fluka/Sigma) or BSA (Sigma) in PBS with 0.1 % Tween 20 (PBS-T) (for details see Table 3-5), followed by incubation at 4°C overnight with the primary antibody: After washing with PBS-T for 30 min, Horseradish peroxidase (HRP)-conjugated secondary antibodies (Table 3-6) were applied to the membranes and incubated for one hour at RT. To detect the labeled proteins the ECL-plus reagent (Amersham, Buckinghamshire, UK) was applied for one min. To quantify the western blot results, the intensity of the bands were measured with ImageJ software and divided by the intensity of the bands of the housekeeping proteins Glyceraldehyde-3-Phosphate Dehydrogenase (GAPDH) or actin.

Table 3-5 Primary antibodies used for western blot analysis

Antibody	GAPDH	Actin	Spectrin BDP$_N$	Spectrin SBDP	GFAP
Company	Chemicon, USA	Chemicon, USA	Bahr lab, USA	Chemicon, USA	Sigma
Subtype	mouse IgG1	mouse IgG1	rabbit polyclonal	mouse IgG1	rabbit polyclonal
Concentration	1:250	1:1000	1:300	1:1000	1:1000
Blocking solution	5% milk PBS-T	5% milk PBS-T	5% BSA PBS-T	5% milk PBS-T	5% milk PBS-T

Table 3-6 Secondary antibodies used for western blot analysis

Antibody	Donkey α Rabbit HRP-conjugated	Sheep α Mouse HRP-conjugated
Company	Amersham, USA	Amersham, USA
Subtype	anti-rabbit IgG	anti-mouse IgG
Concentration	1:5000	1:5000
Blocking solution	5% milk or BSA	5% milk or BSA

3.9 Collection of cerebrospinal fluid

Brown Norway rats were anaesthetized with intraperitoneal injection of ketamine 10 % (0.6 ml / kg; Serumwerk, Bernburg, Germany) and xylazine 2 % (0.3 ml / kg; Riemser, Greifswald, Germany) and placed in a stereotactic frame. The skin was incised mediosagittally, and a hole was drilled into the skull at a 31° angle above the cisterna magna (2.7 mm dorsal from the intraaural line). Then a needle was placed on top of the hole and slowly lowered 7.2 mm. The needle then was lowered down in 1 mm steps (up to 4 mm) to collect cerebrospinal fluid from the cisterna magna. Once obtained, the CSF was aliquoted and stored at -80 ℃.

3.10 Serum collection

After animals were sacrificed with CO_2, blood was collected by heart puncture. Blood was coagulated overnight at 4 ℃, centrifuged at 4 ℃ for 15 minutes at 13,000 rpm and the supernatant aliquoted and stored at -80 ℃.

3.11 Enzyme Linked Immunosorbent Assay (ELISA)

To determine the concentration of different cytokines, the neurodegenerative marker tau and anti-MOG antibodies in the serum and CSF the ELISA technique was used.

3.12 ELISA with serum samples

In serum samples the titre of anti-MOG antibody was measured. Samples from healthy, sham immunised animals and MOG-immunised animals at different timepoints after immunisation and onset of clinical symptoms were measured, using the following protocol:

Whole recombinant MOG was diluted in PBS to a concentration of 5 µg / ml and 100 µl of the solution was to coat each well of a 96 wells microtitre plate. The plate was then incubated overnight at 4 °C. The next day the antigen solution was removed and the plate was washed three times with PBS containing 0.05 % Tween (PBS-T). For blocking, 200 µl of 5 % BSA in PBS was pipetted into each well and the plate stayed overnight at 4 °C. The next day the blocking buffer was removed and the plate was washed four times with PBS-T. Serum samples were diluted to 1:100.000, 1:250.000 and 1:500.000 and 100 µl of each dilution was added in duplicate to an antigen-coated well. After two hours incubation at RT, the samples were removed and the plate was washed four times in PBS-T. 100 µl of secondary goat anti-rat antibody (1:5000) in blocking buffer was added to each well and incubated for two hours at RT. The antibody solution was removed and the plate was washed four times with PBS-T. 100 µl per well of TMB (Sigma) was added and the reaction was stopped after 15 min by adding 0.16M H_2SO_4. Absorbance was measured at 450 nm.

3.13 Multi-spot assays (collaboration with Prof.Dr. Markus Otto and his group)

For the measurement of different cytokines and the neurodegenerative marker total tau/phospho-tau in the CSF, a different approach was necessary due to the small sample size. It is possible to measure several cytokines with one sample of 25 µl by using multi-spot 96 well-plates. In these plates the bottom of the wells is not coated with a single antigen but there are small spots (4, 7 or 10) coated with different antibodies. In Figure 3.1 is an example of a 7 spot plate which recognizes different cytokines. The cytokine plate and a plate for total tau/phosphor-tau (Meso Scale Discovery, Gaithersburg, USA) were analyzed on a Sector Imager 6000 (Meso Scale

Discovery). Concentrations in multispot ELISA assays were calculated with Graph Pad Prism (Graph Pad Software Inc., La Jolla, USA).
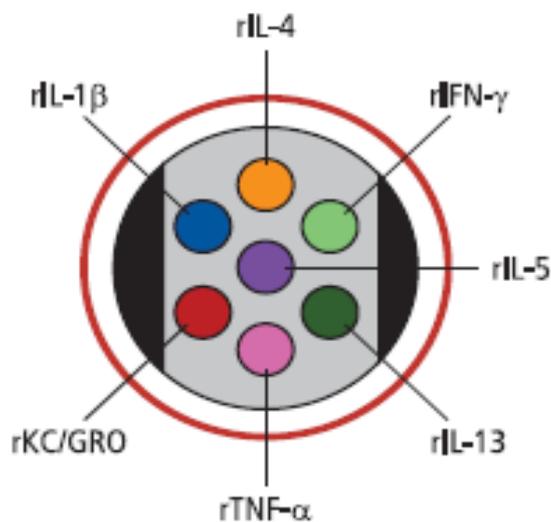
Figure 3.1 Example of a 7 spot plate available for rat CSF

The picture shows the bottom of one well of a 96 well multispot plate. Each well is coated with 7 spots with antibodies against different cytokines. With this technique one sample of 25 µl is sufficient to detect the concentration of 7 different cytokines.

For the multi-spot assays the following protocols were used:

7 spot cytokine assay:

In each well of the cytokine plate 25 µl of rat serum cytokine assay diluent (RSC) were pipetted and the plate was incubated for 30 minutes at RT with vigorous shaking. By diluting the calibrator stock solution (MSD) in RSC a seven point calibration curve (0, 9.8, 39, 156, 625, 2500, 10.000 and 40.000 pg / ml) was prepared. Then 25 µl of CSF sample or calibrator were pipetted into the wells and the plate was incubated for two hours at RT on a tumbling table. The plate wash then washed 3 times with PBS-T and 25 µl of antibody detection solution (diluted to 1 µg / ml in rat serum cytokine antibody diluent) were added to each well before the plate was incubated for one hour at RT on a tumbling table. The plate was washed 3 times in PBS-T and 150 µl of 2x read buffer (diluted in dH_2O) were added to each well. Immediately after adding the read buffer the plate was analysed with the Sector Imager 6000.

Multi-spot phosphor-tau/total tau assay:

In each well of the cytokine plate, 25 µl of blocking solution A (3 % Blocker A in Tris Wash Buffer) were pipetted and the plate was incubated for 1h at RT with vigorous shaking and then washed with Tris Wash Buffer. By diluting the calibrator stock solution (MSD) in 10 % Blocker A in Tris Wash Buffer an eleven point calibration curve (0, 10, 30, 100, 300, 1000, 3000, 10.000, 30.000, 100.000, 300.000 and 1.000.000 pg / ml) was prepared. Then 25 µl of CSF sample or calibrator were pipetted into the wells and the plate was incubated for one hour at RT on a tumbling table. The plate wash then washed 4 times with Tris Wash Buffer and 25 µl of antibody detection solution (diluted to 10 nM in antibody dilution buffer) were added to each well and the plate was incubated for one hour at RT on a tumbling table. The plate was washed 4 times with Tris Wash Buffer and 150 µl of 1x read buffer (diluted in dH_2O.) were added to each well. To avoid bubbles in the wells the reverse pipetting technique was used in this step. Immediately after adding the read buffer, the plate was analysed with the Sector Imager 6000.

3.14 Manganese-enhanced Magnetic Resonance Imaging (MEMRI)

Animals underwent MRI prior to immunisation, on d3 p.i., d5 p.i., d7 p.i., d10 p.i. and d1 of EAE. Sham-immunised animals were used as controls. For each timepoint/parameter a minimum of three animals were investigated.

Anaesthesia was induced with 4% isoflurane in oxygen at a rate of 2 l / min. The animals were placed in the MRI and anesthesia was maintained with 2 % isoflurane in 1l / min oxygen. All measurements were performed using a 9.4 Tesla Bruker Biospec Avance III machine and either a transmit/receive mouse body quadratur coil (for optic nerves) or a saddle-shaped surface coil with a 2x2 array setup (for retinas). Signal intensities were measured with Paravision (Bruker) and false colour images were made with image J.

Different protocols were used for optic nerves and retinas:

Optic nerve protocols:

To verify the correct positioning of the animal in the machine a tri-pilot scan was performed. For positioning of the scan area a T2-weighted sagittal Rapide Acquisition with Relaxation Enhancement (RARE) scan (TR/TE = 5000 ms / 57 ms) was performed and positioning was checked with a T2-weighted coronal RARE scan (TR/TE = 2300 ms / 39.6 ms). This scan was also used to monitor changes in the diameter of the optic nerve during the disease course. For measuring of manganese enhancement a T1-weighted 3D FLASH scan was performed with a TR/TE of 25 ms / 4.3 ms.

After acquisition of pre-contrast T1-weighted 3D FLASH images, animals were injected with 20 mg / kg $MnCl_2$ dissolved in 1 ml saline at a rate of 100 µl / min. T1-weighted 3D Flash scans were then performed 10, minutes after $MnCl_2$ injection and in some animals also 60 and 120 minutes and 24 hours after $MnCl_2$ injection.

Retina protocols:

To verify the correct positioning of the animal in the machine a tri-pilot scan was performed. For positioning of the scan area a T2-weighted sagittal RARE scan (TR/TE = 5000 ms / 57 ms) was performed and positioning was checked with a T2-weighted coronal RARE scan (TR/TE = 2300 ms / 39.6 ms). For measuring of manganese enhancement a T1-weighted MSME scan (TR/TE = 320 ms / 9.1 ms) was performed. After acquisition of pre-contrast T1-weighted MSME images, animals were injected with 10 mg / kg $MnCl_2$ dissolved in 1 ml saline at a rate of 100 µl / min. T1-weighted MSME scans were performed 10 minutes, one hour and two hours after injection. For blocking experiments healthy animals and animals at d5 p.i were injected with the NMDA receptor blocker MK 801 40 minutes prior to $MnCl_2$ injection. The blocker was injected i.p. at a dosage of 2 mg / kg in 1 ml saline. The control group received an i.p. saline injection of the same volume.

3.15 Treatment study with calpeptin

Animals were Fluorogold-labelled one week prior to immunisation as described previously in 3.3. From the day of immunisation onwards, animals received i.p. injections twice daily with 250 µg / kg calpeptin (Santa Cruz, USA) in saline until they

were sacrificed on d5 p.i., d10 p.i., or d1 of EAE. Calpeptin was solved in DMSO at a concentration of 10 mg / ml. The control group received an equivalent volume of saline with DMSO twice daily. Animals were sacrificed on either d10 p.i. or d1 of EAE to count Fluorogold-labelled RGCs. Western blot was performed on animals sacrificed on day 5 p.i. to verify reduced calpain activity after calpeptin treatment by using an antibody against BDP_N, as described in 3.8. Histopathological staining with LFB and Bielschowsky silver impregnation and immunohistochemistry with antibodies against CD3, ED1 and β-APP (as described in 3.6.1, 3.6.2, 3.7.1 and 3.7.3) were performed on optic nerve sections at d1 of EAE to assess possible changes in severity of optic neuritis after calpeptin treatment.

3.16 Statistical analysis

Statistical significance of the data concerning changes in axonal and RGC densities, changes in demyelination, number of infiltrating cells, relative optical density in western blot bands and signal enhancement in MRI was assessed with the two-tailed t-test and two levels of significance were defined: $*p \leq 0.05$ to be significant, $**p \leq 0.01$ to be very significant. Error bars represent standard error of the mean (SEM). For all statistical analyses excel, version 2003, (Microsoft Office, Microsoft Corporation, USA) was used.

4 Results

4.1 Disease course

EAE is an animal model of multiple sclerosis that shares many aspects with the human disease, including inflammation and axonal loss. Brown Norway rats are known to be susceptible to antibody-mediated diseases and unlike in other rat strains immunisation with MOG causes severe demyelination of the optic nerve and a high incidence of optic neuritis (Meyer *et al.*; 2001)., also a common early symptom of MS, that leads to axonal degeneration and apoptotic death of RGCs (Diem *et al.*; 2005a), which makes them a suitable model to investigate neurodegenerative changes in a setting that closely resembles MS.

After Brown Norway rats were immunised they were scored daily for clinical symptoms according to a clinical score (2.2 Induction and evaluation of EAE). The average day of onset was d17.25 ± 0.82 (n=17) following immunisation, with onset occurring between d10 and d23 p.i. 62.5% of the immunised animals developed clinical symptoms of EAE.
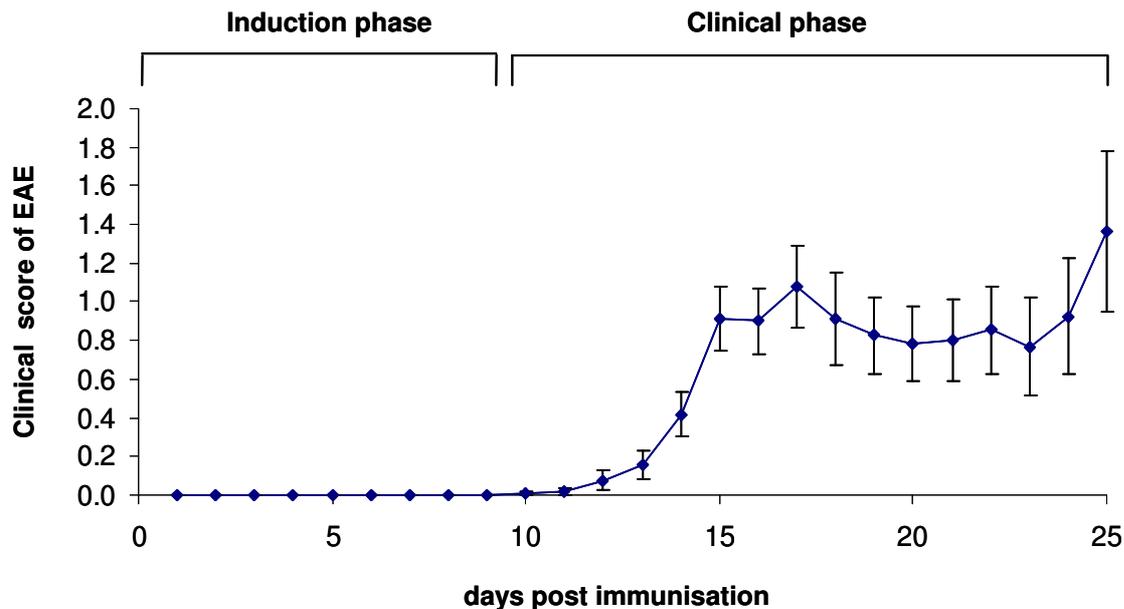
Figure 4.1 Time course of EAE

After immunisation with MOG, animals where scored daily for clinical symptoms. The earliest onset was on d10 p.i., average onset was on d17 p.i. In the induction phase no clinical symptoms (which represent spinal cord involvement) could be seen.

4.2   Loss of RGCs started during the induction phase

In MS optic neuritis is often the first symptom and also many patients have at least one episode of optic neuritis during the course of their illness (The Optic Neuritis Study Group, 2008). The loss of RGCs can occur secondary to optic neuritis, expressing hallmarks of apoptotic death (Meyer *et al.*; 2001). To assess how early in the course of EAE neurodegeneration within the retina could be seen RGCs were labelled with fluorogold, a fluorescent dye. The majority of axons from RGCs project into the superior colliculi and when the dye is injected into the superior colliculi it is transported retrogradely into the cell body of RGCs (Simon and Thanos, 1998). The labelled RGCs were then counted in healthy animals and sham-immunised animals (Figure 4.2, A) and in MOG immunised animals at d5 p.i and d7 p.i. (Figure 4.2, B) and at d1 of EAE (Figure 4.2, C) and d8 of EAE (Figure 4.2, D). The numbers of RGCs per mm^2 in sham-immunised animals were similar to those in healthy (1771.06 ± 85.07 cells / mm^2 in sham-immunised animals and 1756.47 ± 121.17 cells / mm^2 in healthy animals), which proves that the loss of RGCs is a MOG-specific event. The number of RGCs decreased significantly on d5 p.i ($*p \leq 0.05$) to 1474.83 ± 66.61 cells / mm^2 and to 1282.99 ± 57.09 cells / mm^2 on d7 p.i. Although a decrease was

seen between d5 p.i. and d7 p.i., it was not significant (Figure 4.2, E). This showed that degeneration of RGCs started before the onset of clinical symptoms.
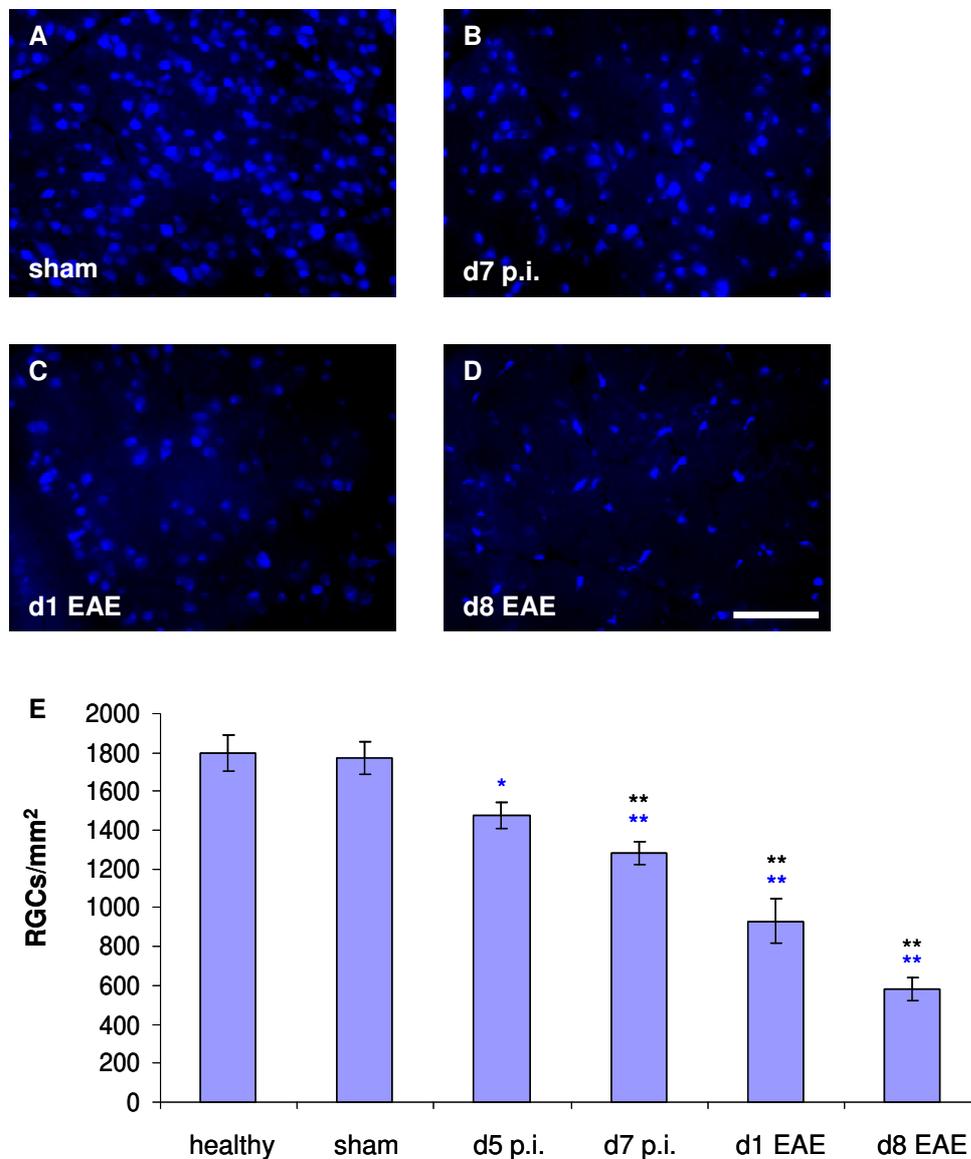
Figure 4.2 Number of Fluorogold-labelled RGCs was reduced from d5 p.i. onwards (data and pictures provided by Dr. Richard Fairless)
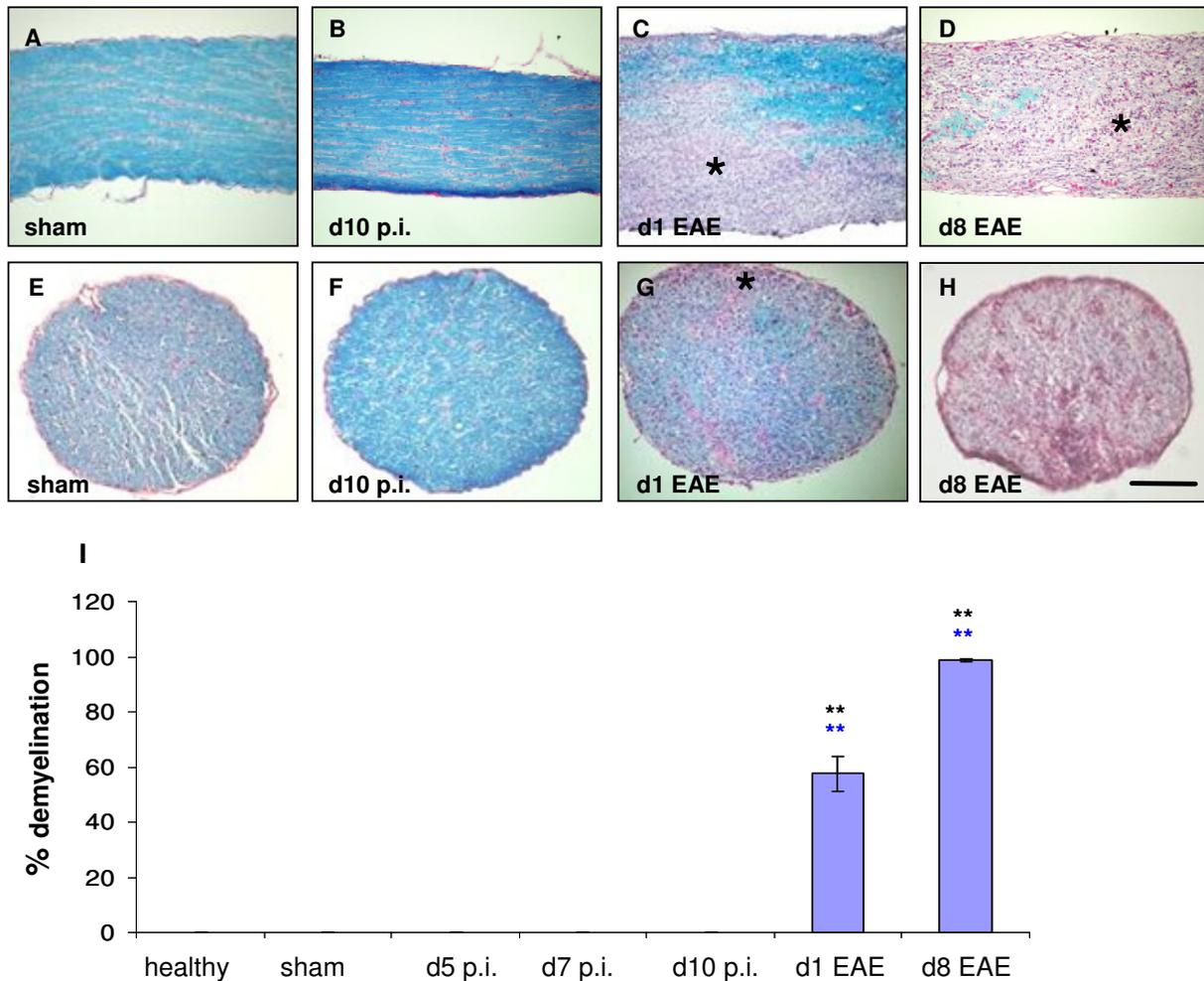
Representative images were taken from sham-immunised animals (A), d7 p.i. (B), d1 of EAE (C) and d8 of EAE (D).Numbers of RGCs in sham-immunised animals were similar to those of healthy animals. Cell counts showed a significant decrease in the numbers of RGCs from d5 p.i. onwards when compared to retinas of sham-immunised animals (E). (* = $p \leq 0.05$, ** = $p \leq 0.01$. ** = significant to healthy, *, ** =significant to sham, n = 4 for all timepoints). Scale bar = 50 µm.

4.3 Onset of optic neuritis did not correlate with onset of RGC degeneration

Since the clinical score is only a correlate of spinal cord lesion load, the time course of optic neuritis was examined to assess how it correlates with the early degeneration of RGCs seen in Figure 4.2. Demyelination, infiltration with inflammatory cells and axonal pathology in the optic nerve were examined.

4.3.1 No demyelination could be observed in the induction phase

To assess how early in the disease course demyelination starts, longitudinal- and cross-sections of ONs were stained with Luxol Fast Blue (LFB). LFB binds to the hydrophobic myelin protein and produces a blue colour in myelinated areas, whereas Schiff´s reagent stains cytoplasm and connective tissue pink. In healthy and sham-immunised animals and on d5 p.i., d7 p.i. and d10 p.i., the ON is fully myelinated (Figure 4.3 A, B, E and F). By d1 of EAE, there was a significant increase in demyelinated area (57.57 ± 6.35 %, Figure 4.3 C, G, I) and by d8 of EAE the ONs were nearly completely demyelinated (98.84 ± 0.41 %, Figure 4.3, D, H, I). In addition the whole area of the optic nerve was measured to look for optic nerve swelling. There was significant swelling on d5, d7 and d10 p.i. when compared to healthy but swelling was also observed in sham-immunised animals and is therefore likely to be a byproduct of the immunisation and since no degeneration of RGCs could be observed in sham-immunised animals not involved in degeneration. On d1 and d8 of EAE profound optic nerve swelling could be observed (Figure 4.4) when compared to both healthy and sham-immunised animals.

Figure 4.3 Myelin specific staining (LFB) during the disease course shows that demyelination starts at d1 of EAE

Demyelination was examined with LFB staining of ON cross and longitudinal sections. Representative images were taken from sham-immunised animals (A, E), d10 p.i. (B, F), d1 of EAE (C, G) and d8 of EAE (D, H). Demyelination started on d1 of EAE at d8 of EAE the nerves were nearly completely demyelinated. Asterisks indicate demyelinated areas. (I) shows the percentage of demyelination in ON cross-sections. (** = p ≤ 0. 01. ** = significant to healthy, ** = significant to sham, n = 3 for all timepoints). Scale bar = 100 µm
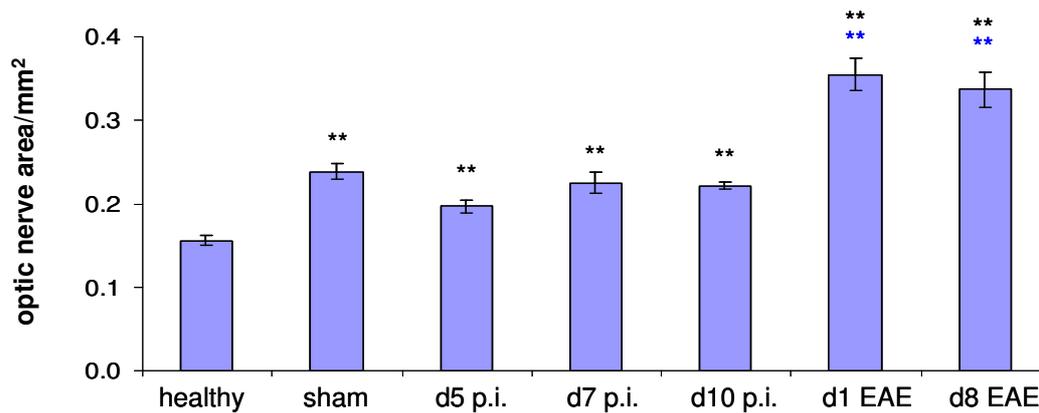
Figure 4.4 Area of the optic nerve measured from cross-sections

The area of the optic nerve was measured from cross-sections. It was significantly increased in sham-immunised animals and during the induction phase and also on d1 and 8 of EAE when compared to both healthy and sham-immunised animals. (** = p ≤ 0. 01. ** = significant to healthy, ** = significant to sham, n = 3 for all timepoints).

4.3.2 No axonal loss could be observed during the induction phase

To assess if the numbers of axons within the ON during the course of optic neuritis are reduced, cross-sections were stained with Bielschowsky´s silver impregnation. On d5, d7 and d10 p.i, the numbers of axons were similar to the ones in healthy and sham-immunised animals (Figure 4.5, A, B). The number of surviving axons was reduced on d1 of EAE and to a greater extent on d8 of EAE (Figure 4.5, C and D). The percentage of surviving axons decreased significantly (**p ≤ 0, 01) from healthy and sham-immunised animals to d1 of EAE and to d8 of EAE (Figure 4.5, E). To examine if subtle axonal injury occurs in the induction phase the concentration of tau in the CSF was measured. Elevated tau concentration in the CSF can for example be observed in patients with TBI and is considered a potential marker for clinical outcome (Zemlan *et al.*, 1999; Zemlan *et al.*, 2001; Ost *et al.*, 2006). Most studies show elevated tau concentration in MS patients even though this finding is not unanimous (reviewed by Tumani *et al.*, 2008). For this a multi-spot ELISA was used. No increase in tau concentration could be observed during the induction phase but tau concentration was significantly increased on d1 and d8 of EAE when compared to healthy and sham-immunised animals (Figure 4.6), correlating with the data obtained with Bielschowsky´s silver impregnation.
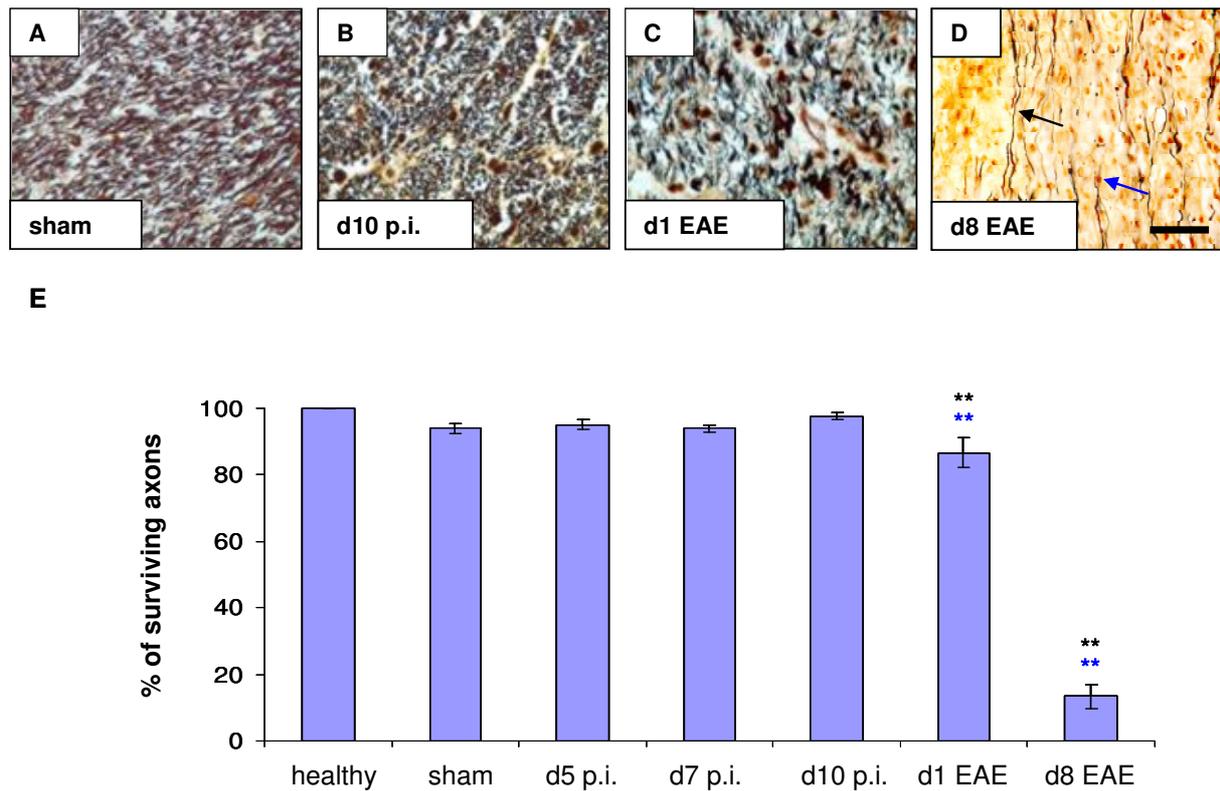
Figure 4.5 Bielschowsky´s silver impregnation showed reduced number of axons on d1 and d8 of EAE

Axonal loss was examined using Bielschowsky´s silver impregnation on ON cross-sections. Representative images were taken from sham-immunised animals (A), d10 p.i. (B), d1 of EAE (C) and d8 of EAE (D). On d1 of EAE the number of axons was significantly reduced and on d8 of EAE only a few axons remained. Arrows indicate axons (black) and macrophages (blue). (E) Quantification of the number of surviving axons. (** = p ≤ 0. 01. ** =significant to healthy, ** =significant to sham, n = 3 for all timepoints). Scale bar = 25 μm
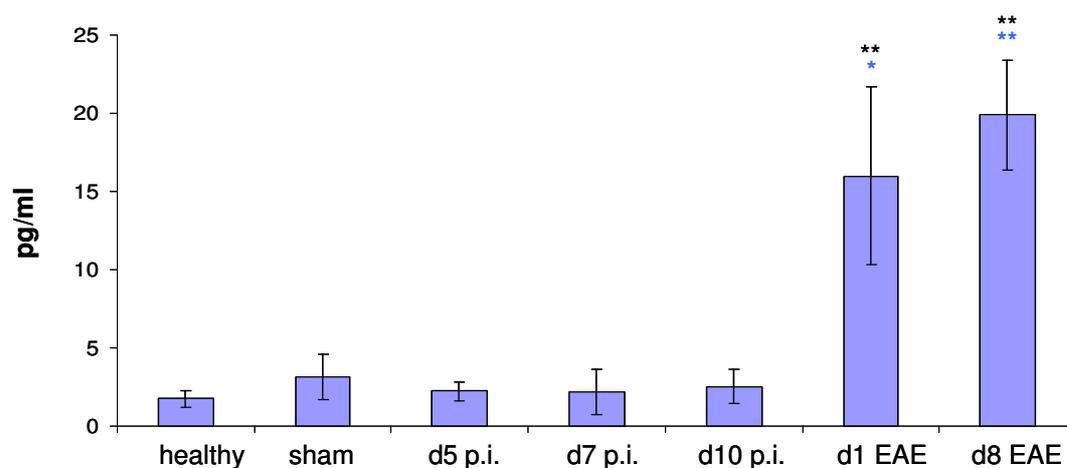

Figure 4.6 Concentration of tau in the CSF was elevated on d1 and d8 of EAE

Tau concentration was significantly elevated on d1 and d8 of EAE when compared to healthy and sham controls. (* = p ≤ 0.05, ** = p ≤ 0.01. ** = significant to healthy, *, ** = significant to to sham, n = 5 for d7 p.i, n = 6 for sham, d10 p.i., d1 and d8 of EAE, n = 7 for d5 p.i. and n = 9 for healthy)

4.3.3 No infiltration with CD3 positive cells could be observed in the induction phase

T-cells are considered to play a fundamental role in immunopathogenesis in EAE. Autoreactive T-cells (against myelin proteins such as MBP) cause EAE symptoms in healthy recipient animals, emphasizing their importance in disease induction (Ben-Nun *et al.*, 1981). Sham-immunised animals do not develop clinical symptoms, confirming that MOG-specifity of the T-cell-mediated disease induction. To asses how early during the disease course infiltration with T-cells in the optic nerve starts, an antibody against CD3 was used. Clusters of differentiation (CD) are cell surface molecules which can be used to distinguish different types of immune cells since they have unique expression patterns. In addition to CD45 which is expressed by all types of leucocytes, T-cells express the CD3 antigen. Only occasionally CD3-positive cells could be found in healthy and sham-immunised animals and before the onset of EAE (Figure 4.7 A and B). On d1 and d8 of EAE the number of CD3 positive cells was elevated (Figure 4.7 C and D). The number increased significantly (*$p \leq 0.05$) from 1.11 ± 0.54 cells / mm^2 in healthy and 1.11 ± 0.41 cells / mm^2 in sham-immunised animals to 170.13 ± 66.45 cells / mm^2 on d1 of EAE and 121.71 ± 27.89 cells / mm^2 on d8 of EAE (Fig 3.7 E).
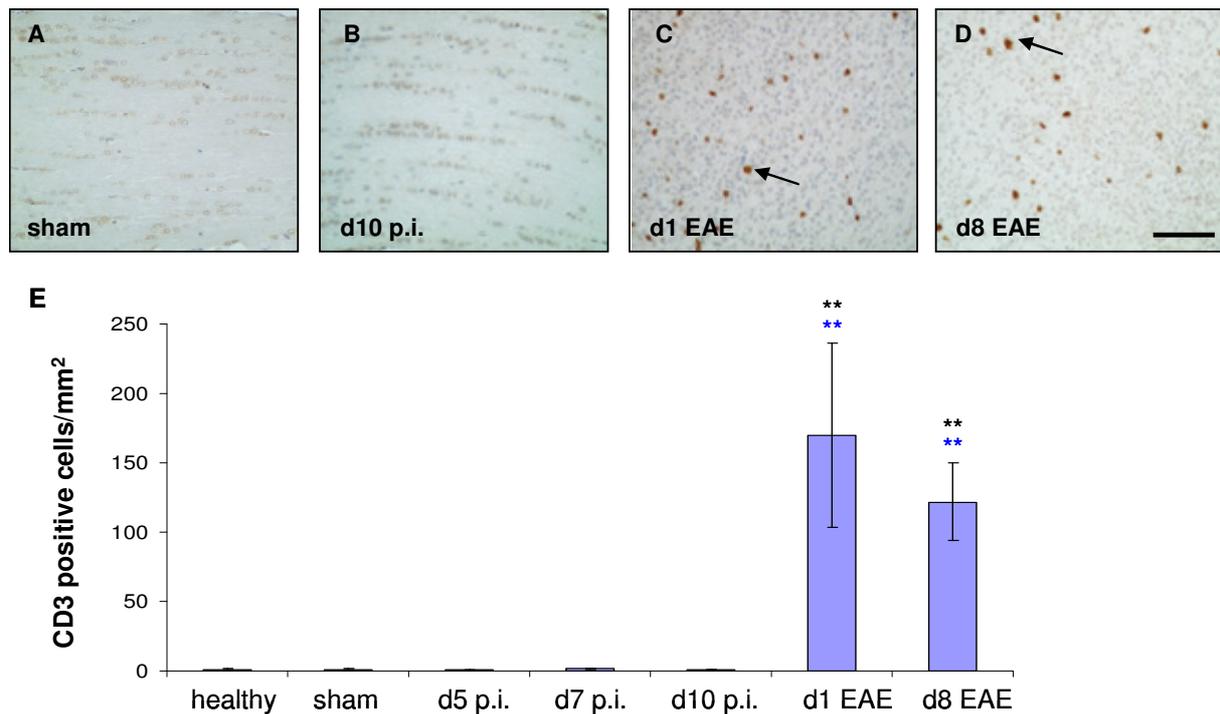
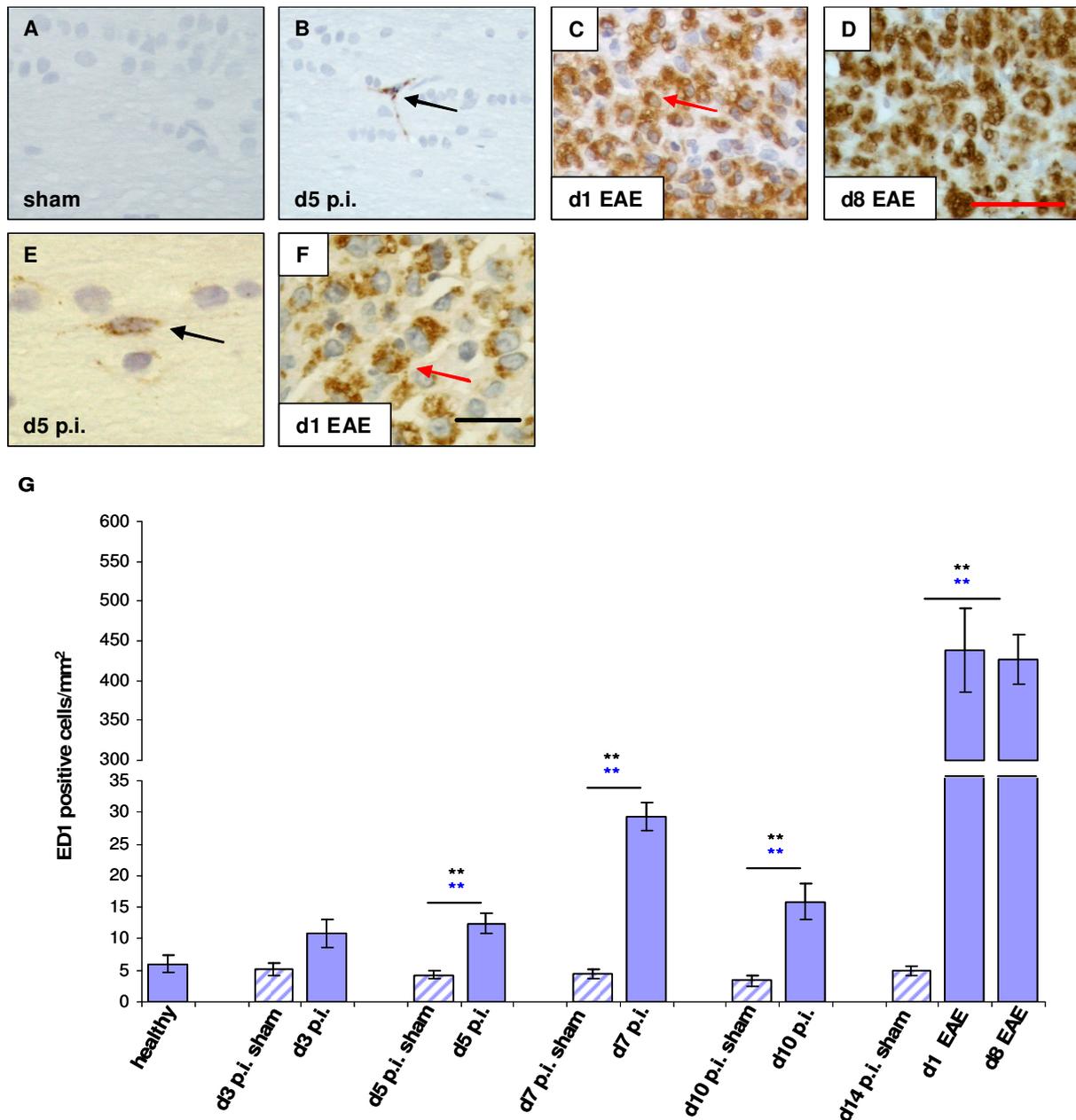**Figure 4.7 Number of CD3 positive cells was increased on d1 and d8 of EAE**

The number of T-cells was examined using an antibody against CD3 on ON cross-sections. Representative images were taken from sham-immunised animals (A), d10 p.i. (B), d1 of EAE (C) and d8 of EAE (D). In the induction phase only occasional CD3 positive cells could be seen (A, B). Their number increased significantly on d1 and d8 of EAE (C, D). Arrows indicate CD3 positive cells. (E) Quantification of CD3 positive cells / mm^2 (** = $p \leq 0.01$. ** = significant to healthy, ** = significant to sham, n = 3 for healthy, sham, d10 p.i. and d1 of EAE, n = 4 for d5 p.i., d7 p.i. and d8 of EAE). Scale bar = 50 µm

The fact that RGC degeneration in our model started before the onset of optic neuritis is of particular interest considering recent publications suggesting the possibility of primary retinal pathology where patients not affected by optic neuritis show signs of retinal pathology such as macular thinning and loss of RGCs (Syc *et al.*, 2011; Saidha *et al.*, 2011).

4.4 Increase in number of ED1 positive cells in the optic nerve started during the induction phase

Besides T-cells, microglia/macrophages are a main part of the inflammatory response and their numbers correlate with axonal loss in acute lesions (Ferguson *et*

*al.,*1997; Trapp *et al.*, 1998). They can secrete pro-inflammatory cytokines and toxic mediators thus contributing to axonal loss during optic neuritis. The ED1 antigen can be found on activated microglia and macrophages. On d5 p.i., d7 p.i. and d10 p.i, ED1 positive cells displayed a microglia-like phenotype (Figure 4.8, B), with long thin processes (del Rio Hortega, 1932) and only weak staining around the cell-body**.** After the onset of EAE a robust increase in cells numbers could be seen and the ED1 positive displayed strong staining of the whole cell membrane and a foamy shape similar to that described for macrophages (del Rio Hortega, 1932) (Figure 4.8; C and D). These results were confirmed with an antibody against the proinflammatory cytokine EMAP II, which is expressed by activated microglia and macrophages. Staining with this antibody showed similar results, with increased numbers of microglia-like shaped cells (Figure 4.8, E) during the induction phase and macrophage-like cells after the onset of EAE (Figure 4.8, F).The number of ED1 positive cells amounted 6.00 ± 1.35 cells / mm^2 in healthy animals and increased to 12.44 ± 1.66 cells/mm^2 on d5 p.i, 29.33 ± 2.31 cells / mm^2 on d7 p.i, 15.83 ± 2.78 cells / mm^2 on d10 p.i, 437.95 ± 52.66 cells / mm^2 on d1 of EAE and 427.43 ± 31.03 cells / mm^2 on d8 of EAE. There was a significant (**$p \leq 0.01$) increase at these timepoints when compared to healthy animals and corresponding sham-controls.

Figure 4.8 Number of ED1 positive cells was increased from d5 p.i. onwards

The number of microglia/macrophages was examined using an antibody against ED1 on ON longitudinal sections. Representative images were taken from sham-immunised animals (A), d5 p.i. (B), d1 of EAE (C) and d8 of EAE (D). The results were confirmed with immunohistochemistry with EMAP II, another antibody against activated microglia/macrophages (E, F). In the induction phase the ED1 and EMAP II positive cells showed a microglia-like appearance with long, thin processes (B, E). After the onset of clinical symptoms they looked like macrophages, with stronger expression of ED1/EMAP II and a foamy appearance (C, D, and F). The number of ED1 positive cells was increased significantly from day 5 p.i. onwards when compared to healthy animals and corresponding sham controls. Arrows indicate microglia-like cells (black) and macrophage-like cells (red). (G) Quantification of ED1 positive cells / mm^2 (** = p ≤ 0. 01. ** = significant to healthy, ** = significant to corresponding sham control, n = 3 for shams, n = 4 for d7 p.i., d10 p.i., d1 and d8 of of EAE, n = 5 for healthy and d5 p.i. and n = 6 for d3 p.i.). Scale bar = 50 µm.

4.5 Proliferation of microglia and macrophage-like ED1 positive cells started during the induction phase

In order to assess if the microglia and macrophage-like cells which can be seen during the course of EAE are proliferating, an antibody against the Proliferating Cell Nuclear Antigen (PCNA), which can be found in the nuclei of cells during the DNA synthesis phase of the cell cycle, was used in combination with ED1. For immunohistochemistry it was decided to use SG as a substrate for PCNA and DAB as a substrate for ED1 because PCNA positive and negative cells are easier to distinguish when stained with SG.

Longitudinal sections of ONs were then double stained with antibodies against PCNA and ED1. ED1$^+$ cells and ED1$^+$ + PCNA$^+$ cells were counted. The total number of ED1$^+$ cells was increased from d5 p.i. onwards, as was already shown in Figure 4.8, G. The percentage of ED1 and PCNA$^+$ positive cells was significantly increased from healthy (38.77 ± 7.19 %) to d5 p.i (62.95 ± 6.14 %), d7 p.i (58.77 ± 6.71 %) and d1 of EAE (60.45 ± 2.80 %). When compared to sham-immunised animals the number of proliferating cells was increased on d5 p.i. and d1 of EAE, demonstrating that ED1 positive cells proliferate in the induction and clinical phases of EAE.
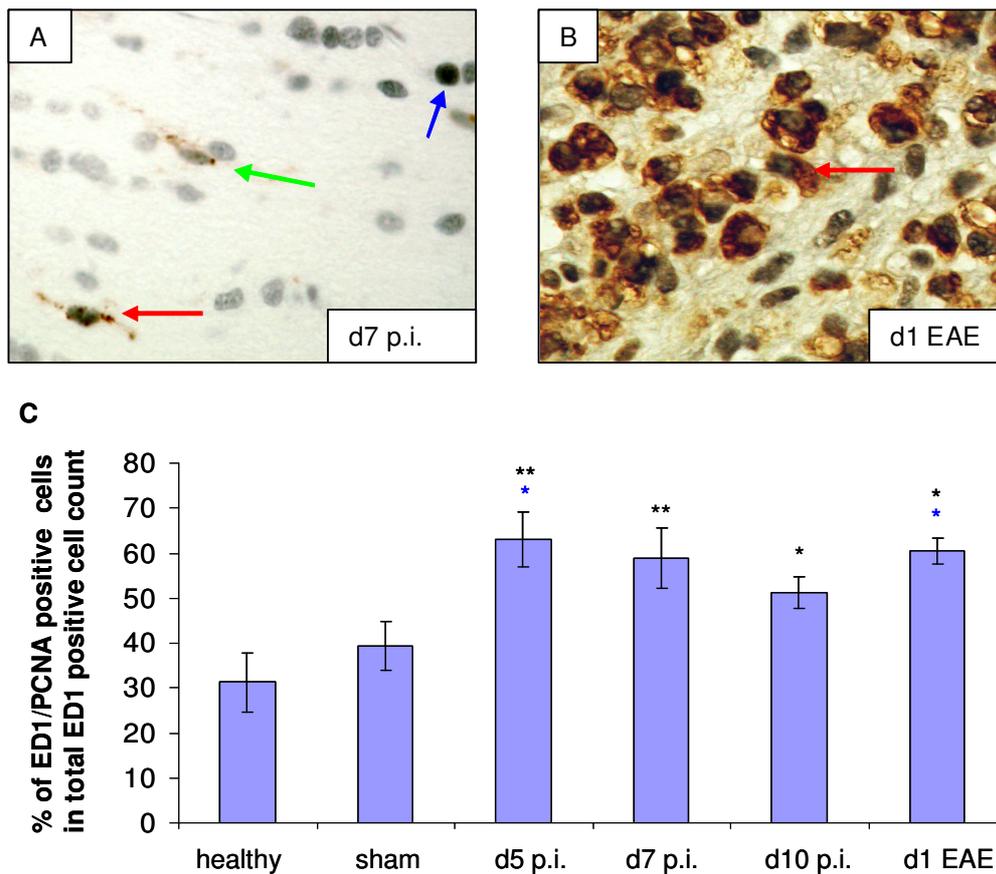
Figure 4.9 Proliferation of ED1 positive cells started during the induction phase

Representative images were taken at d7 p.i (A) and d1 of EAE (B). Red arrows indicate ED1 and PCNA positive cells, blue arrows indicate PCNA positive cells and green arrows indicate ED1 positive cells. (C) Percentage of ED1 and PCNA positive cells / mm^2 (* = p ≤ 0.05, ** = p ≤ 0.01, *, ** = significant to healthy, *,** = significant to to sham, n = 3 for sham, d5 p.i., d10 p.i and d1 of EAE, n = 4 for d7 p.i. and n = 5 for healthy). Scale bar = 50 μm

4.6 Animals can develop optic neuritis independently from clinical symptoms

The following part addresses the possibily that the development of optic neuritis is a distinct process to the formation of spinal cord lesions and thus clinical symptoms. 62.5% of immunised animals developed EAE (Figure 4.11), but for the remaining 37.5% which did not develop clinical signs of EAE, it was decided to investigate their optic nerves for pathological signs of optic neuritis. Eight animals which did not develop clinical EAE symptoms by d30 p.i. were sacrificed. The ONs of four animals were made into longitudinal sections, the ONs from the other four into cross sections.

Cross-sections were stained with LFB and Bielschowsky and antibodies against ED1 and CD3 were used on longitudinal sections. The ONs could be divided into two groups: One group showed no demyelination and no reduction in numbers of axons when compared to sham-immunised animals (Figure 4.10, A, B, I and J, blue columns). The other group showed substantial demyelination and reduced number of axons. The demyelination and loss of axons in this group was significantly increased (**$p \leq 0.01$) when compared to sham-immunised animals and demyelination and axonal loss was also significantly higher than on d1 of EAE (Figure 4.10, E, F, I and J, red columns).

In addition, immunohistochemistry against ED1 and CD3 was performed on the longitudinal sections. The group with no demyelination shows a significant increase in infiltrating CD3-positive cells (Figure 4.10, C and K) but numbers are smaller than at d1 of EAE. There is also a significant increase in ED1 positive cells which show a microglia-like shape (Figure 4.10 D and L, blue column).

The group with demyelination showed robust infiltration of CD3 positive cells (Figure 4.10, G and K, red column) and macrophage-like ED1 positive cells (Figure 4.10, H). The number of ED1 positive cells was significantly (**$p \leq 0.01$) elevated compared to sham-immunised animals and d10 p.i. (Figure 4.10, L, red column).

This shows that optic neuritis can be developed independently from clinical symptoms and that demyelination is highly correlated with the presence of infiltrating cells.
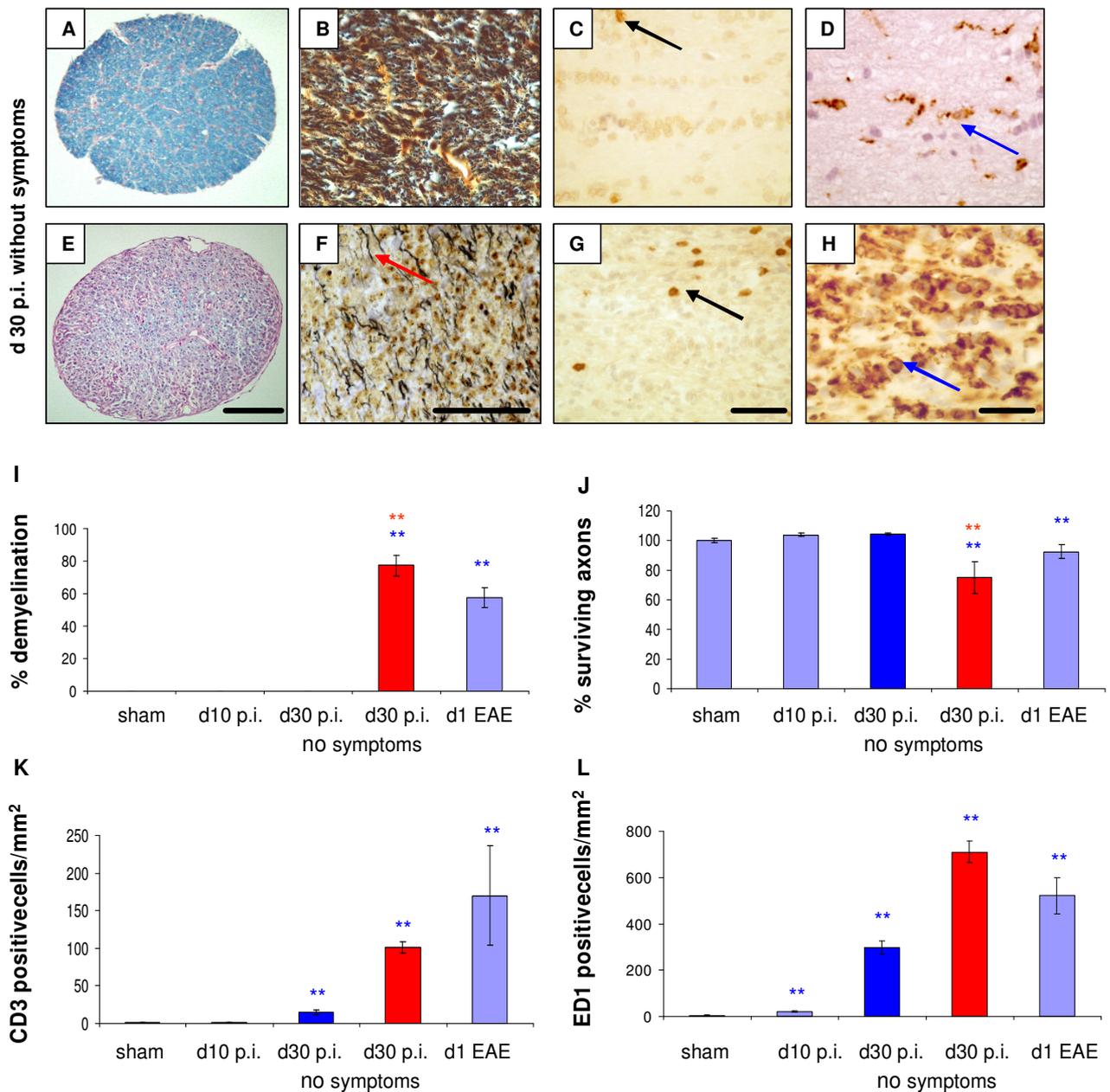
Figure 4.10 Some animals without clinical symptoms of EAE still developed optic neuritis

Representative images of two optic nerves from animals with no clinical symptoms (A-D and E-H)
Representative images from an ON with no signs of optic neuritis (A-D). Nerve showed no demyelination (A), no change in axonal density (B), some CD3 positive cells (C) and ED1 positive cells with a microglia-like shape (D). Representative images from an optic nerve with optic neuritis (E-H). The ON was demyelinated (E), the number of axons was reduced (F), many CD3 positive cells could be seen (G) and ED1 positive cells showed a macrophage-like shape (H). Arrows indicate axons (red), CD3 positive cells (black) and ED1 positive cells (blue).The extent of demyelination and axonal loss was significantly higher than on d1 of EAE (I, J). The number of CD3 positive and ED1 positive cells was elevated in the group without demyelination and was strongly elevated in nerves showing demyelination and axonal loss, again comparable to d1 of EAE (K, L) (** = $p \leq 0.01$, ** = significant to sham, ** = significant to d1 of EAE, n = 3 for sham, d10 p.i and d1 of EAE, n = 4 for animals without symptoms). Scale bar = 100 µm A, C, D, F and 50 µm B, E.
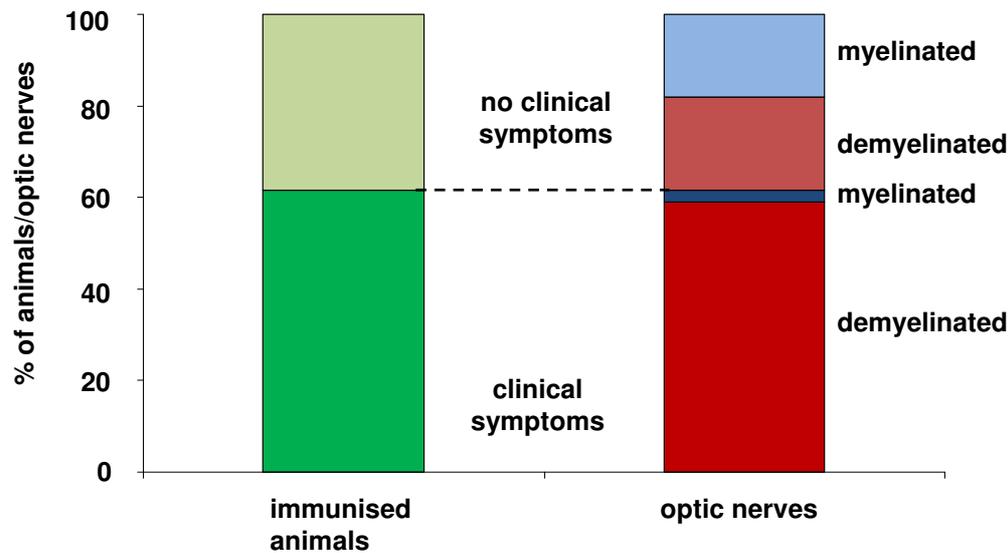
**Figure 4.11 The incidence of optic neuritis was much higher than the incidence of clinical symptoms**

62.5% of the immunised animals developed EAE and in this group only one ON showed no signs of optic neuritis. In the group without symptoms 53% of the examined ONs showed demyelination. The overall incidence of optic neuritis is 78.4% and thus higher than the incidence of EAE.

In summary 53% of the ONs of animals without clinical symptoms show extensive demyelination (Figure Figure 4.11) and also axonal loss and 50% of the longitudinal ON sections show elevated numbers of CD3 positive and ED1 positive cells with a macrophage-like morphology, all hallmarks of optic neuritis. The incidence of optic neuritis is therefore higher (78.4%) than the incidence of clinical symptoms (62.5%). It is possible that the optic nerve is more vulnerable due to smaller diameter and it is known that MOG expression is higher in the optic nerve than the spinal cord (Betelli *et al.*, 2003).

4.7 Anti-MOG antibodies were increased during the induction phase

The role of antibodies against myelin proteins in pathogenesis in MS has been studied extensively but studies show conflicting results as to their usefulness in predicting relapses of MS and their overall involvement in pathogenesis. Immunisation with MOG, a protein located on the surface of the myelin sheath, induces EAE in a variety of species usually accompanied by only a low grade of

demyelination (Gold *et al.*, 2006). Brown Norway rats are particularly susceptible to antibody-mediated diseases and immunisation with MOG causes a severe demyelinating autoantibody response. In order to determine if anti-MOG antibodies could be involved in the previously observed early degeneration of RGCs (Figure 4.2), serum samples from different timepoints after immunisation and onset of clinical symptoms were compared to serum from healthy and sham-immunised animals, using the ELISA technique. The antibody titre was significantly elevated from d10 p.i onwards (Figure 4.12), preceding the onset of clinical symptoms but started several days after onset of RGC degeneration, suggesting that anti-MOG antibodies are not involved in early degeneration of RGCs.
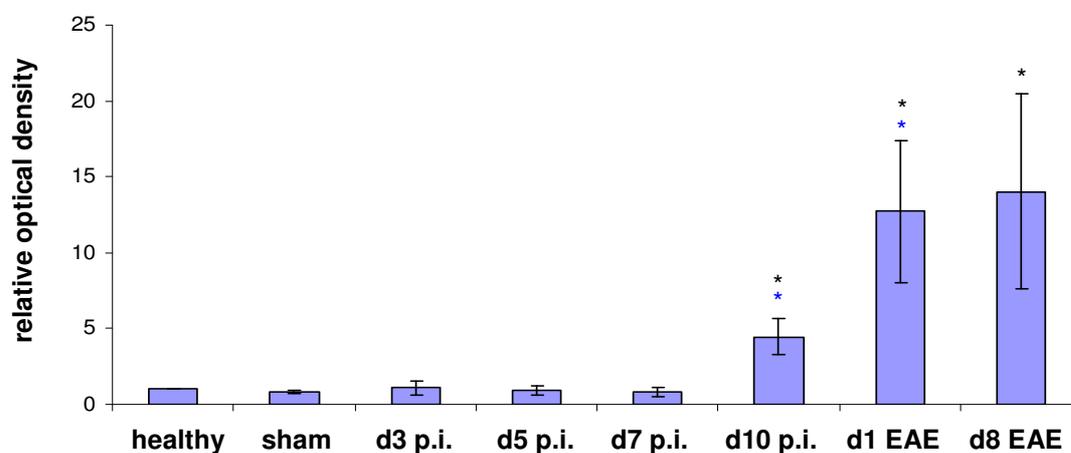

Figure 4.12 The concentration of MOG antibody was elevated from d10 p.i. onwards

The MOG antibody concentration was significantly elevated from d10 p.i onwards when compared to healthy and sham controls. (* = p ≤ 0. 05. * = significant to healthy, * = significant to sham, n = 4 for all timepoints).

4.8   Increased number of ED1 positive cells in the retina correlated with onset of RGC degeneration

An increase in the number of ED1 positive cells was observed in the optic nerve during the induction phase and microglia/macrophages could be involved in the early loss of RGCs, therefore their presence in the retina was examined. The number of ED1 positive cells was increased significantly from d5 p.i onwards during the induction phase (Figure 4.13, C). In healthy animals the number of cells was 2.3 ± 0.11 cells / mm. On d5 p.i., d7 p.i. and d10 p.i the number of cells was

4.6 ± 0.23 cells / mm, 3.38 ± 0.21 cells / mm and 3.43 ± 0.26 cells / mm, which was significantly (**p ≤ 0.01) higher than in healthy animals and corresponding sham controls (**p ≤ 0.01 and *p ≤ 0.05). There was no significant increase in sham-controlls when compared to healthy animals.After the onset of EAE the number of ED1 positive cells was reduced to 2.27 ± 0.22 cells / mm on d1 of EAE which was only significantly higher compared to the corresponding sham control. The ED1 positive cells showed a microglia-like shape during the disease course (Figure 4.13 A and B).
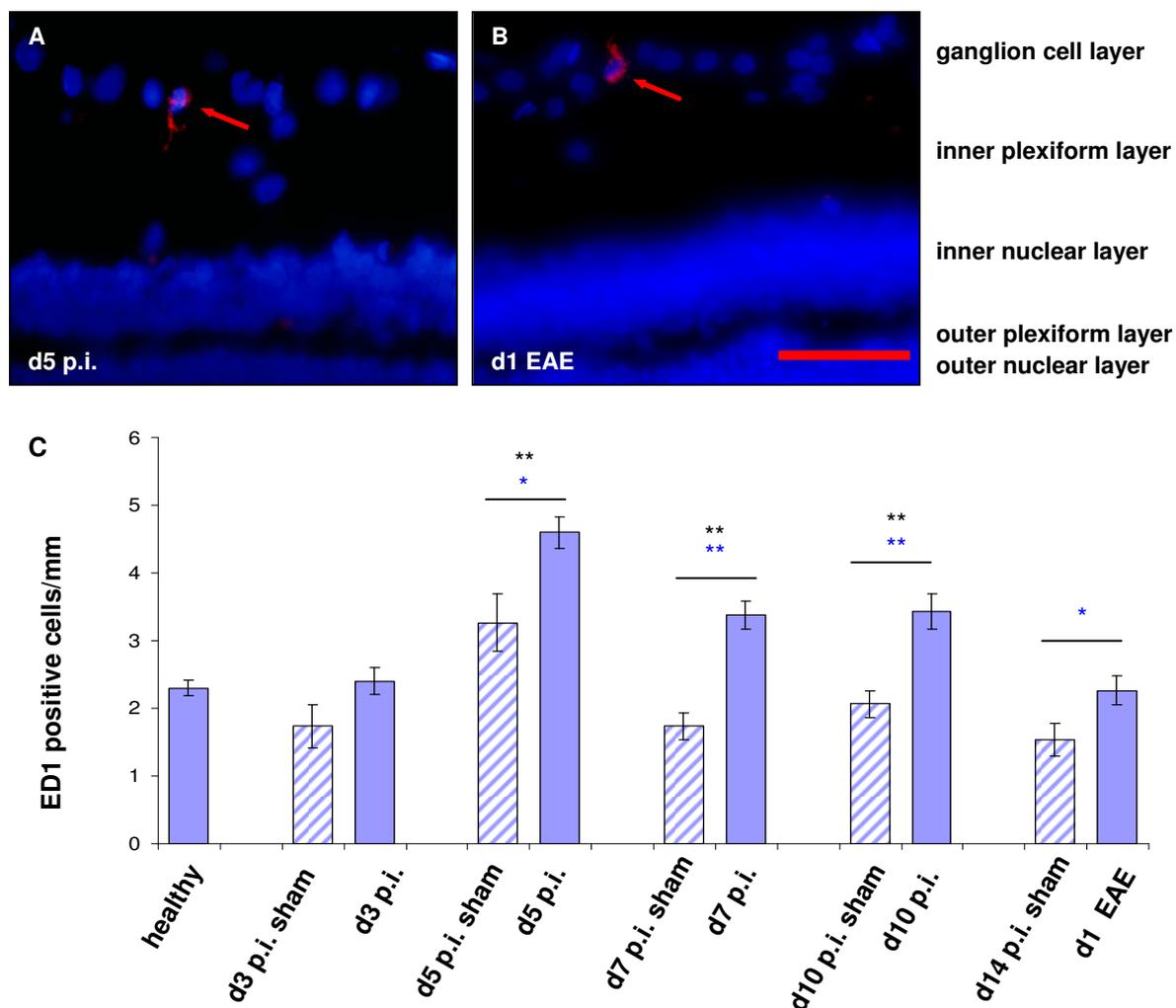
Figure 4.13 Number of ED1 positive cells in retinal ganglion cell layer was increased from d5 p.i. onwards

ED1 positive cells show a microglia-like morphology in the induction phase (A) and also after onset of EAE (B). The increase in ED1 positive cells was significant in the induction phase of the disease when compared to healthy animals and corresponding sham controls. After the onset of EAE the number of ED1 positive cells was reduced (C). (* = p ≤ 0. 05, ** = p ≤ 0. 01. ** = significant to healthy, *,** = significant to corresponding sham, n = 3 for shams, d3 p.i., d5 p.i., d10 p.i and d1 of EAE, n = 4 for d7 p.i.). Scale bar = 50 μm.

4.9   Increased GFAP expression in the retina correlated with microglial activation and onset of RGC degeneration

In addition to microglia, the retina contains two types of macroglial cells: Müller cells and astrocytes. Astrocytes are located in the ganglion cell layer and nerve fibre layer and express the glial fibrillary acidic protein (GFAP). Müller cells are located in the inner nuclear layer (cell body) with processes projecting to the inner and outer plexiform layer (Reichenbach *et al.*, 1989) and only express detectable levels of GFAP after retinal insults (Bignami and Dahl, 1979; Björklund and Dahl, 1985). Astrocytes become reactive after various insults, and can be identified by elevated expression of GFAP and thicker processes (hypertrophy) (Latov *et al.*, 1979; Brock and O'Callaghan, 1987; Eng *et al*, 2000). Activation of microglia/macrophages and astrocytosis are often found in parallel after insults to CNS tissue with cytokine signalling providing a mean of communication between these cell types during inflammation (Dong and Benveniste, 2001). In order to assess if the activation of microglia is accompanied by increased reactivity in aystrocytes and Müller cells, immunohistochemistry with an antibody against GFAP was performed. This revealed increased expression in the ganglion cell layer and also GFAP-positive processes in the inner plexiform layer from d5 p.i. onwards, when compared to healthy and sham-immunised animals (Figure 4.14 A, B and C), suggesting increased activation of astrocytes and probably Müller cells. Western blots with retina lysates were performed to quantify the changes in GFAP expression. A significant increase in GFAP expression could be seen from d5 p.i. onwards when compared to healthy and sham-immunised animals (Figure 4.14, D and E). These results suggest that reactive gliosis in the retina started on d5 p.i., correlating with microglial activation and onset of RGC degeneration.
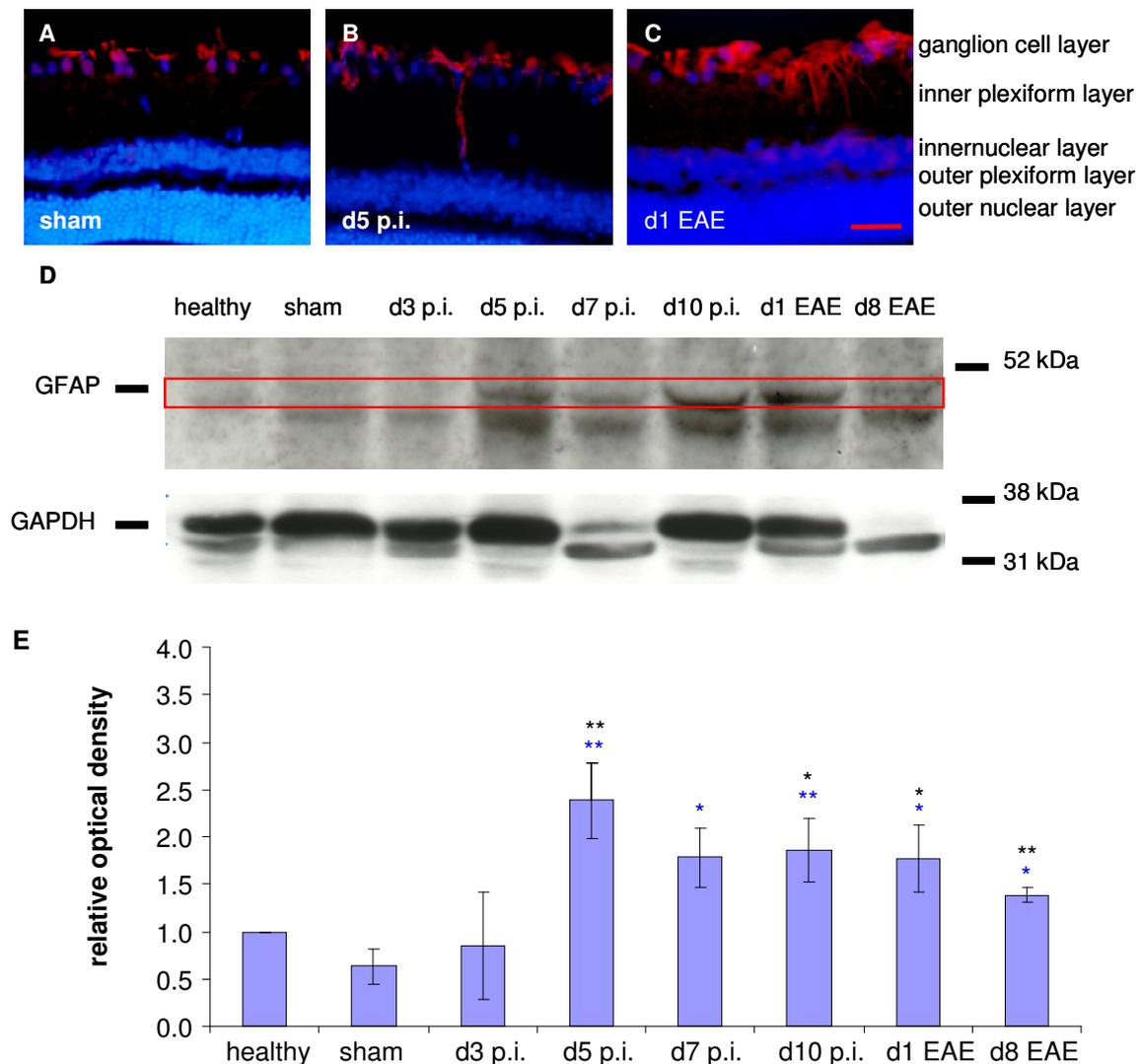
Figure 4.14 GFAP expression in the retina was upregulated from day 5 p.i. onwards

Representative images were taken from sham-immunised animals (A), d5 p.i (B) and d1 EAE (C). Increased GFAP expression could be seen from d5 p.i onwards, which was confirmed with western blot analysis (D, E) (* = p ≤ 0. 05, ** = p ≤ 0. 01. *, ** = significant to healthy, *, ** = significant to sham, n = 4 for d8 of EAE, n = 5 for d3 p.i., d5 p.i. and d1 of EAE, n = 6 for healthy and d10 p.i. and n = 7 for sham and d7 p.i.). Scale bar = 50 μm.

4.10 Cytokine concentrations were not elevated during the induction phase

Concentrations of several cytokines are elevated in the CSF of MS patients, for example it has been proposed that the chemokine CXCL13 can be used to predict

conversion from CIS to MS (Brettschneider *et al.*, 2010). Cytokines have also been implied in the early activation of microglia (Marik *et al.*, 2007). With the multispot assay technique the concentration of several cytokines in the CSF was measured. There was no detectable change in concentration of Il-4, IL-5, IL-13, IL-1β, IFN-γ and TNF-α during the induction phase and after onset of clinical symptoms. The concentration of GRO (CXCL1) increased significantly (*p ≤ 0.01) on d1 of EAE (Figure 4.15). CXCL1 is a chemokine that is released by reactive astrocytes and binds to the CXCR2 receptor which is expressed on neutrophils and responsible for their chemotactic response (Bozic *et al.*, 1995; Van Damme *et al.*, 1997), thus promoting inflammation.
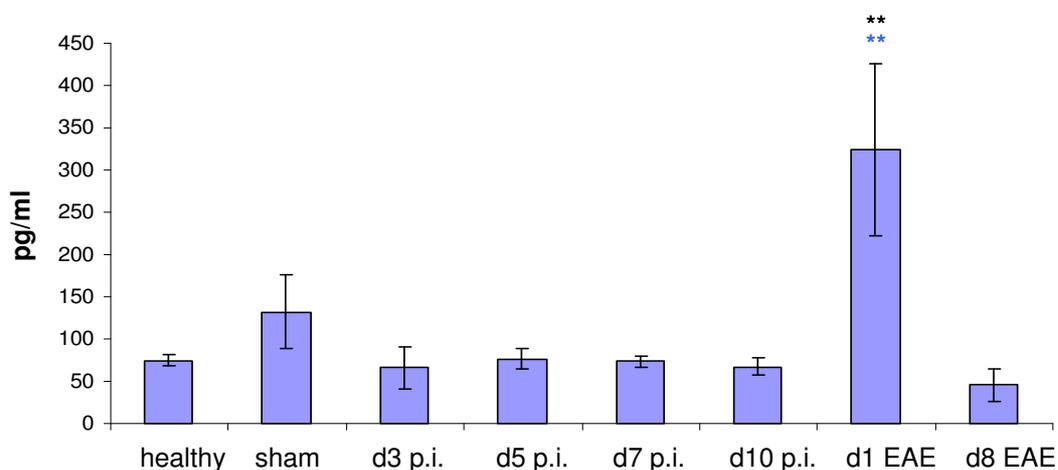
Figure 4.15 Concentration of CXCL1 in the cerebrospinal fluid is elevated at d1 of EAE
The CXCL1 concentration was significantly elevated at d1 of EAE when compared to healthy and sham controls. (** = p ≤ 0. 01. ** = significant to healthy, ** = significant to sham, n = 3 for d3 p.i., d7 p.i.and d10 p.i., n = 4 for sham, d1 and d8 of EAE, n = 6 for d5 p.i. and n = 7 for healthy).

4.11 Manganese enhancement in the retina and optic nerve started during the induction phase

To address the timing of calcium influx during the disease course of EAE, manganese-enhanced MRI (MEMRI) was performed, using manganese chloride (MnCl$_2$) as a contrast agent in T1-weighted MRI. Manganese ions (Mn^{2+}) are able to enter cells via the same entry pathways as calcium ions, such as voltage-dependent calcium channels (VDCCs) (Lin and Koretsky; 1997; Takeda, 2002) and ionotropic glutamate receptors, and therefore manganese-enhanced MRI can be used to

monitor calcium influx in the retina and the optic nerve. In addition MRI was used to monitor anatomical changes in the optic nerve.

4.11.1 Optic nerve swelling could be seen in the induction phase and after onset of optic neuritis

T2-weighted RARE scans were used to measure changes in the width of the optic nerve during the disease course. There was a significant increase in sham-immunised animals and d10 p.i. when compared to healthy animals (Figure 4.16, D) and no difference between sham-immunised animals and d10 p.i. (Figure 4.16, A, B and D). At d1 of EAE there was a significant increase compared to both healthy and sham-immunised animals (Figure 4.16, C and D). This agrees with the results from measuring the area of the optic nerve (Figure 4.4) showing that the previously observed results from the histophathological staining are not caused by artefacts due to the fixation process.
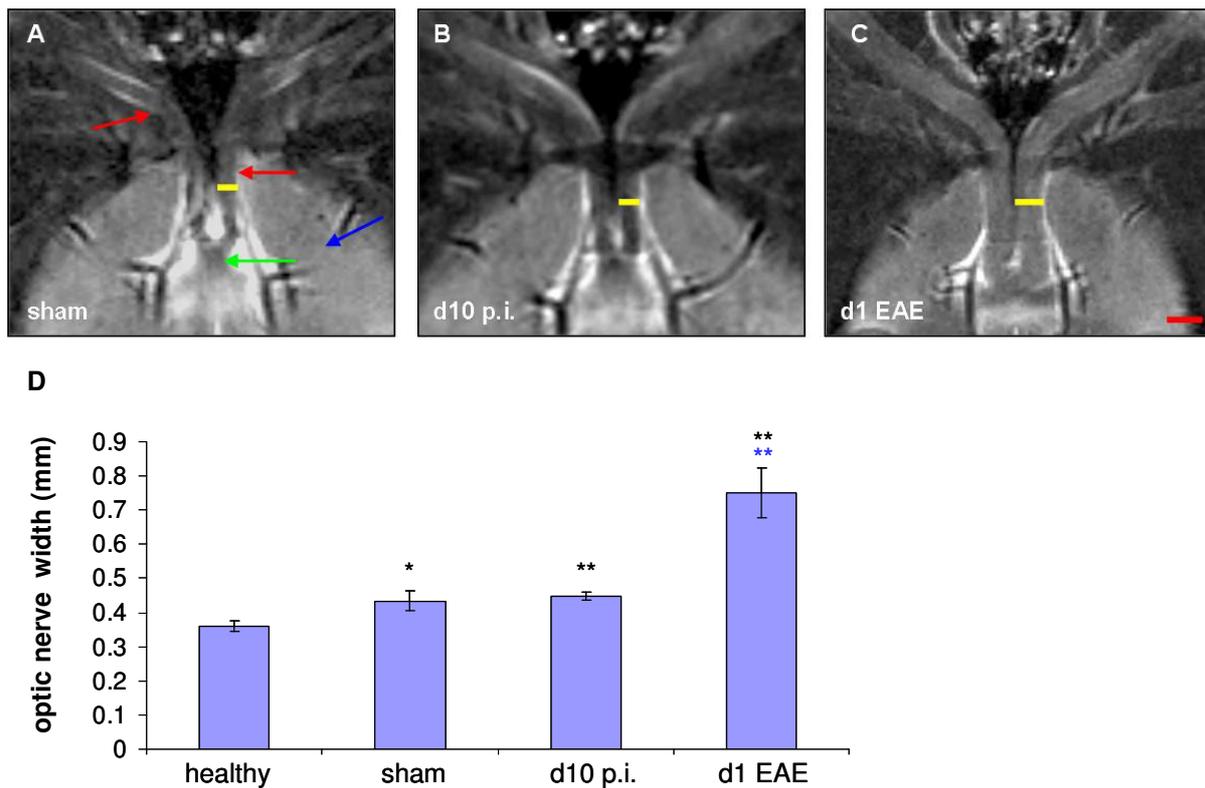
Figure 4.16 Width of the optic nerve is increased on d1 of EAE

Representative images of T2-weighted scans were taken from sham-immunised animals (A), d10 p.i (B) and d1 of EAE (C). Arrows indicate the brain (blue), optic nerves (red) and optic chiasm (green). The yellow line indicates where the width was measured. There is a significant increase in the width of the optic nerve in sham-controls and d10 p.i when compared to healthy animals but no difference between d10 p.i. and sham control. There is a significant increase in width on d1 of EAE when compared to both healthy and sham. (D) Measurement of optic nerve width. (* = $p \leq 0.05$, ** = $p \leq$ 0.01. *,** = significant to healthy, ** = significant to sham, n = 4 for sham, n = 5 for d1 of EAE, n = 6 for healthy and n = 9 for d10 p.i.). Scale bar = 1 mm.

4.11.2 Manganese enhancement in the optic nerve could be seen from d10 p.i. onwards

After positioning with T2-weighted RARE scans, 3D FLASH scans were performed. To find the timepoint were the signal enhancement is most prominent, three sick animals (d1 EAE) were injected with $MnCl_2$ and signal intensity was measured before injection (Figure 4.17, A), 10 minutes after injection (Figure 4.17, B), one hour (Figure 4.17, C) and two hours (Figure 4.17, D) after injection. In two animals intensity was also measured 24 hours after injection.

The signal enhancement was slightly stronger 10 minutes after injection when compared to the one hour timepoint and stayed stable between one and two hours after injection. 24 hours after injection there was still small but significant increase in signal intensity (Figure 4.17, E). Since the signal enhancement was strongest 10 minutes after injection, this timepoint was choosen for further measurements.
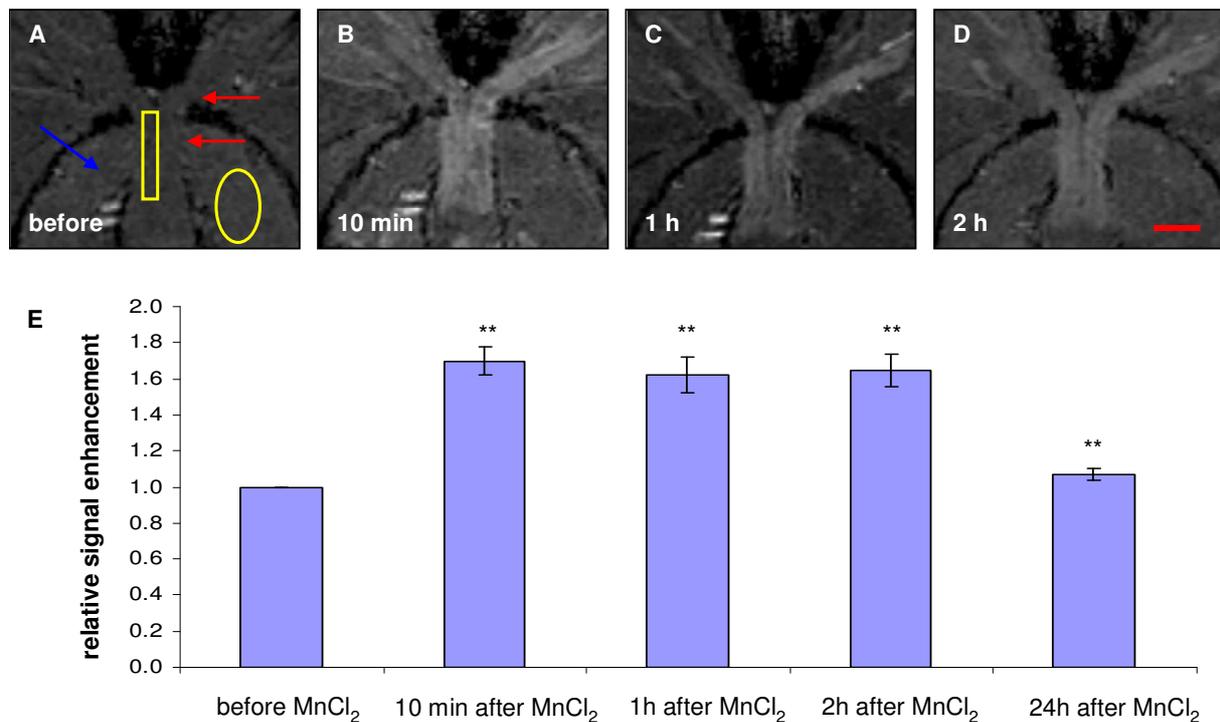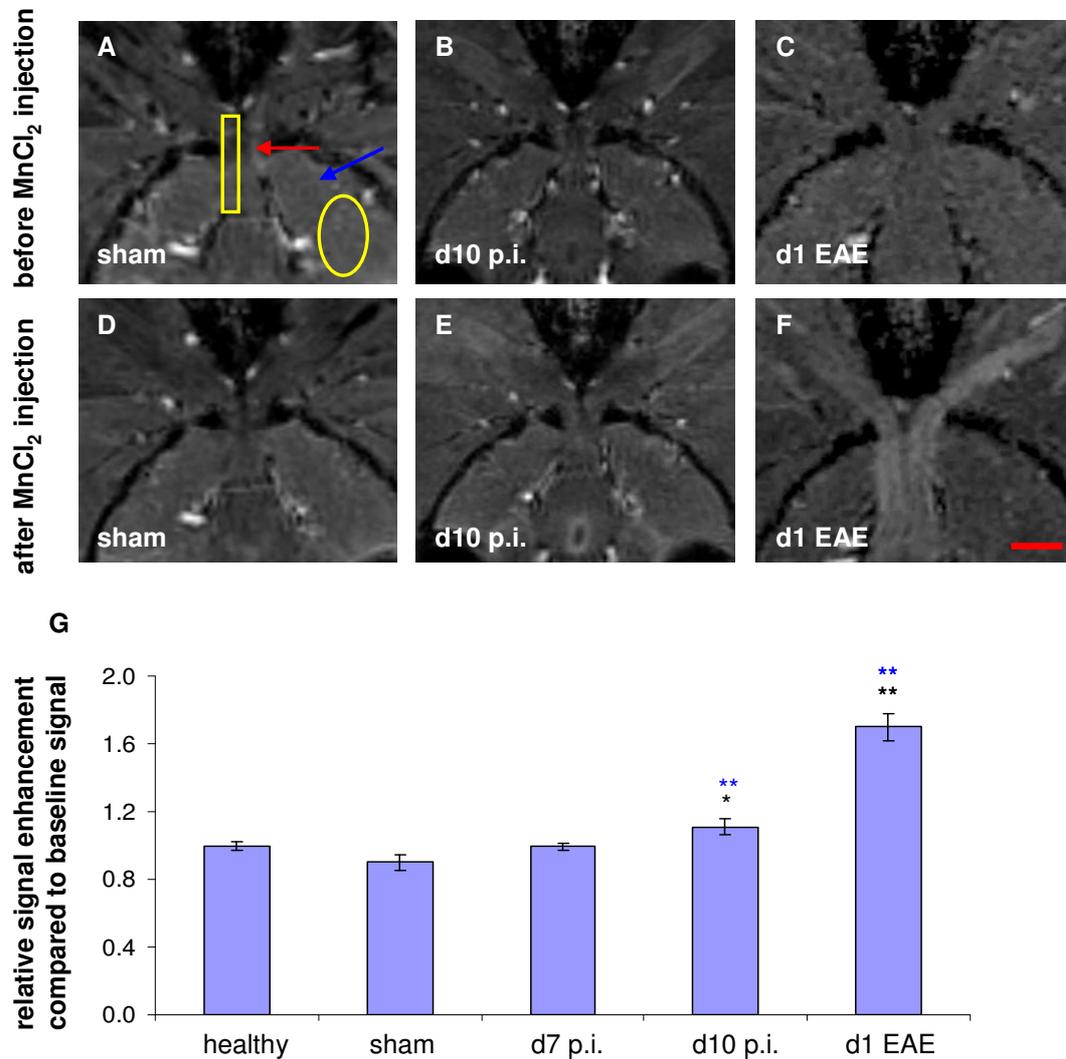

Figure 4.17 Time course of signal enhancement after MnCl$_2$ injection at d1 of EAE
Representative images of T1-weighted scans show the baseline value before injection (A), and the same nerve 10 minutes, one hour and two hours after MnCl$_2$ injection (B),(C) and (D). The signal intensity was increased significantly 10 minutes after injection when compared to the baseline value. One hour after injection the signal intensity was slightly reduced and stayed stable between one and two hours. At 24 hours the signal intensity was greatly reduced but still significantly elevated (E). Arrows indicate the brain (blue) and optic nerves (red). The yellow rectangles and ellipses indicate the area measured for signal intensity. (** = $p \leq 0.01$, n = 2 for the 24 hour scan, n = 5 for other timepoints). Scale bar = 2 mm.

To examine the time course of manganese enhancement, signal intensity was measured in healthy and sham-immunised animals, on d7 and d10 p.i and on d1 of EAE before MnCl$_2$ injection (Figure 4.18, A, B and C) and 10 minutes after injection (Figure 4.18, D, E and F). There was no difference between healthy (signal intensity 0.99 ± 0.02), sham-immunised animals (signal intensity 0.90 ± 0.05) and on d7 p.i. (signal intensity 0.99 ± 0.02). There was a significant increase in manganese enhancement on d10 p.i. (signal intensity 1.11 ± 0.05) and on d1 of EAE (signal

intensity 1.70 ± 0.08) when compared to sham-immunised and healthy animals (Figure 4.18, G).

Figure 4.18 Manganese enhancement in the optic nerve during the course of optic neuritis.
Representative images of T1-weighted scans show the baseline value before $MnCl_2$ injection in sham-immunised animals (A), d10 p.i (B) and d1 of EAE (C) and the same nerve 10 minutes after injection (D-F). Arrows indicate the brain (blue) and optic nerves (red). The yellow rectangles and ellipses indicate the area measured for signal intensity. No change in signal enhancement could be seen on d7 p.i when compared to healthy and sham-immunised animals. There was a significant increase on d10 p.i and d1 EAE. (* = $p \leq 0.05$, ** = $p \leq 0.01$, *, ** = significant to healthy, ** = significant to sham, n = 3 for healthy and d7 p.i., n = 4 for sham, n = 5 for d1 of EAE and n = 6 for d10 p.i.). Scale bar = 2 mm.

4.11.3 Manganese enhancement in the retina could be seen from d5 p.i. onwards

After positioning with T2-weighted RARE scans, MSME scans were performed before and after injection of $MnCl_2$. To find the timepoint after injection where the signal enhancement is most prominent, animals at d5 p.i were injected with $MnCl_2$ and signal intensity was measured before injection (Figure 4.19, C), 10 minutes after injection (Figure 4.19, D), one hour (Figure 4.19, E) and two hours (Figure 4.19, F) after injection. Signal intensity was increased significantly 10 minutes after injection and reached its peak one hour after injection (Figure 4.19, G) and this timepoint was used for further experiments.

To examine the time course of manganese enhancement, signal intensity was measured in healthy and sham-immunised animals, on d3 p.i, d5 p.i., d10 p.i. and on d1 of EAE before $MnCl_2$ injection and one hour after injection.

Signal intensity after $MnCl_2$ injection in healthy, sham-immunised animals and at d3 p.i. was very similar (Figure 4.20, G). From d5 p.i. onwards $MnCl_2$ injection caused a profound increase in signal enhancement (Figure 4.20, B-F) and signal intensity was significantly increased when compared to healthy and sham-immunised animals (Figure 4.20, G). The fact that manganese enhancement can be seen from d5 p.i. onwards, correlating with onset of RGC degeneration suggest that calcium influx might play a role in the death of RGCs at this timepoint.
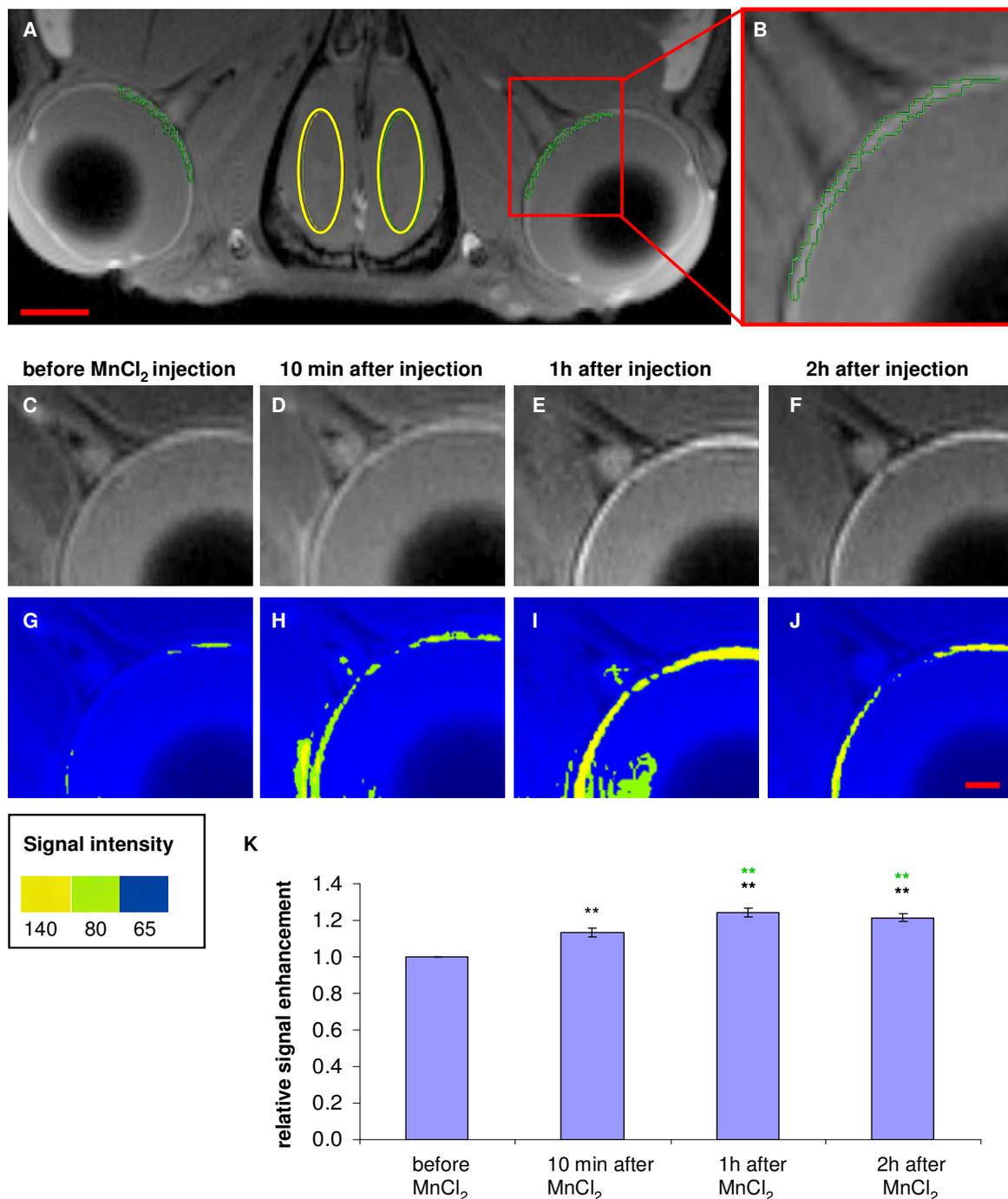
Figure 4.19 Signal enhancement in the retina is highest one hour after MnCl$_2$ injection

Representative image of a T1-weighted scan at d5 p.i. shows which areas of the retina and brains were measured (A and B). The yellow ellipses indicate the brain area measured as control for signal intensity and the green are indicates the area of the retina that was measured.

Signal intensity was measured before MnCl$_2$ injection (C), 10 minutes after injection (D), one hour after injection (E) and two hours after injection (F). The same images are shown as false colour images (G-J). The signal intensity was significantly increased 10 minutes after injection and highest one hour after injection. (K) Measurement of signal intensity (** = p ≤ 0.01. ** = significant to before injection, ** = significant to 10 minutes after injection, n = 4 for the 10 minutes scan, n = 5 for one and two hour scans) Scale bar = 2 mm in A and 1 mm in C-J.

before MnCl$_2$ injection

after MnCl$_2$ injection

Signal intensity

140   80   65
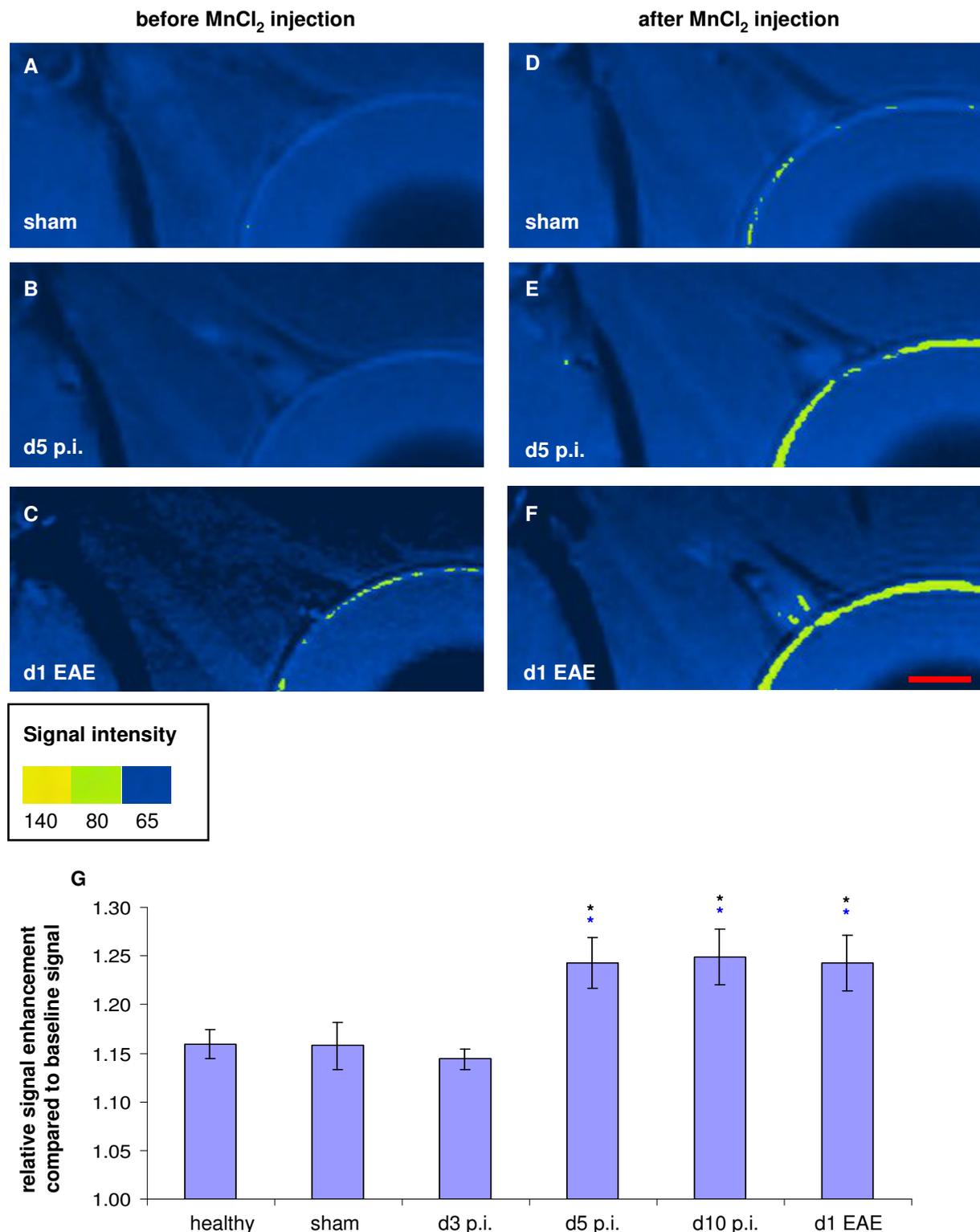
Figure 4.20 Manganese enhancement in the retina started during the induction phase

Representative images of T1-weighted scans show the baseline value before MnCl$_2$ injection in sham-immunised animals (A), d5 p.i (B) and d1 EAE (C) and one hour after MnCl$_2$ injection (D, E, F). There was a significant increase on d5 p.i., d10 p.i. and d1 of EAE when compared to healthy and sham-immunised animals (G).Since the baseline value before injection was set to one, the scale was also set to one as a minimum value. (* = p ≤ 0.05. * = significant to healthy, * = significant to sham, n = 4 for healthy, sham, d3 p.i., d10 p.i. and d1 of EAE, n = 5 for d5 p.i.) Scale bar = 1 mm).

4.11.4 Treatment with the NMDA receptor blocker MK 801 reduced manganese enhancement in the retina

The NMDA receptor (ionotropic glutamate receptor) has been shown to play an important role in retinal degeneration. Blockade of the receptor with the antagonist MK-801 reduces death of cultured RGCs after glutamate exposure (Pang *et al.*, 2007) and also reduces calcium influx in cultured RGCs (Hartwick *et al.*, 2008). In the following experiments the role of the NMDA receptor in the previously observed manganese enhancement was examined. Animals were taken at d5 p.i. because there was strong signal enhancement at this timepoint (Figure 4.20, G) and the early manganese enhancement correlates with onset of RGC degeneration.

Signal intensity was measured in healthy animals and at d5 p.i before and one hour after $MnCl_2$ injection. Animals were injected with MK801 40 minutes prior to $MnCl_2$ injection; the control group received a saline injection. At d5 p.i. there was a significant increase in signal enhancement in the control group when compared to the healthy control group (Figure 4.21, A, B and E), as was already shown in untreated animals. In the animals treated with MK801 a significant reduction in signal intensity could be seen at d5 p.i (Figure 4.21 B, D, and F) suggesting that influx through NMDA receptors contributes to manganese enhancement.
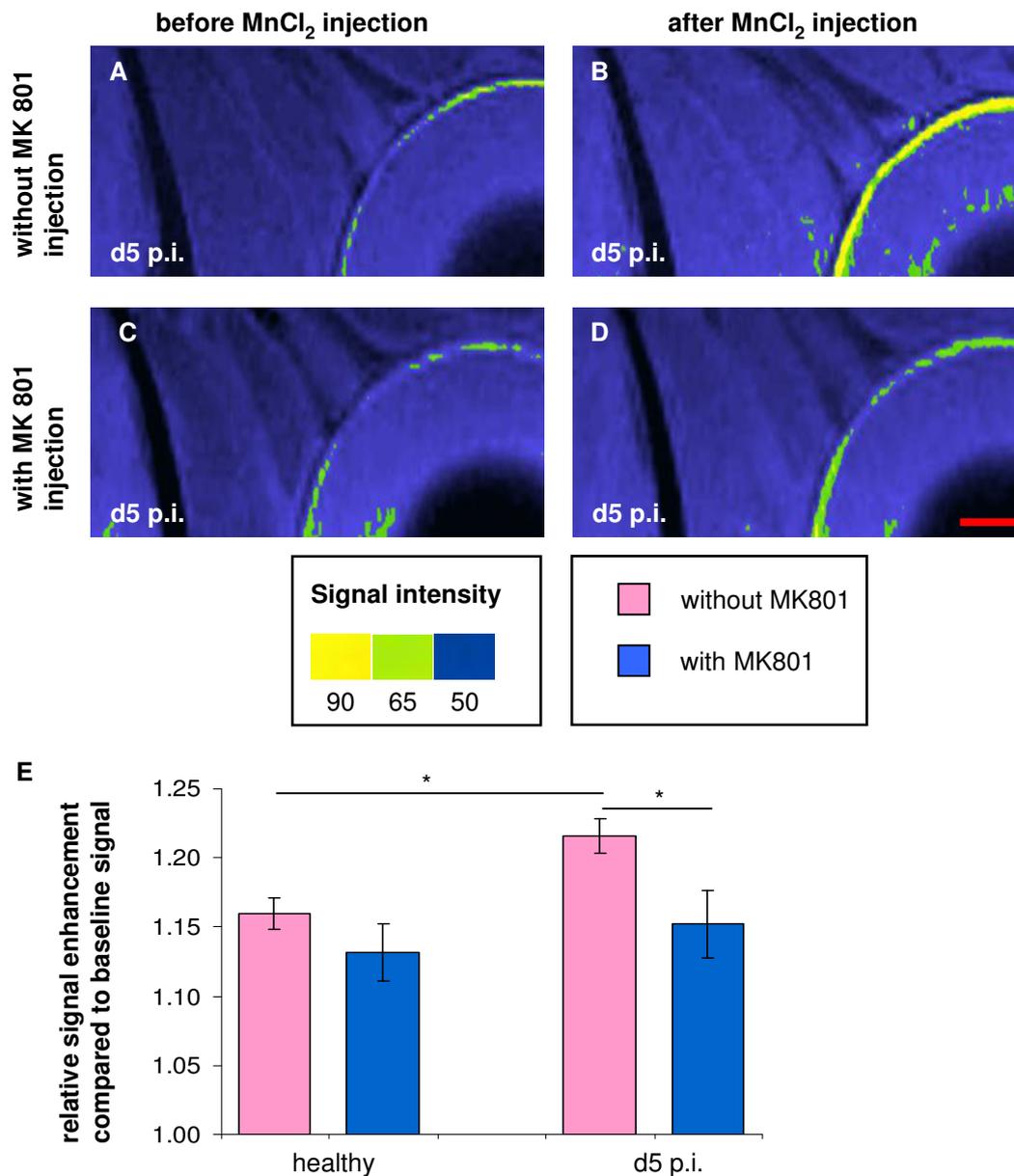
Figure 4.21 Treatment with the NMDA receptor blocker MK801 significantly reduced manganese enhancement at d5 p.i

Representative images of T1-weighted scans show a retina at d5 p.i. before MnCl$_2$ injection with saline injection (A) and one hour after MnCl$_2$ injection (B) and at d5 p.i. with injection of MK 801 (C) and one hour after injection of MnCl$_2$ (D). The injection of MnCl$_2$ caused a significant increase in signal intensity at d5 p.i. when compared to healthy animals (E) and signal intensity was decreased significantly at d5 p.i. in animals that received MK801 but not in healthy animals (E). (* = $p \leq 0.05$, n = 4 for healthy and d5 p.i. with saline and d5 p.i. with MK801, n = 6 for healthy with MK801). Scale bar = 1 mm.

4.12 Increased amount of BDP$_N$ in the retina and optic nerve could be observed during the induction phase

The loss of RGCs can be seen very early in the disease course. A mechanism implicated in pathology in both acute neurodegenerative disorders and chronic neurodegenerative diseases is an increase in calpain activity as a result of calcium dysregulation (Vosler *et al.*, 2008). A commonly used method for measuring increased calpain activity is using an antibody against spectrin breakdown products (SBDPs). Spectrin is a cytoskeletal protein which can be cleaved into different SBDPs by caspase 3 and calpain. Calpain cleavage leads to breakdown products with a size of 145 kDa and 150 kDa. Caspase 3 cleavage produces breakdown products with a size of 120 kDa and 150 kDa. An antibody that recognizes all the breakdown products was used first but since the breakdown products are difficult to distinguish due to their similar sizes, an antibody specific for one of the calpain cleaved breakdown products was later used (BDP$_N$ against the 145 kDa breakdown product).

4.12.1 Elevated concentration of BDP$_N$ in the optic nerve correlated with manganese enhancement

With the antibody against all breakdown products two bands of approximatley 150 kDa in size could be seen. Due to the very similar size (Figure 4.22) it was impossible to quantify these bands. Therefore the antibody against BDP$_N$ was used to quantify changes in the amount of spectrin breakdown product and thus calpain activity.
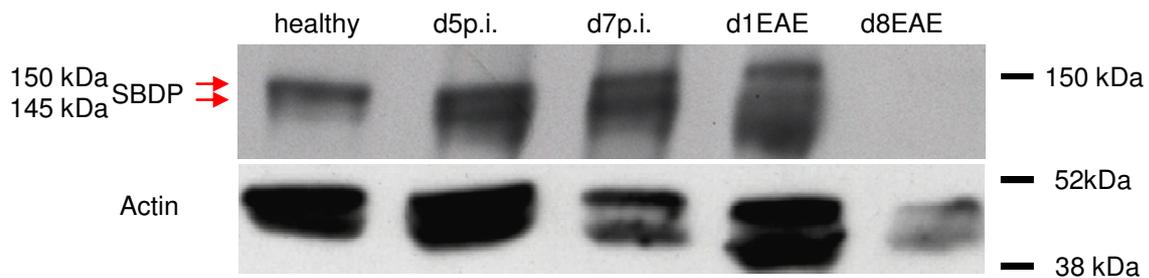
Figure 4.22 An antibody against caspase-3 and calpain cleaved spectrin produced bands to similar in size to be quantified

Initially an antibody was used that recognizes spectrin breakdown products produced by calpain and caspase-3 cleavage. Since the cleavage products are very similar in size (145 kDa for calpain and 150 kDa for caspase-3, indicated with red arrows), quantification was not possible. For further experiments an antibody that only recognises one of calpain-mediated spectrin breakdown products was used.

As expected, with the antibody specific against BDP_N, 145 kDa only one band can be seen in the western blot (Figure 4.23 , A). The relative level of BDP_N is elevated in sham-immunised animals and on d3 p.i., d5 p.i. and d7 p.i. when compared to healthy animals and significantly elevated from d10 p.i. onwards when compared to sham-immunised animals (Figure 4.23, B). This correlates well with the results from manganese enhanced MRI where enhancement could be seen at d10 p.i. and d1 of EAE. In the optic nerve no axonal loss can be seen at d10 p.i.; the activation of calpain might therefore correlate with subtle axonal changes prior to axonal loss.

A

B
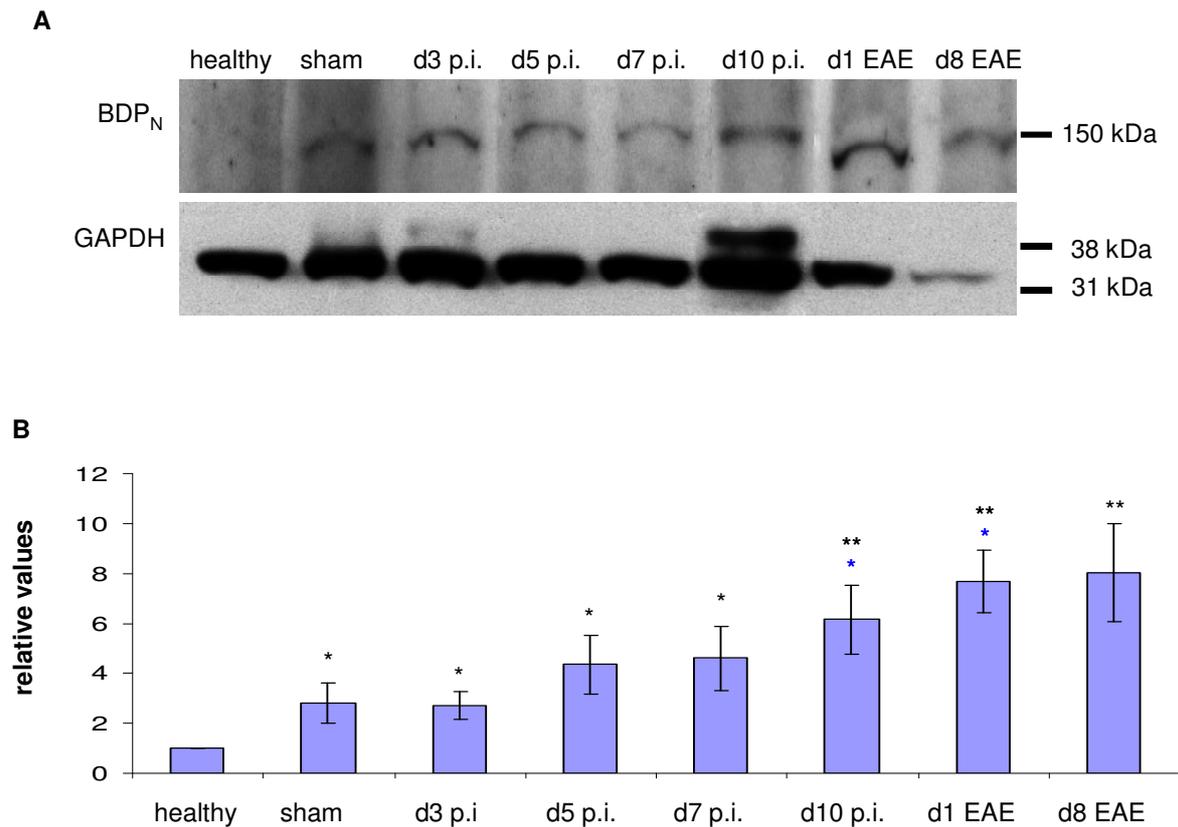
Figure 4.23 Calpain-specific spectrin breakdown product (BDP$_N$) in optic nerves was elevated from d10 p.i. onwards

An antibody specific to BDP$_N$ showed one band at 145 kDa (A). GAPDH was used as a loading control. (B) There was an increase in BDP$_N$ in sham-immunised animals and between d3 p.i. and d7 p.i. when compared to healthy animals and a further significant increase on d10 p.i. when compared to both healthy and sham-immunised animals. The increase in BDP$_N$ indicates increased calpain activity from d10 p.i. onwards. (* = p ≤ 0.05, ** = p ≤ 0.01. *, ** = significant to healthy, *, ** = significant to sham, n = 4 for sham, n = 5 for d10 p.i. and d8 of EAE, n = 6 for healthy, d7 p.i. and d1 of EAE, n = 7 for d3 p.i. and d5 p.i.).

4.12.2 Onset of elevated concentration of BDP$_N$ in the retina correlated with manganese enhancement and degeneration of RGCs

For the retinal lysates only the antibody for the calpain-mediated spectrin breakdown was used. The relative level of BDP$_N$ was significantly elevated on d5 p.i. and d7 p.i., when compared to both sham-immunised and healthy animals (Figure 4.24 A, B). There was also a slight increase at d10 and d1 of EAE which was only siginificant compared to healthy animals.

The onset of increased amount of BDP$_N$ at d5 p.i. correlated with the result from manganese enhanced MRI where increased signal intensity could be seen from d5 p.i. onwards (Figure 4.20, G) and also correlated with the onset of RGC degeneration.
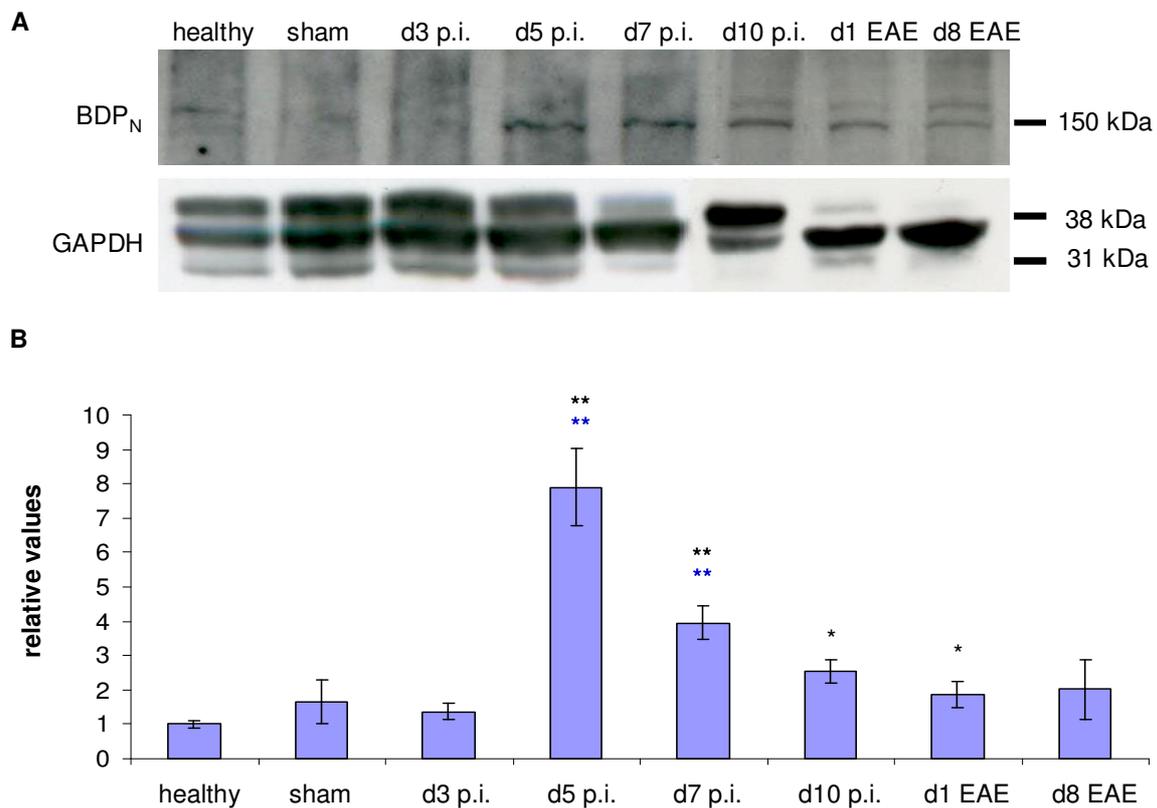
Figure 4.24 Calpain-specific spectrin breakdown product in retina was elevated on days 5 and 7 p.i.

An antibody specific to the calpain-cleaved spectrin breakdown product showed one band at 147 kDa (A). GAPDH was used as a loading control. (B) Relative levels of spectrin breakdown product. The increase in spectrin breakdown product indicates an increase in calpain activity on d5 and d7 p.i. (* = p ≤ 0.05, ** = p ≤ 0.01. *, ** = significant to healthy, ** = significant to sham, n = 4 for d3 p.i, n = 6 for d5 p.i., n = 7 for d10 p.i.and d8 of EAE, n = 10 for sham, d7 p.i. and d1 of EAE).

4.13 Calpeptin treatment reduced RGC degeneration in the induction and clinical phase and reduced symptoms of optic neuritis

The previous results imply that calpain activity is increased during the induction phase of EAE in both the retina and optic nerve. In the retina we see evidence of elevated calcium influx (shown by increased signal enhancement in manganese-enhanced MRI), starting at d5 p.i., correlating with onset of RGC degeneration.

Increased activity of the calcium-activated protease calpain can also be seen starting at d5 p.i. To determine if calpain activity plays a crucial role in early degeneration of RGCs, and could therefore be a potential target for neuroprotective therapies, calpain activity was inhibited with calpeptin.

In addition calpain activity has been implicated to play a role in T-cell migration (Butler *et al.*, 2009). Calpeptin treatment might therefore also be able to reduce inflammatory infiltration and subsequent demyelination and axonal loss after onset of optic neuritis. Animals were treated twice daily with an i.p. injection of 250 µg / kg calpeptin from the day of immunisation onwards. To confirm that the treatment strategy reduced calpain activity, lysates were taken from retinas at d5 p.i. and calpain activity was examined with the antibody against calpain-specific spectrin breakdown product. There was a trend towards decreased calpain activity after calpeptin treatment when compared to untreated animals but it was not significant (p=0.055), (Figure 4.25). There was no significant difference in the day of onset of clinical symptoms beetween the saline treated (d15.25 ± 0.75 p.i.) and calpeptin treated (d16.2 ± 1.24 p.i.) group (Figure 4.26) and also no difference in severity of symptoms.

A

B
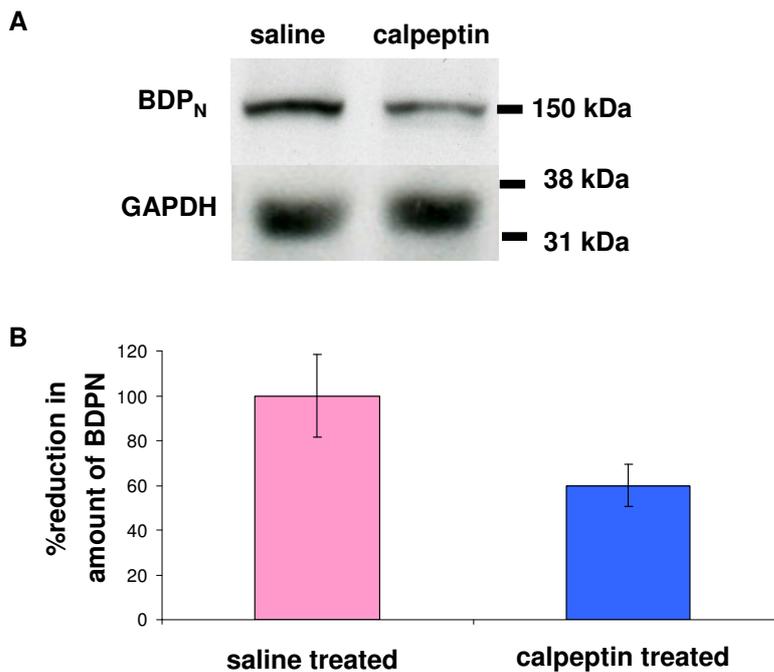
Figure 4.25 A trend towards decreased amount of BDP$_N$ in retina lysated after calpeptin treatment could be observed

(A) Western blot of retinal lysates at d5 p.i from animals treated with calpeptin and from control animals injected with saline. (B) A trend towards decreased amount of calpain-specific spectrin breakdown product could be seen, but it was not significant (p = 0.055, n = 7 for both groups).
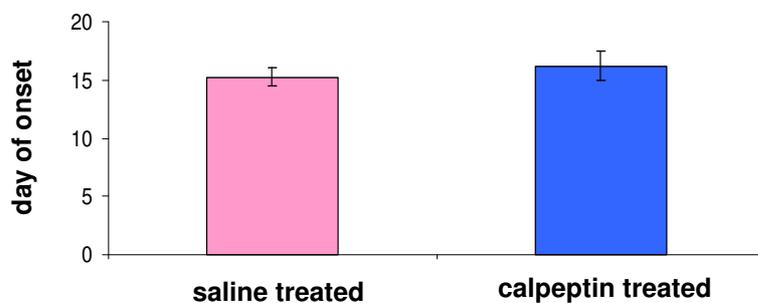
Figure 4.26 No delay in day of onset of clinical symptoms was observed with calpeptin treatment

Animals from the two groupts (calpeptin treated and saline treated) were scored daily for clinical symptoms. There was no significant difference in day of onset in the two groups. (n = 4 for saline treated and n = 5 for calpeptin treated)

Animals were taken at d1 of EAE for histopathological and immunohistochemical staining. Treatment with calpeptin reduced the number of infiltrating CD3 positive cells in the optic nerve significantly (Figure 4.27, C) from 114.67 ± 24.61 cells / mm^2 in saline treated animals to 47.9 ± 14.66 cells / mm^2 in calpeptin treated animals.

The number of ED1 positive cells was also significantly reduced (Figure 4.28, C) from 988.06 ± 206.6 cells / mm^2 in saline treated animals to 206.6 ± 126.476 cells / mm^2 in calpeptin treated animals.

saline treated   calpeptin treated
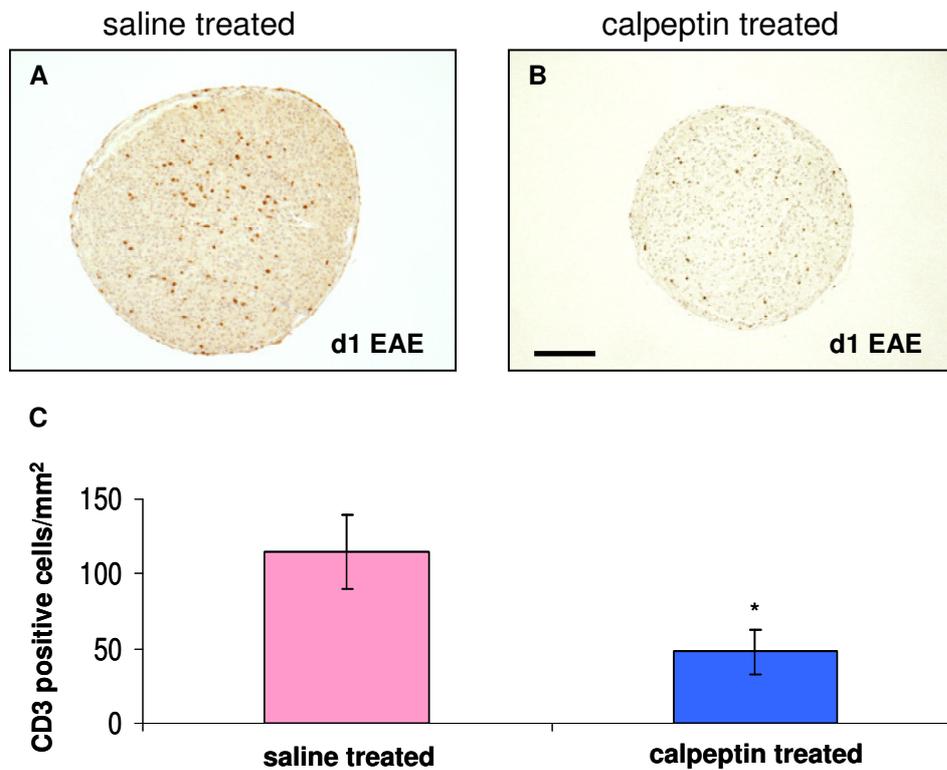
Figure 4.27 Calpeptin treatment reduced the number of CD3 positive cells in the optic nerve at d1 of EAE

The number of T-cells was examined using an antibody against CD3 on ON cross-sections. Representative images were taken from a saline treated animal (A) and an animal treated with calpeptin (B).The number of CD3 positive cells was significantly decreased in optic nerves of calpeptin treated animals (C). (* = $p \leq 0.05$, n = 4 for both groups). Scale bar = 50 µm.
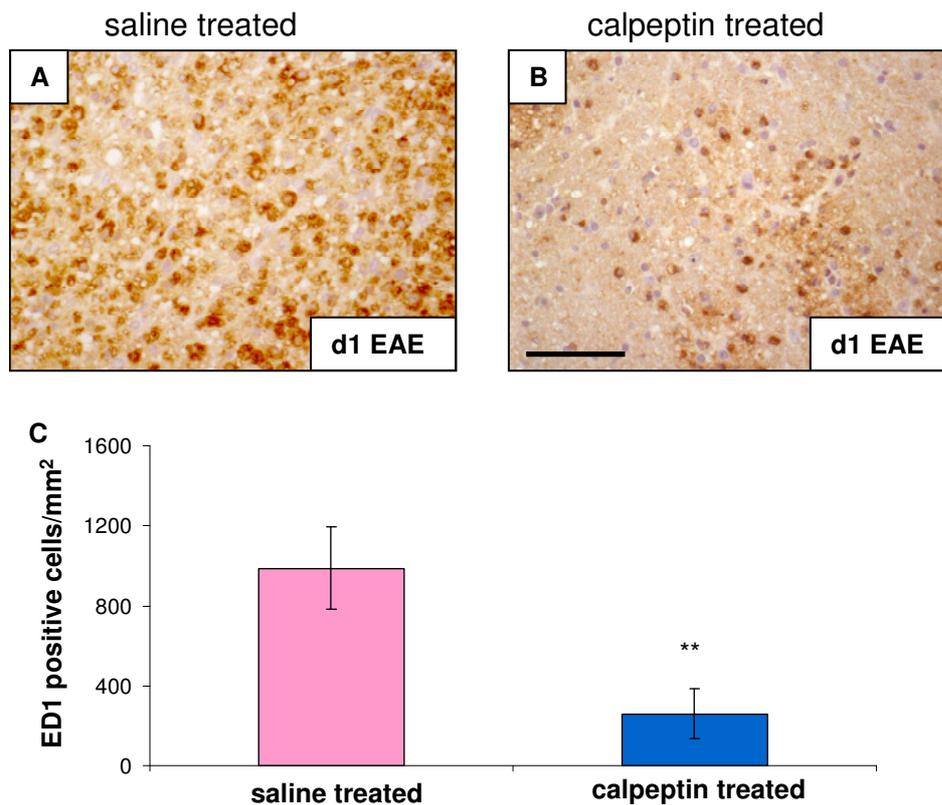
Figure 4.28 Calpeptin treatment reduced the number of ED1 positive cells in the optic nerve at d1 of EAE

The number of microglia/macrophages was examined using an antibody against ED1 on ON cross-sections. Representative images were taken from a saline treated animal (A) and an animal treated with calpeptin (B).The number of ED1 positive cells was significantly decreased in optic nerves of calpeptin treated animals (C). (* = $p \leq 0.05$, n = 4 for both groups). Scale bar = 50 μm.

LFB staining showed that demyelination was significantly decreased after calpeptin treatment from 48.35 ± 5.51% in saline treated animals to 13.65 ± 3.65 % in calpeptin treated animals (Figure 4.29, A-C). Since Bielschowsky silver impregnation is not a very sensitive marker for subtle axonal changes, an antibody against APP was used to examine disturbances in axonal transport. There was a significant decrease in APP positive axons from 1121.75 ± 187.97 axons / mm^2 in saline treated animals to 580.46 ± 123.75 axons / mm^2 in calpeptin treated animals (Figure 4.30, A-C).

Figure 4.29 Calpeptin treatment reduced demyelination in the optic nerve at d1 of EAE

Demyelination was asessed with LFB staining on ON cross-sections. Representative images were taken from a saline treated animal (A) and an animal treated with calpeptin (B).The demyelinated area was significantly decreased in optic nerves of calpeptin treated animals (C). (** = p ≤ 0. 01, n = 4 for both groups). Scale bar = 100 µm.

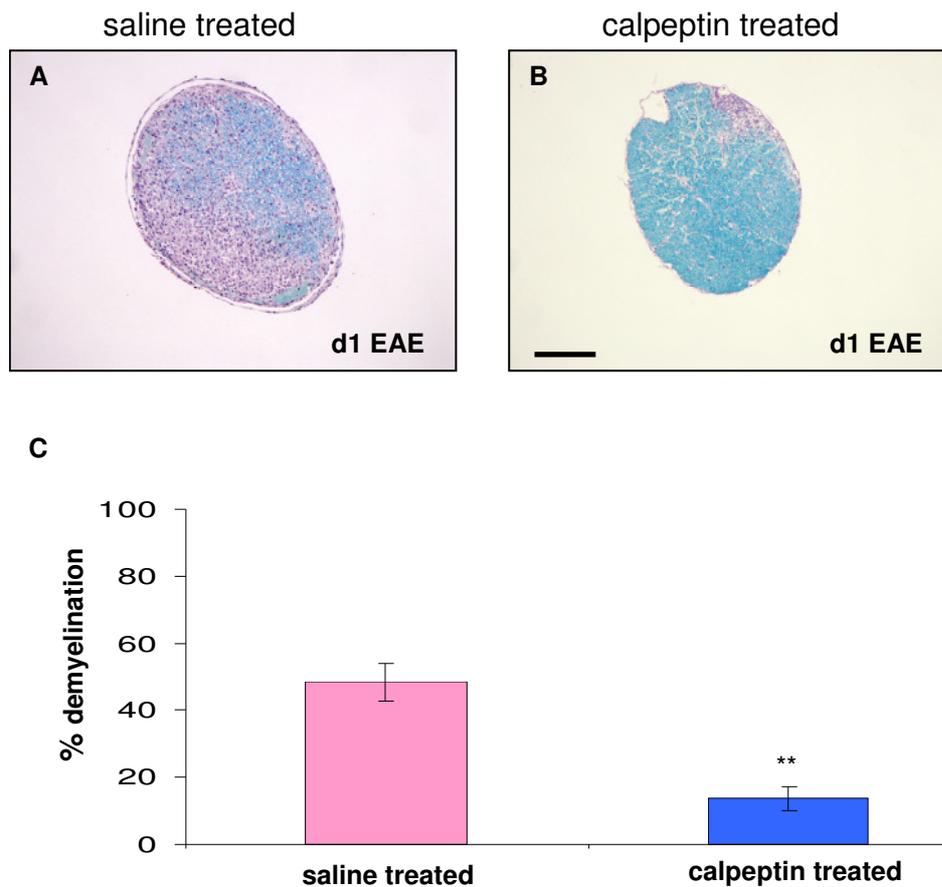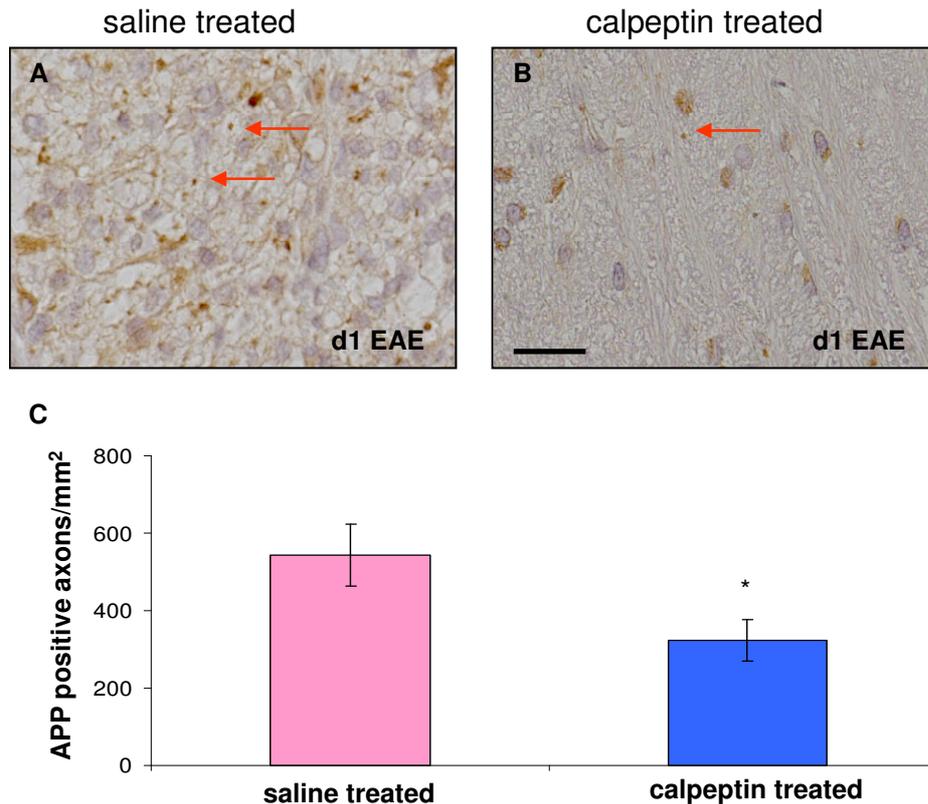**Figure 4.30 Calpeptin treatment reduced number of APP positive cells in the optic nerve at d1 of EAE**

Disturbed axonal transport was examined using an antibody against APP on ON cross-sections. Representative images were taken from a saline treated animal (A) and an animal treated with calpeptin (B). The number of APP positive axons was significantly decreased in optic nerves of calpeptin treated animals (C). (* = $p \leq 0.05$, n = 4 for both groups). Scale bar = 50 μm.

As mentioned before calpain activity plays an important role in apoptotic cell death and reduced calpain activity might contribute to survival of RGCs. Animals were sacrificed either on d10 p.i. or d1 of EAE and the number of Fluorogold-labelled RGCs in the retina was counted. Treatment with calpeptin increased the number of surviving RGCs significantly (*$p \leq 0.05$) at d10 p.i (Figure 4.31, A and B) from 1021.86 ± 57.17 cells / mm^2 in saline treated animals to 1200.25 ± 49.41 cells / mm^2 in calpeptin treated animals (Figure 4.31, E). There was also a significant increase (**$p \leq 0.01$) at d1 of EAE (Figure 4.31, C and D) from 726.86 ± 62.37 cells / mm^2 in saline treated animals to 1045.57 ± 41.77 cells / mm^2 in calpeptin treated animals (Figure 4.31, E).

saline treated   calpeptin treated
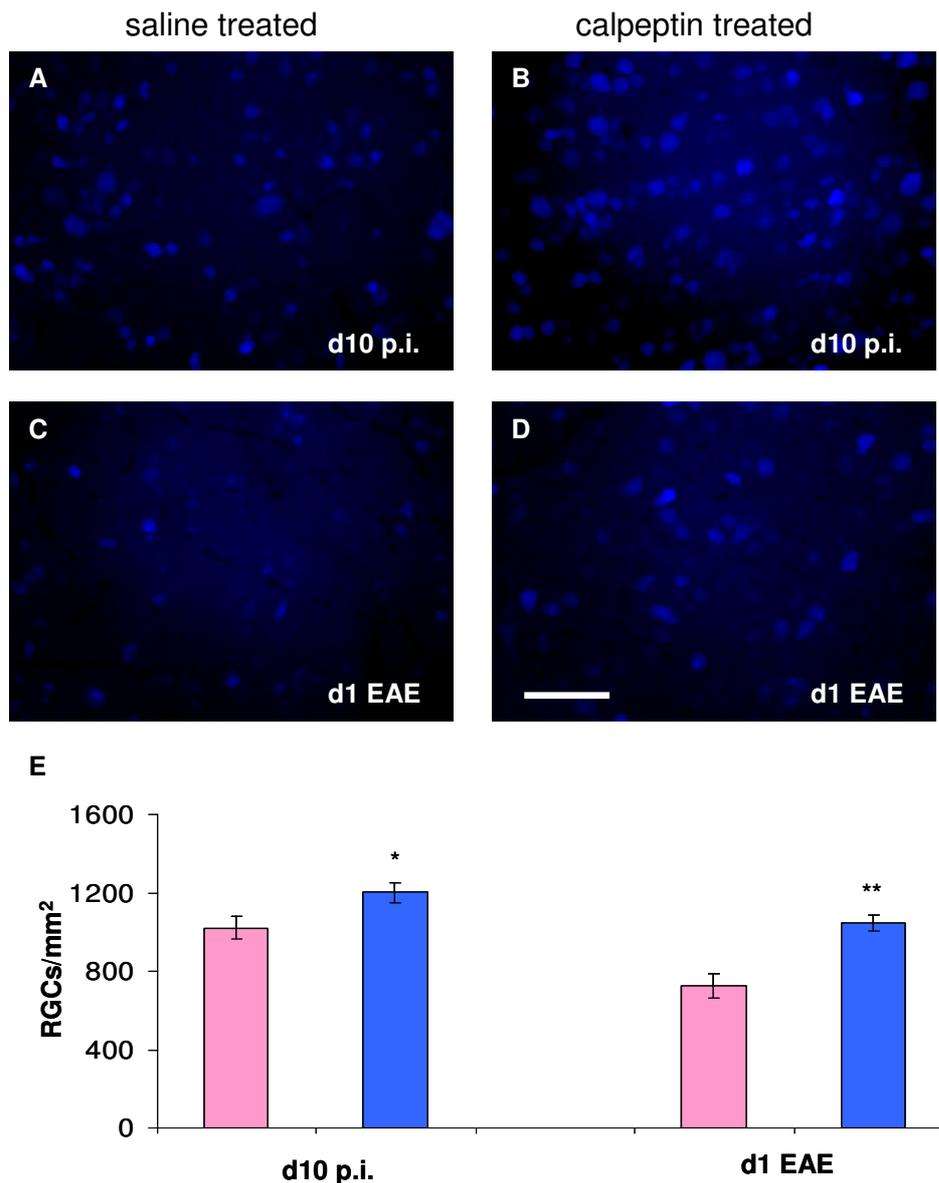
Figure 4.31 Calpeptin treatment increased the number of surviving RGCs

Numbers of surviving RGCs were assessed by counting Fluorogold-labelled cells in the retinas from animals sacrificed either on d10 p.i. or d1 of EAE. Representative images were taken from saline treated animals at d10 p.i. (A) and at d1 of EAE (C) and from calpeptin treated animals at d10 p.i. (B) and d1 of EAE (D). Cell counts showed a significant increase in the number of RGCs both at d10 p.i. and d1 of EAE in the animals treated with calpeptin. (* = $p \leq 0.05$, ** = $p \leq 0.01$, n = 3 for d1 of EAE calpeptin treated, n = 4 for d1 EAE saline treated, n = 6 for d10 p.i. saline treated and n = 8 for d10 p.i. calpeptin treated).

The above result that calpeptin treatment significantly reduces death of RGCs in the induction phase, strongly suggests that calcium influx and subsequent calpain activation play an important role in early degeneration of RGCs and that calpain inhibitiors could be a potential therapy for early neurodegeneration. In addition calpeptin treatment sifnificantly reduced inflammatory infiltration after onset of optic

neuritis, confirming results in spinal cord of Lewis rats with EAE where treatment with calpeptin reduced inflammatory infiltration and demyelination (Guyton *et al.*, 2010), suggesting that calpain inhibitors could also be considered as anti-inflammatory therapy.

5   Discussion

5.1   RGC death does not only occur secondary to axonal damage

Death of RGCs is believed to mainly occur secondary to axonal damage of the ON during optic neuritis, and is further demonstrated by experiments showing that this death shares apoptotic pathways similar to those induced by axotomy (Isenmann *et al.,* 1997; (Kermer *et al.*, 1999; Kermer *et al.,* 2000; Meyer *et al.*; 2001; Hobom *et al.*, 2004). In our model the number of RGCs is significantly reduced on d5 p.i. (Figure 4.2) more than a week before the average onset of clinical symptoms (Figure 4.1), confirming previous results from our group (Hobom *et al.*, 2004). During the induction phase, before onset of clinical symptoms no demyelination, infiltration with T-cells or axonal loss was observed in the optic nerve (Figure 4.3, Figure 4.5, Figure 4.7). The optic nerve swelling that was observed in the induction phase (Figure 4.4 and Figure 4.16) is likely to represent a subclinical event with no impact on other parameters as is has also been observed in sham-immunised animals where no degeneration of RGCs or increased activation of microglia has been observed.

The timing of optic neuritis, axonal loss and death of RGCs shows that RGCs die prior to onset of optic neuritis and even before loss of their axons, thus it appears that the degeneration of RGCs is a direct primary event. This result is of special interest in the light of recent publications, suggesting the possibility of a primary retinopathy in MS patients with no history of optic neuritis (Saidha *et al.*, 2011, Syc *et al.*, 2011).

5.2   Activated microglia in the retina and optic nerve as a potential source for excitotoxic glutamate levels

Microglia reside in the CNS and participate in innate immunity and adaptive immune response of the CNS (Garden and Möller, 2006). In the healthy brain, microglia can be found in a resting form, with long, thin processes that are moving in order to scan the environment (Hanisch and Kettenmann, 2007). Activation of microglia/macrophages, which can be identified by the expression of ED1, has been described to be a part of numerous insults to the CNS including ischemia, traumatic

injury, infections and autoimmune diseases (Kreutzberg, *et al.*, 1996; Gehrmann *et al.*, 1995) In our model activated microglia can be found in the retina and optic nerve prior to the onset of optic neuritis, correlating with the onset of RGC degeneration. After onset of optic neuritis the ED1 positive cells in the optic nerve show a macrophage-like shape which is in agreement with studies showing recruitment of blood-borne macrophages into the CNS after onset of EAE (Huitinga *et al.*, 1995; Polman *et al.*, 1986) as well as morphological changes of intrinsic microglia after insult (Kato *et al.*, 2003; Garden and Möller, 2006). In the optic nerve ED1 positive cells were found to be proliferating both in the induction phase and after onset of clinical symptoms, confirming their activation because activated microglia/macrophages express markers for proliferation (Kato *et al.*, 2003)

Activation of microglia has been suggested as an early event in lesion formation in the brain of MS patients. Activated microglia have been observed during development of lesions in normal-appearing white matter (NAWM) in MS patients in the absence of demyelination (De Groot *et al.*, 2001; van der Valk & Amor, 2009) and studies also showed a stage in lesion formation where microglia were activated prior to T-cell infiltration and demyelination (Barnett and Prineas, 2004; Gay *et al.*, 1997). It was shown that axonal/oligodendrocyte pathology at nodal and paranodal regions in the NAWM of MS patients correlates with microglial activation rather than infiltration of T-cells and in the spinal cord of mice with MOG-induced EAE microglial activation also correlates with disruption of the nodal/paranodal region and can be seen before the onset of clinical symptoms in the absence of inflammatory infiltration and demyelination (Howell *et al.*, 2010) and are likely to involve excitotoxic insult to oligodendrocytes. In our model microglial activation can also be seen in the optic nerve during the induction phase and might therefore contribute to axonal changes that precede inflammation, demyelination and axonal loss.

In the retina, microglial activation correlated with RGC degeneration, which started prior to the onset of optic neuritis. The fact that microglial activation is an early event in lesion formation and correlates with death of RGCs, underlines the importance of microglial activation and as a target for early intervention/neuroprotective therapies. The antibioticum minocycline, which inhibits microglial activation (Yrjänheikki *et al.*, 1998; Tikka *et al.*, 2002), is currently examined as a possible anti-inflammatory and neuroprotective therapy in several diseases including MS, ALS and Parkinson´s disease as it shows beneficial effects in animal models of these diseases and also in

models of stroke and TBI (reviewed by Yong *et al.*, 2004). Experiments in animals with optic neuritis and after optic nerve axotomy show that minocycline treatment is beneficial for RGC survival and several mechanisms are suggested, including reduced glutamate concentration as a result of decreased microglial activation and upregulation of glutamate transporters in astrocytes (Maier *et al.*, 2007). Since both activation of microglia and astrocytes can be observed during the induction phase in the retina, minocycline could prove beneficial in reducing early death of RGCs.

The mechanism by which microglia are activated in the absence of robust T-cell infiltration is unclear but it has been proposed that small numbers of perivascular T-cells might mediate BBB disturbances and cause influx of pro-inflammatory cytokines and/or fibrin which may then activate microglia (Marik *et al.*, 2007) and experiments in our model showed localised disturbance in the integrity of the blood-retinal-barrier during the induction phase (Fairless *et al.*, under revision).

As mentioned above a mechanism by which microglia could contribute to early neurodegeneration of retinal ganglion cells and axonal damage is glutamate toxicity. Activated microglia and macrophages can secrete glutamate (Piani *et al.*, 1991; Takeuchi *et al.*, 2005; Takeuchi *et al.*, 2006, Barger *et al.*, 2007). Inhibition of glutaminase and blocking of gap junctions with carbenoxolone (CBX) decreased extracellular concentration of glutamate in microglial cultures and also reduced death of co-cultured neurons (Yawata *et al.*, 2008). Treatment with CBX attenuated symptoms in mice with EAE and promoted survival of neurons in culture with LPS-stimulated activated microglia (Shijie *et al.*, 2009). Since activation of microglia correlates well with onset of RGC degeneration, excitotoxicity caused by microglial glutamate release is a potential contributor to early RGC death. As mentioned before activation of microglia correlates with axoglial alterations in NAWM of patients and spinal cord in rats with EAE; the authors (Howell *et al.*, 2010) suggest a role for microglia-derived glutamate since oligodendrocytes are vulnerable to excitotoxicity (Matute *et al.*, 1997) and exposing spinal cords to glutamate causes paranodal myelin retraction (Fu *et al.,* 2009).

5.3 Reactive astrocytes and Müller cells can have beneficial and detrimental effects on neuronal survival

In the retina two types of macroglia can be found: Astrocytes and Müller cells. Astrocytes are restricted to the ganglion cell layer and nerve fiber layers, Müller cell bodies are located in the inner nuclear layer and project processes throughout the retina. These glial cells perform a variety of different, overlapping functions, among them providing growth factors, ion buffering and maintaining homeostasis of neurotransmitters, including glutamate by taking it up via sodium-dependent glutamate transporters. In the retina the Glutamate Aspartate Transporter (GLAST) is the principle transporter for maintaining low glutamate concentration (Rauen *et al.*, 1998; Harada *et al.*, 1998) and is expressed both in Müller cells and astrocytes (Otori *et al.*, 1994). One of the most common markers for altered glial reactivity is GFAP (Norton *et al.*, 1992; Lam *et al.*, 1995; Chen and Weber, 2002) and increased GFAP expression can be found in retinal injuries such as ischemia and glaucoma (Osborne *et al.*, 1991; Wang *et al.*, 2000). In this study an increase in GFAP expression could be seen from d5 p.i. onwards, both in the retinal ganglion cell layer and also in the inner plexiform layer (Figure 4.14), suggesting increased reactivity in astrocytes and Müller cells.

There are several mechanisms by which glial cells can contribute to both neurodegeneration and neuroprotection. Glial cells provide trophic support for neuronal cells, and upon injury, increased expression of neurotophic factors and growth factors can promote neuronal survival (reviewed by Bringman *et al.*, 2009; Nair *et al.*, 2008). Astrocytes and Müller cells can secrete pro-inflammatory cytokines including IL-6 and TNF-α (Dong and Benveniste, 2001; Yoshida *et al.*, 2001), and chemokines, contributing to neuronal injury, but TNF-α has also been implied in rescue of RGCs after optic nerve axotomy (Diem *et al.*, 2001). Chemokine expression of astrocytes has been shown to play a role in microglia/macrophage activation in secondary progressive MS (Tanuma *et al.*, 2006). Reactive astrocytes show elevated levels of inducible nitric oxide synthase (iNOS) when exposed to elevated hydrostatic pressure (Neufeld and Liu, 2003). iNOS produces nitric oxide (NO) and which can damage both axons and neurons (Smith *et al.*, 2001, Morgan *et al.*, 1999). A beneficial role of reactive gliosis during the acute phase of EAE is supported by studies where astrocytosis was inhibited in mice with EAE and an

increased infiltration with macrophages and more severe disease course could be observed, suggesting a role for reactive astrocytosis in controlling leukocyte infiltration (Voskuhl *et al.*, 2009; Toft-Hansen *et al.*, 2011). As mentioned before, glial glutamate transporters are important for maintaining low extracellular glutamate concentration and malfunction of glutamate transporters can contribute to increased glutamate levels, causing exctitotoxic damage to neurons. Down-regulation of GLAST has been observed in spinal cord astrocytes in Lewis rats with EAE (Ohgoh *et al.*, 2002) and downregulation of GLAST was observed in astrocytes co-cultured with autoreactive T-cells (Korn *et al.*, 2005), suggesting reactive gliosis and subsequent impairment of glutamate uptake as a mechanism contributing to glutamate-mediated neuronal death.

5.4 Increased concentration of biomarkers in the CSF and blood did not correlate with early degeneration of RGCs

In MS patients, intensive efforts have been directed at the identification of biomarkers from body fluids, especially blood and CSF, in order to get a better understanding of MS pathogenesis and to predict the conversion to MS after a first clinical episode, disease course and future disability, selection of patients for individual treatment and for monitoring disease activity and treatment response (Tumani *et al.*, 2009; Dujmovic, 2011).

There are several categories of potential biomarkers, among them are markers indicating changes in the immune system (cytokines such as TNF-α, different interleukins and IFN-γ), markers connected to demyelination and humoral immune response (anti-MOG and anti-MBP antibodies) and markers for neuroaxonal damage (tau, Neurofilament L and H) (Tumani *et al.*, 2009; Dujmovic, 2011; Bielekova and Martin, 2004).

CSF levels of pro-inflammatory cytokines are usually elevated in MS patients and increased concentrations of IFN-γ and TNF-α have also been found in the CSF of mice with EAE (Willenborg *et al*, 1995). Microglia can be both recipients of and secrete pro-inflammatory cytokine such as IL-1β, IFN-γ and TNF-α (Hinkerohe *et al.*, 2005; Hanisch, 2002). Since it has been proposed that liberation of pro-inflammatory cytokines might contribute to early activation of microglia (Marik *et al.* 2007), the CSF

of rats both from the induction phase and after onset of clinical symptoms was examined for changes in the concentration of several cytokines. No changes could be seen in the concentration of Il-4, IL-5, IL-13, IL-1β, IFN-γ or TNF-α during the induction or clinical phase. It might be possible that the assay used was not sensitive enough to detect changes since increased expression of TNF-α mRNA parallels disease course during EAE (Issazadeh *et al.*, 1995) and increased TNF-α concentration in the CSF of Lewis rats with EAE has been observed (Villarroya *et al.*, 1996), suggesting that increased concentrations of cytokines are likely to be observed at least after onset of clinical symptoms. There was a significant increase in the concentration of CXCL1 on d1 of EAE (Figure 4.15). CXCL1 is secreted by reactive astrocytes and activated microglia/macrophages and binds to the CXCR2 receptor which is expressed on neutrophils and responsible for their chemotactic response (Bozic *et al.*, 1995; Van Damme *et al.*, 1997), thereby promoting inflammation.

As mentioned before neurodegeneration has become a focus of research because clinical disability correlates with neurodegeneration and axonal pathology (De Stefano *et al.*, 1998; Bjartmar and Trapp, 2003). A potential biomarker for axonal degeneration is the microtubule-associated protein tau. Tau protein concentration has been investigated in numerous studies in MS patients. Most studies show a significant increase in tau concentration in the CSF of patients but this finding is not unanimous (reviewed by Tumani *et al.*, 2008). In our model, a significant increase in tau protein concentration could be seen on d1 and d8 of EAE, correlating with axonal loss observed with Bielschowsky silver impregnation (Figure 4.5 and Figure 4.6). Axonal changes during the induction phase might not have been extended enough to raise tau concentration to detectable levels which may provide further evidence that RGC degeneration is occurring before widescale axonal damage.

Immunisation with MOG is known to elicit a humoral immune response in our model and a significant increase in the concentration of anti-MOG antibodies in the serum was observed from d10 p.i. onwards in my experiments (Figure 4.12), thus preceeding the onset of clinical symptoms. A significant increase in the number of activated microglia could be seen in MOG-immunised animals but not in sham-immunised controls at the same time point (Figure 4.8 and Figure 4.13), emphasizing the MOG-specifity of microglial activation. However, a detectable level of anti-MOG antibodies was first observed 5 days after onset of microglial activation and RGC

degeneration, suggesting that microglial activation is not directly mediated by anti-MOG antibodies.

5.5 Optic neuritis can be developed independently from clinical symptoms

Not all immunised animals developed clinical symptoms of EAE. Animals without symptoms were sacrificed on d30 p.i. and the ONs were examined for signs of optic neuritis. In 50% of the ONs, the ED1 positive cells had a microglia-like phenotype and no demyelination could be seen (Figure 4.10; D and A). The number of ED1 positive cells was significantly higher than on d10 p.i. (Figure 4.10, L). A possible explanation might be the longer time period after immunisation in which more of the resident microglia can be activated and also more CD3 positive cells could be seen compared to healthy and sham-immunised animals, contributing to microglial activation.

The remaining 50% of the ONs showed strong demyelination and reduced axonal density (Figure 4.10, E and F). Both demyelination and reduction in axonal density were significantly more severe in these animals than in animals sacrificed on d1 of EAE. Animals developed clinical symptoms on average by d17 p.i. and were then sacrificed, whereas animals without clinical symptoms were sacrificed on d30 p.i. Assuming that they developed optic neuritis around the same time the more extensive demyelination and axonal loss could be explained by the longer period of time after onset of optic neuritis.

These results show that animals can develop optic neurits independently from spinal cord symptoms and that the incidence of optic neuritis is much higher than that of EAE. In patients with MS, optic neuritis is often one of the first symptoms therefore it is not surprising that animals with EAE also develop optic neuritis early. The possibility remains that animals with optic neuritis would have developed spinal cord symptoms later on. Reasons for the early development of optic neuritis without the occurrence of spinal cord symptoms could be for one the higher permeability of the BBB around the optic nerve when compared to the permeability of the BBB at the spinal cord which could lead to higher numbers of infiltrating inflammatory cells

around the ON. It has been shown that the BBB at the ON head is incomplete and thus more permeable than in other areas (Tso *et al.*, 1975; Hu *et al.*, 1998; Hofman *et al.*, 2001). The higher expression of MOG in the ON compared to expression in the spinal cord (Betelli *et al.*, 2003) could lead to more extensive immune response in the ON after infiltration with MOG specific T-cells.

5.6 Calcium influx in the retina and optic nerve started during the induction phase and in the retina it correlated with onset of RGC degeneration

In the retina a significant increase in contrast enhancement could be seen on d5 p.i, d10 p.i and d1 of EAE (Figure 4.20), suggesting an increase in calcium influx. The onset of manganese enhancement correlated well with microglial activation in the retina and onset of RGC degeneration. Experiments with the NMDA-receptor inhibitor MK801 showed that contrast enhancement is significantly reduced at d5 p.i when animals are pretreated with the inhibitor (Figure 4.21), suggesting a role for calcium influx via NMDA-receptors at this timepoint. Since treatment with MK801 reduces calcium influx and glutamate-induced cell death in cultured RGCs (Pang *et al.*, 2007; Hartwick *et al.*, 2008), NMDA receptor modulation might also be considered as a therapeutical target to decrease early death of RGCs. In the optic nerve a significant increase in manganese enhancement could be seen from d10 p.i. onwards (Figure 4.18). It has been shown that exposing spinal cords to glutamate causes paranodal myelin retraction and a subsequent increase in axonal calcium influx can be observed at these exposed paranodes (Fu *et al.*, 2009). Subtle myelin abnormalities starting prior to onset of optic neuritis might make these exposed structures more vulnerable to T-cell or antibody-mediated attacks (Howell *et al.*, 2010) and axons showing alterations and increased calcium influx during the induction phase are therefore likely to be the first affected after onset of optic neuritis.

5.7 Increased calpain activity in the optic nerve and retina correlated with calcium influx and onset of RGC degeneration

In the retina, the amount of calpain-mediated spectrin breakdown product is significantly increased on d5 and d7 p.i, suggesting increased calpain activity. Since onset of RGC degeneration correlates with increased amounts of spectrin breakdown product, increased calpain activity is likely to be involved in early death of RGCs. This is supported by *in vitro* data demonstrating that calpain activity is increased in cultured RGCs after serum starvation and calcium ionophore treatment and that calpain inhibitors promote cell survival in these experiments (Mc Kernan *et al.*, 2007). Additionally, the calpain inhibitor SNJ-1945 ameliorated retinal degeneration in an animal model of glaucoma (Oka *et al.*, 2006a). Proteolysis and hyperphosphorylation of tau have been proposed as neurotoxic (Azuma and Shearer, 2008) and calpain may play a role in both processes. Induction of hypoxia in rat retinas leads to the production of a calpain-specific spectrin breakdown product, proteolysis of pro-caspase 3 and proteolysis of tau. The calpain inhibitor SJA6017 partially inhibited the production of these fragments (Tamada *et al.*, 2005). In a rat model of glaucoma, elevated pressure leads to proteolysis of tau, spectrin and p35 in the retina (Oka *et al.*, 2006, b). There is increasing evidence of cross-talk between the calpain and caspase system (Camins *et al.*, 2006). As mentioned before calpain can cleave pro-caspase 3 into an active form and caspase 3 can cleave the calpain inhibitor calpastatin. These findings make it very plausible that the increased calpain activity in this model plays a crucial role in the early degeneration of RGCs. The reduction in spectrin breakdown product later on might be due to further degradation of spectrin into products that are no longer recognized by the specific antibody.

In the optic nerve calpain activation can bee seen from d10 p.i. onwards, correlating with increased manganese enhancement. As mentioned before, calpain can cleave several cytoskeletal proteins, among them β4-spectrin and ankyrin (Hall *et al.*, 1987; Lövfenberg and Backmann, 1999). β4-spectrin binds ankyrin G to the plasma membrane and actin cytoskeleton (Berghs *et al.*, 2000; Bennett and Baines, 2001) and in the nodes of Ranvier and the axonal initial segment (AIS), the localization of Na_V-channels is highly correlated with that of β4-spectrin and ankyrin G (Kordeli *et al.*, 1995; Bennett and Baines, 2001). In β4-spectrin and ankyrin null neurons, voltage-gated sodium channels are not clustered correctly (Komada and Soriano,

2002). Increased calcium concentration causes a concentration-dependent calpain-mediated proteolysis of β4-spectrin and ankyrin G at the AIS and loss of ion channel clustering. Inhibition of calpain was sufficient to preserve the structure of the AIS (Schafer *et al.*, 2009). The molecular organisation at the nodes of Ranvier is very similar with the same β4-spectrin and ankyrin G-based cytoskeleton (Susuki and Rasband, 2008), suggesting similar results. Increased calpain activation during the induction phase could therefore contribute to subtle axonal changes, including more diffuse localisation of sodium channels around the nodes of Ranvier.

5.8 Reduced degeneration of RGCs and reduced severity of optic neuritis under calpeptin treatment suggests a role for increased calpain activity in these events

Treatment with the calpain inhibitor calpeptin is known to reduce the capability of T-cells to migrate into the CNS and to reduce inflammation, demyelination and axonal loss in the spinal cord (Guyton *et al.*, 2010). In our model, treatment with calpeptin from the day of immunisation onwards reduced infiltration with T-cells and macrophages, demyelination and accumulation of APP in the optic nerve. There was also significant reduction of RGC death during the clinical phase, likely to be connected to reduced severity of optic neuritis, confirming results from experiments in Lews rats with EAE where calpeptin treatment reduced death of RGCs after onset of optic neuritis (Smith *et al.*, 2011). As mentioned before in our model RGC degeneration starts in the induction phase of EAE, prior to onset of optic neuritis. The early death of RGCs is accompanied by increased microglial activation in the retina, calcium influx and increased amount of calpain-specific spectrin breakdown product, suggesting an increase in calpain activity. It has been shown that calpeptin treatment reduces death of cultured RGCs after calcium influx, suggesting that calpain activity is an important factor in RGC degeneration caused by elevated calcium concentration (Das *et al.*, 2006). Treatment with calpeptin significantly reduced the degeneration of RGCs in the induction phase. These results suggest that increased calpain activity plays an important role in the early degeneration of RGCs which can be observed in our model and that calpeptin treatment could be considered as a potential neuroprotective therapy.

References

1. Aizenman, E.; Frosch, M.P.; Lipton, S.A. Responses mediated by excitatory amino acid receptors in solitary retinal ganglion cells from rat J Physiol.;396:75-91 (1988)

2. Araújo, I.M.¸Carreira, B. P.¸Pereira, T.; Santos, P.F.; Soulet, D, Inácio, A.; Bahr, B.A.; Carvalho, A.P.; Ambrósio, A.F.; Carvalho, C.M. Changes in calcium dynamics following the reversal of the sodium-calcium exchanger have a key role in AMPA receptor-mediated neurodegeneration via calpain activation in hippocampal neurons Cell Death Differ. 14(9):1635-46 (2007)

3. Arnold, A.C. Evolving management of optic neuritis and multiple sclerosis Am J Ophthalmol. 139(6):1101-8 (2005)

4. Azuma, M.; Shearer, T.R. The Role of Calcium-Activated Protease Calpain in Experimental Retinal Pathology Survey of Ophthalmology, Volume 53, Issue 2, Pages 150-163 (2008)

5. Bähr, M. Live or let die - retinal ganglion cell death and survival during development and in the lesioned adult CNS Trends Neurosci. 23(10):483-90 (2000)

6. Balashov, K.E.; Rottman, J.B.; Weiner, H.L.; Hancock, W.W. CCR5(+) and CXCR3(+) T cells are increased in multiple sclerosis and their ligands MIP-1alpha and IP-10 are expressed in demyelinating brain lesions Proc Natl Acad Sci U S A. 96(12):6873-8 (1999)

7. Bano, D.; Young, K.W.; Guerin, C.J.; Lefeuvre, R.; Rothwell, N.J.; Naldini, L.; Rizzuto, R.; Carafoli, E.; Nicotera, P. Cleavage of the plasma membrane Na+/Ca2+ exchanger in excitotoxicity Cell. 28;120(2):275-85 (2005)

8.   Barcellos, L.F.; Oksenberg, J.R.; Green, A.J.; Bucher, P.; Rimmler, J.B.; Schmidt, S.; Garcia, M.E.; Lincoln, R.R.; Pericak-Vance, M.A.; Haines, J.L.; Hauser, S.L.; Multiple Sclerosis Genetics Group Genetic basis for clinical expression in multiple sclerosis Brain. 125(Pt 1):150-8 (2002)

9.   Barger, S.W., Goodwin, M.E.; Porter, M.M.; Beggs, M.L. Glutamate release from activated microglia requires the oxidative burst and lipid peroxidation J. Neurochem 101(5): 1205-1213 (2007)

10. Barnett, M.H.; Prineas, J.W. Relapsing and remitting multiple sclerosis: pathology of the newly forming lesion Ann Neurol. 55(4):458-68 (2004)

11. Baron, J.L.; Madri, J.A.; Ruddle, N.H.; Hashim, G.; Janeway, C.A Jr. Surface expression of alpha 4 integrin by CD4 T cells is required for their entry into brain parenchyma J Exp Med. 177(1):57-68 (1993)

12. Beltran, L.; Chaussade, C.; Vanhaesebroeck, B.; Cutillas, P.R. Calpain interacts with class IA phosphoinositide 3-kinases regulating their stability and signaling activity Proc Natl Acad Sci U S A. 108(39):16217-22 (2011)

13. Bennett, V.; Gilligan, D.M. The spectrin-based membrane skeleton and micron-scale organization of the plasma membrane Annu Rev Cell Biol. 9:27-66 (1993)

14. Bennett, V.; Baines, A.J: Spectrin and ankyrin-based pathways: metazoan inventions for integrating cells into tissues. Physiol Rev 81(3):1353-1392 (2001)

15. Ben-Nun, A.; Wekerle, H.; Cohen, I.R. The rapid isolation of clonable antigen-specific T lymphocyte lines capable of mediating autoimmune encephalomyelitis Eur J Immunol. 11(3):195-9 (1981)

16. Berghs, S.; Aggujaro, D.; Dirkx, R.; Maksimova, E.; Stabach, P.; Hermel, J. M.; Zhang, J. P.; Philbrick, W.; Slepnev, V.; Ort, T.; Solimena, M. βIV spectrin, a

new spectrin localized at axon initial segments and nodes of Ranvier in the central and peripheral nervous system. J. Cell Biol. 151:985–1001 (2000)

17. Berkowitz, B.A.; Gradianu, M.; Schafer, S.; Jin, Y.; Porchia, A.; Iezzi, R.; Roberts, R. Ionic Dysregulatory Phenotyping of Pathologic Retinal Thinning with Manganese-Enhanced MRI Invest Ophthalmol Vis Sci. 49(7):3178-84(2008)

18. Berkowitz, B.A.; Roberts, R.; Oleske, D.A.; Chang, M.; Schafer, S.; Bissig, D.; Gradianu, M. Quantitative mapping of ion channel regulation by visual cycle activity in rodent photoreceptors in vivo, Invest. Ophthalmol. Vis. Sci. 50:1880-5 (2009)

19. Betelli, E.; Pagany, M.; Weiner, H.L.; Linington, C.; Sobel, R.A.; Kuchroo, V.K. Myelin oligodendrocyte glycoprotein-specific T cell receptor transgenic mice develop spontaneous autoimmune optic neuritis J Exp Med. 197(9):1073-81 (2003)

20. Bielekova, B.; Martin, R. Development of biomarkers in multiple sclerosis Brain 127 (7): 1463-1478 (2004)

21. Bignami, A.; Dahl, D. The radial glia of Müller in the rat retina and their response to injury. An immunofluorescence study with antibodies to the glial fibrillary acidic (GFA) protein Exp Eye Res. 28(1):63-9 (1979)

22. Bjartmar, C.; Trapp, B.D. Axonal degeneration and progressive neurologic disability in multiple sclerosis Neurotox Res. 5(1-2):157-64 (2003)

23. Björklund, H.; Dahl, D. Glial fibrillary acidic protein (GFAP)-like immunoreactivity in the rodent eye. Comparison between peripheral glia of the anterior uvea and central glia of the retina J Neuroimmunol. 8(4-6):331-45 (1985)

24. Black, J.A.; Liu, S.; Hains B.C.; Saab C.Y.; Waxman S.G. Long-term protection of central axons with phenytoin in monophasic and chronic-relapsing EAE Brain 129(12), 3196-3208 (2006)

25. Bozic, C.R.; Kolakowski, L.F Jr.; Gerard, N.P.; Garcia-Rodriguez, C.; von Uexkull-Guldenband, C.; Conklyn, M.J.; Breslow, R.; Showell, H.J.; Gerard C. Expression and biologic characterization of the murine chemokine KC J Immunol. 154(11):6048-57 (1995)

26. Bozzali, M.; Wrabetz, L. Axonal signals and oligodendrocyte differentiation Neurochem Res. 29(5):979-88 (2004)

27. Bradley, W.G. Recent views on amyotrophic lateral sclerosis with emphasis on electrophysiological studies Muscle Nerve. 10(6):490-502 (1987)

28. Brettschneider, J.; Czerwoniak, A.; Senel, M.; Fang, L.; Kassubek, J.; Pinkhardt, E.; Lauda, F.; Kapfer, T.; Jesse, S.; Lehmensiek, V.; Ludolph, A.C.; Otto, M.; Tumani, H. The chemokine CXCL13 is a prognostic marker in clinically isolated syndrome (CIS) PLoS One.5(8):e11986 (2010)

29. Bringmann, A.; Iandiev, I.; Pannicke, T.; Wurm, A.; Hollborn, M.; Wiedemann, P.; Osborne, N.N.; Reichenbach, A. Cellular signaling and factors involved in Müller cell gliosis: neuroprotective and detrimental effects Prog Retin Eye Res. 28(6):423-51 (2009)

30. Brock, T.O.; O'Callaghan, J.P. Quantitative changes in the synaptic vesicle proteins synapsin I and p38 and the astrocyte-specific protein glial fibrillary acidic protein are associated with chemical-induced injury to the rat central nervous system J Neurosci. 7(4):931-42 (1987)

31. Brück, W. The pathology of multiple sclerosis is the result of focal inflammatory demyelination with axonal damage J Neurol. 252 Suppl 5:v3-9 (2005)

32. Burnashev, N.; Monyer, H.; Seeburg, P.H.; Sakmann, B. Divalent ion permeability of AMPA receptor channels is dominated by the edited form of a single subunit Neuron 8(1):189-98 (1992)

33. Butler, J.T.; Samantaray, S.; Beeson, C.C.; Ray, S.K.; Banik, N.L. Involvement of calpain in the process of Jurkat T cell chemotaxis J Neurosci Res. 15;87(3):626-35 (2009)

34. Camins A, Verdaguer E, Folch J, Pallàs M. Involvement of calpain activation in neurodegenerative processes CNS Drug Rev.12(2):135-48 (2006)

35. Cardone, M.H.; Roy, N.; Stennicke, H.R.; Salvesen, G.S.; Franke, T.F.; Stanbridge, E.; Frisch, S.; Reed, J.C. Regulation of cell death protease caspase-9 by phosphorylation Science. 282(5392):1318-21 (1998)

36. Cenni, M.C.; Bonfanti, L.; Martinou, J.C.; Ratto, G.M.; Strettoi, E.; Maffei, L. Long-term survival of retinal ganglion cells following optic nerve section in adult bcl-2 transgenic mice Eur J Neurosci. 8(8):1735-45 (1996)

37. Chang, A.; Tourtellotte, W.W.; Rudick, R.; Trapp, B.D. Premyelinating Oligodendrocytes in Chronic Lesions of Multiple Sclerosis N. Engl. J. Med., 346(3): 165 – 173 (2002)

38. Charcot, J.-M. "Histologie de la sclerose en plaques". Gazette des hopitaux (Paris) 41: 554–55 (1868)

39. Clineschmidt, B. V.; Williams, M.; Witoslawski, J. J.; Bunting, P. R.; Risley, E. A.; Totaro, J. A. Restoration of shock-suppressed behavior by treatment with (+)-5-methyl-10,11-dihydro-5H-dibenzo[a, d]cyclohepten-5, 10-imine (MK-801), a substance with potent anticonvulsant, central sympathomimetic, and apparent anxiolytic properties Drug Development Research, 2: 147–163 (1982)

40. Coles, A.J.; Cox, A.; Le Page, E.; Jones, J.; Trip, S.A.; Deans, J.; Seaman, S.; Miller, D.H.; Hale, G.; Waldmann, H.; Compston, D.A. The window of therapeutic opportunity in multiple sclerosis: evidence from monoclonal antibody therapy J Neurol. 253(1):98-108 (2006)

41. Compston, A.; Coles, A. Multiple Sclerosis Lancet 359(9313), 1221-31 (2002)

42. Confavreux, C.; Vukusic, S. Age at disability milestones in multiple sclerosis Brain. 129(Pt 3):595-605 (2006)

43. Committee on Multiple Sclerosis Clinical and biological features. In: Joy, J.E.; Johnston, J.B. Jr Multiple sclerosis status and strategies for the future National Academics Press s. 30 (2001)

44. Cua, D.J.; Sherlock, J.; Chen, Y.; Murphy, C.A.; Joyce, B.; Seymour, B.; Lucian, L.; To, W.; Kwan, S.; Churakova, T.; Zurawski, S.; Wiekowski, M.; Lira, S.A.; Gorman, D.; Kastelein, R.A.; Sedgwick, J.D. Interleukin-23 rather than interleukin-12 is the critical cytokine for autoimmune inflammation of the brain Nature 421(6924):744-8 (2003)

45. Curtis, D.R.; Johnston, G.A. Amino acid transmitters in the mammalian central nervous system. Ergeb Physiol 69:97–188 (1974)

46. Czogalla, A.; Sikorski, A. F. Spectrin and calpain: a 'target' and a 'sniper' in the pathology of neuronal cells. Cellular and molecular life sciences: CMLS ; 62(17):1913-24 (2005)

47. Das, A.; Garner, D.P.; Del Re, A.M.; Woodward, J.J.; Kumar, D.M.; Agarwal, N.; Banik, N.L.; Ray, S.K. Calpeptin provides functional neuroprotection to rat retinal ganglion cells following Ca2+ influx Brain Res. 1084(1):146-57 (2006)

48. Danke, N.A.; Koelle, D.M.; Yee, C.; Beheray, S.; Kwok, W.W. Autoreactive T cells in healthy individuals J Immunol. 15;172(10):5967-72 (2004)

49. Datta, S.R.; Dudek, H.; Tao, X.; Masters, S.; Fu, H.; Gotoh, Y.; Greenberg, M.E. Akt phosphorylation of BAD couples survival signals to the cell-intrinsic death machinery Cell. 91(2):231-41 (1997)

50. Del Rio-Hortega, P.: Microglia. In: Penfield, W. Cytology and cellular pathology of the nervous system p. 483-534 (1932)

51. De Groot, C.J.; Bergers, E.; Kamphorst, W.; Ravid, R.; Polman, C.H.; Barkhof, F.; van der Valk, P. Post-mortem MRI-guided sampling of multiple sclerosis brain lesions: increased yield of active demyelinating and (p)reactive lesions. Brain 124:1635-45 (2001)

52. De Stefano, N.; Matthews, P.M.; Fu, L.; Narayanan, S.; Stanley, J.; Francis, G.S.; Antel, J.P.; Arnold, D.L. Axonal damage correlates with disability in patients with relapsing-remitting multiple sclerosis. Results of a longitudinal magnetic resonance spectroscopy study Brain. 121 (Pt 8):1469-77 (1998)

53. Detels, R.; Visscher, B.R.; Malmgren, R.M.; Coulson, A.H.; Lucia, M.V.; Dudley, J.P. Evidence for lower susceptibility to multiple sclerosis in Japanese-Americans Am J Epidemiol. 105(4):303-10 (1977)

54. Diem, R.; Meyer, R.; Weishaupt, J.H.; Bahr, M. Reduction of potassium currents and phosphatidylinositol 3-kinase-dependent AKT phosphorylation by tumor necrosis factor-(alpha) rescues axotomized retinal ganglion cells from retrograde cell death in vivo J Neurosci.;21(6):2058-66 (2001)

55. Diem, R., Sättler, M.B., Maier, K., Bähr, M., Molecular mechanisms of neuronal apoptosis in chronic inflammatory CNS diseases. Signal Trans. 5, 250–255 (2005a)

56. Diem, R.; Taheri, N.; Dietz, G.P.; Kuhnert, A.; Maier, K.; Sättler, M.B.; Gadjanski, I.; Merkler, D.; Bähr, M. HIV-Tat-mediated Bcl-XL delivery protects retinal ganglion cells during experimental autoimmune optic neuritis Neurobiol Dis. 20(2):218-26 (2005b)

57. Dujmovic, I. Cerebrospinal Fluid and Blood Biomarkers of Neuroaxonal Damage in Multiple Sclerosis Multiple Sclerosis International Volume 2011: 1-18 (2011)

58. Dutta, R.; McDonough, J.; Yin, X.; Peterson, J.; Chang, A.; Torres, T.; Gudz, T.; Macklin, W.B.; Lewis, D.A.; Fox, R.J.; Rudick, R.; Mirnics, K.; Trapp, B.D. Mitochondrial dysfunction as a cause of axonal degeneration in multiple sclerosis patients Ann Neurol. 59(3):478-89 (2006)

59. Ebers, G.C.; Sadovnick, A.D.; Risch, N.J. A genetic basis for familial aggregation in multiple sclerosis. Canadian Collaborative Study Group Nature 377(6545):150-1 (1995)

60. Eng, L.F.; Ghirnikar, R.S.; Lee, Y.L. Glial fibrillary acidic protein: GFAP-thirty-one years (1969-2000) Neurochem Res. 25(9-10):1439-51 (2000)

61. Engelhardt, B.; Ransohoff, R.M. The ins and outs of T-lymphocyte trafficking to the CNS: anatomical sites and molecular mechanisms Trends Immunol. 26(9):485-95 (2005)

62. Ferguson, B.; Matyszak, M.K.; Esiri, M.M.; Perry, V.H. Axonal damage in acute multiple sclerosis lesions Brain. 120 (Pt 3):393-9 (1997)

63. Fisher J.B.; Jacobs D.A.; Markowitz C.E.; Galetta S.L.; Volpe N.J.; Nano-Schiavi, ML.; Baier, M.L.; Frohman, E.M.; Winslow, H.; Frohman, T.C.; Calabresi, P.A.; Maguire, M.G.; Cutter, G.R.; Balcer, L.J. Relation of visual function to retinal nerve fiber layer thickness in multiple sclerosis Ophthalmol 113:324-32 (2006)

64. Fonnum, F. Glutamate: a neurotransmitter in mammalian brain J Neurochem.;42(1):1-11 (1984)

65. Franklin, R.J.M. Why does remyelination fail in multiple sclerosis? Nat Rev Neurosci 3(9): 705-14 (2002)

66. Fu, Y.; Sun, W.; Shi, Y.; Shi, R.; Cheng, J.X. Glutamate excitotoxicity inflicts paranodal myelin splitting and retraction PLoS One.; 4 (8) (2009)

67. Gadjanski, I.; Boretius, S.; Williams, S.K.; Lingor, P.; Knöferle, J.; Sättler, M.B.; Fairless, R.; Hochmeister, S.; Sühs, K.W.; Michaelis, T.; Frahm, J.; Storch, M.K.; Bähr, M.; Diem, R. Role of n-type voltage-dependent calcium channels in autoimmune optic neuritis.Ann Neurol. 66(1):81-93 (2009)

68. Garcia-Valenzuela, E.; Gorczyca, W.; Darzynkiewicz, Z.; Sharma, S.C. Apoptosis in adult retinal ganglion cells after axotomy J Neurobiol. 25(4):431-8 (1994)

69. Garden, G.A.; Möller, T. Microglia biology in health and disease J Neuroimmune Pharmacol. 1(2):127-37 (2006)

70. Gay, F.W.; Drye, T.J.; Dick, G.W.; Esiri, M. M. The application of multifactorial cluster analysis in the staging of plaques in early multiple sclerosis. Identification and characterization of the primary demyelinating lesion Brain 120 (8): 1461-1483 (1997)

71. Gehrmann, J.; Matsumoto, Y.; Kreutzberg, G.W. Microglia: intrinsic immuneffector cell of the brain Brain Res Brain Res Rev. (3):269-87 (1995)

72. George, E.B.; Glass, J.D.; Griffin, J.W. Axotomy-induced axonal degeneration is mediated by calcium influx through ion-specific channels J Neurosci. 15(10):6445-52 (1995)

73. Gil-Parrado, S.; Fernández-Montalván, A.; Assfalg-Machleidt, I.; Popp, O.; Bestvater, F.; Holloschi, A.; Knoch, T.A.; Auerswald, E.A.; Welsh, K.; Reed, J.C.; Fritz, H.; Fuentes-Prior, P.; Spiess, E.; Salvesen, G.S.; Machleidt, W.

Ionomycin-activated calpain triggers apoptosis. A probable role for Bcl-2 family members J Biol Chem. 277(30):27217-26 (2002)

74. Gold, R.; Linington, C.; Lassmann, H. Understanding pathogenesis and therapy of multiple sclerosis via animal models: 70 years of merits and culprits in experimental autoimmune encephalomyelitis research Brain 129(Pt 8):1953-71 (2006)

75. Goldenberg-Cohen, N.; Dratviman-Storobinsky, O.; Dadon Bar El, S.; Cheporko, Y.; Hochhauser, E. Protective effect of bax ablation against cell loss in the retinal ganglion layer induced by optic nerve crush in transgenic mice J Neuroophthalmol. 31(4):331-8 (2011)

76. Goverman, J.; Woods, A.; Larson, L.; Weiner, L.P.; Hood, L.; Zaller, D.M. Transgenic mice that express a myelin basic protein-specific T cell receptor develop spontaneous autoimmunity Cell.;72(4):551-60 (1993)

77. Green, A.J.; McQuaid, S.; Hauser, S.L.; Allen, I.V.; Lyness R. Ocular pathology in multiple sclerosis: retinal atrophy and inflammation irrespective of disease duration Brain 133:1591-601 (2010)

78. Guyton, M.K.; Brahmachari, S.; Das, A.; Samantaray, S.; Inoue, J.; Azuma, M.; Ray, S.K.; Banik N.L. Inhibition of calpain attenuates encephalitogenicity of MBP-specific T cells J Neurochem110(6):1895-907 (2009)

79. Guyton, M.K.; Das, A.; Samantaray, S.; Wallace, G.C. 4th; Butler, J.T.; Ray, S.K.; Banik, N.L Calpeptin attenuated inflammation, cell death, and axonal damage in animal model of multiple sclerosis J Neurosci Res. 88(11):2398-408 (2010)

80. Hains, B.C and Waxman, S.G. Neuroprotection by Sodium Channel Blockade with Phenytoin in an Experimental Model of Glaucoma Invest. Ophthalmol. Vis. Sci., 46(11):4164 -4169 (2005)

81. Hall T.G.; Bennett, V. Regulatory domains of erythrocyte ankyrin J Biol Chem. 262(22):10537-45 (1987)

82. Hall, P.A.; Levison, D.A.; Woods, A.L.; Yu, C.C.; Kellock, D.B.; Watkins, J.A.; Barnes, D.M.; Gillett, C.E.; Camplejohn, R.; Dover, R.; Waseem, N.H.; Lane, D.P. Proliferating cell nuclear antigen (PCNA) immunolocalization in paraffin sections: an index of cell proliferation with evidence of deregulated expression in some neoplasms J Pathol. 162(4):285-94 (1990)

83. Hanisch U.K. Microglia as a source and target of cytokines Glia 40(2):140-55 (2002)

84. Hanisch, U.K.; Kettenmann, H. Microglia: active sensor and versatile effector cells in the normal and pathologic brain Nat Neurosci 10: 1387-1393 (2007)

85. Hara, M.R.; Snyder, S.H. Cell signaling and neuronal death Annu Rev Pharmacol Toxicol. 47:117-41 (2007)

86. Hartung, H.P.; Gonsette, R.; König, N.; Kwiecinski, H.; Guseo, A.; Morrissey, S.P.; Krapf, H.; Zwingers, T. Mitoxantrone in Multiple Sclerosis Study Group (MIMS) Mitoxantrone in progressive multiple sclerosis: a placebo-controlled, double-blind, randomised, multicentre trial Lancet. 360(9350):2018-25 (2002)

87. Hartwick, A.T.; Hamilton, C.M.; Baldridge, W.H. Glutamatergic calcium dynamics and deregulation of rat retinal ganglion cells J Physiol. 15;586(14):3425-46 (2008)

88. Henderson A.P.D.; Trip A.S.; Schlottmann P.G.; Altmann D.R.; Garway-Heath D.F.; Plant, G.T.; Miller, D.H. An investigation of the retinal nerve fibre layer in progressive multiple sclerosis using optical coherence tomography. Brain 131:277-87 (2008)

89. Henderson, A.P.D.; Altmann, D.R.; Trip, A.S.; Kallis, C.; Jones, S.J.; Schlottmann, P.G.; Garway-Heath, D.F.; Plant, G.T.; Miller, D.H. A serial study

of retinal changes following optic neuritis with sample size estimates for acute neuroprotection trials. Brain 133:2592-602 (2010)

90. Hickey, W.F. The pathology of multiple sclerosis: a historical perspective J Neuroimmunol. 1;98(1):37-44 (1999)

91. Hinkerohe, D.; Smikalla, D.; Haghikia, A.; Heupel, K.; Haase, C.G.; Dermietzel, R.; Faustmann.; P.M. Effects of cytokines on microglial phenotypes and astroglial coupling in an inflammatory coculture model Glia 52(2):85-97 (2005)

92. Hjelmström, P.; Juedes, A.E.; Fjell, J.; Ruddle, N.H. B-cell-deficient mice develop experimental allergic encephalomyelitis with demyelination after myelin oligodendrocyte glycoprotein sensitization. J Immunol. 161: 4480-3 (1998)

93. Hobom. M.; Storch, M.K.; Weissert, R.; Maier, K.; Radhakrishnan, A.; Kramer, B.; Bähr, M.; Diem, R Mechanisms and time course of neuronal degeneration in experimental autoimmune encephalomyelitis Brain Pathol. 14(2):148-57 (2004)

94. Hofman, P.; Hoyng, P.; van der Werf, F.; Vrensen, G.F.; Schlingemann, R.O. Lack of blood-brain barrier properties in microvessels of the prelaminar optic nerve head Invest Ophthalmol Vis Sci 42(5):895-901 (2001)

95. Hollmann, M .; Hartley, M.; Heinemann, S. Ca2+ permeability of KA-AMPA-- gated glutamate receptor channels depends on subunit composition Science 252 (5007): 851-3 (1991)

96. Howell, O.W.; Palser, A.; Polito, A.; Melrose, S.; Zonta, B.; Scheiermann, C.; Vora, A.J.; Brophy, P.J.; Reynolds, R. Disruption of neurofascin localization reveals early changes preceding demyelination and remyelination in multiple sclerosis Brain. 129(Pt 12):3173-85 (2006)

97. Howell, O.W.; Rundle, J.L.; Garg, A.; Komada, M.; Brophy, P.J.; Reynolds, R. Activated microglia mediate axoglial disruption that contributes to axonal injury in multiple sclerosis J Neuropathol Exp Neurol. 69(10):1017-33 (2010)

98. Hu, P.; Pollard, J.; Hunt, N.; Chan-Ling, T. Microvascular and cellular responses in the optic nerve of rats with acute experimental allergic encephalomyelitis (EAE). Brain Pathol 8:475-86 (1998)

99. Huang, W.; Fileta, J.B.; Dobberfuhl, A.; Filippopolous, T.; Guo, Y.; Kwon, G.; Grosskreutz, C.L. Calcineurin cleavage is triggered by elevated intraocular pressure, and calcineurin inhibition blocks retinal ganglion cell death in experimental glaucoma Proc Natl Acad Sci U S A. 102(34):12242-7 (2005)

100. Huh, G.Y.; Glantz, S.B.; Je, S.; Morrow, J.S.; Kim, J.H. Calpain proteolysis of alpha II-spectrin in the normal adult human brain. Neuroscience letters; 316(1):41-4 (2001)

101. Huitinga, I.; Ruuls, S.R.; Jung, S.; Van Rooijen, N.; Hartung, H.P.; Dijkstra CD. Macrophages in T cell line-mediated, demyelinating, and chronic relapsing experimental autoimmune encephalomyelitis in Lewis rats Clin Exp Immunol. 100(2):344-51 (1995)

102. Imaizumi, T.; Kocsis, J.D.; Waxman, S.G. The role of voltage-gated Ca2+ channels in anoxic injury of spinal cord white matter. Brain Res 817, 84-92 (1999).

103. Inglese, M. Multiple sclerosis: new insights and trends AJNR Am J Neuroradiol. (5):954-7 (2006)

104. Isenmann, S.; Wahl, C.; Krajewski, S.; Reed, J.C.; Bähr, M. Up-regulation of Bax protein in degenerating retinal ganglion cells precedes apoptotic cell death after optic nerve lesion in the rat Eur J Neurosci. 9(8):1763-72 (1997)

105. Issazadeh, S.; Ljungdahl, A.; Höjeberg, B.; Mustafa, M.; Olsson, T. Cytokine production in the central nervous system of Lewis rats with experimental autoimmune encephalomyelitis: dynamics of mRNA expression for interleukin-10.; interleukin-12.; cytolysin.; tumor necrosis factor alpha and tumor necrosis factor beta J Neuroimmunol. 61(2):205-12 (1995)

106. Jakobs, .T.C.; Ben, Y.; Masland, R.H. Expression of mRNA for glutamate receptor subunits distinguishes the major classes of retinal neurons, but is less specific for individual cell types Mol Vis. 18;13:933-48 (2007)

107. Johnson, K.P.; Brooks, B.R.; Cohen, J.A.; Ford, C.C.; Goldstein, J.; Lisak, R.P.; Myers, L.W.; Panitch, H.S.; Rose, J.W.; Schiffer, R.B. Copolymer 1 reduces relapse rate and improves disability in relapsing-remitting multiple sclerosis: results of a phase III multicenter, double-blind placebo-controlled trial. The Copolymer 1 Multiple Sclerosis Study Group Neurology. 45(7):1268-76 (1995)

108. Jonas, P.; Burnashev, N. Molecular mechanisms controlling calcium entry through AMPA-type glutamate receptor channels Neuron. 15(5):987-90 (1995)

109. Karschin, A.; Aizenman, E.; Lipton, S.A. The interaction of agonists and noncompetitive antagonists at the excitatory amino acid receptors in rat retinal ganglion cells in vitro J Neurosci. 8(8):2895-906 (1988)

110. Kato, H.; Takahashi, A.; Itoyama, Y. Cell cycle protein expression in proliferating microglia and astrocytes following transient global cerebral ischemia in the rat Brain Res Bull. 60(3):215-21 (2003)

111. Kermer, P.; Klöcker, N.; Labes, M., Thomsen, S.; Srinivasan, A.; Bähr, M. Activation of caspase-3 in axotomized rat retinal ganglion cells in vivo FEBS Lett. 453(3):361-4 (1999)

112. Kermer, P.; Klöcker, N.; Labes, M..; Bähr, M. Insulin-like growth factor-I protects axotomized rat retinal ganglion cells from secondary death via PI3K-

dependent Akt-phosphorylation and inhibition of caspase-3 in vivo. J. Neurosci. 20:722-8 (2000)

113. Kharbanda, S.; Pandey, P.; Schofield, L.; Israels, S.; Roncinske, R.; Yoshida, K.; Bharti, A.; Yuan, Z.M.; Saxena, S.; Weichselbaum, R.; Nalin, C.; Kufe, D. Role for Bcl-xL as an inhibitor of cytosolic cytochrome C accumulation in DNA damage-induced apoptosis Proc Natl Acad Sci U S A. 94(13):6939-42 (1997)

114. Kirk ,J.; Plumb, J.; Mirakhur, M.; McQuaid, S Tight junctional abnormality in multiple sclerosis white matter affects all calibres of vessel and is associated with blood-brain barrier leakage and active demyelination J Pathol. 201:319–27 (2003)

115. Komada, M.; Soriano, P. [Beta]IV-spectrin regulates sodium channel clustering through ankyrin-G at axon initial segments and nodes of Ranvier J Cell Biol. 156(2):337-48 (2002)

116. Kordeli, E.; Lambert, S.; Bennett, V. AnkyrinG. A new ankyrin gene with neural-specific isoforms localized at the axonal initial segment and node of Ranvier J Biol Chem. 270(5):2352-9 (1995)

117. Kornek. B.; Storch, M.K.; Djamshidian, A.; Weissert, R.; Wallstroem, E.; Stefferl, A.; Zimprich, F.; Olsson, T.; Linington, C.; Schmidbauer, M.; Lassmann, H Multiple sclerosis and chronic autoimmune encephalomyelitis: a comparative quantitative study of axonal injury in active, inactive, and remyelinated lesions Am J Pathol. 157(1):267-76 (2000)

118. Kornek. B.; Storch, M.K.; Djamshidian, A.; Weissert, R.; Wallstroem, E.; Stefferl, A.; Zimprich, F.; Olsson, T.; Linington, C.; Schmidbauer, M.; Lassmann, H.; Distribution of a calcium channel subunit in dystrophic axons in multiple sclerosis and experimental autoimmune encephalomyelitis. Brain 124:1114-24 (2001)

119. Korsmeyer, S.J. BCL-2 gene family and the regulation of programmed cell death Cancer Res. 59(7 Suppl):1693s-1700s (1999)

120. Kreutzberg, G.W. Microglia: a sensor for pathological events in the CNS. Trends Neurosci. 19, 312–318(1996)

121. Kuhlmann, T.; Lingfeld, G.; Bitsch, A.; Schuchardt, J.; Brück, W. Acute axonal damage in multiple sclerosis is most extensive in early disease and decreases over time. Brain 125 (10):2202-12 (2002)

122. Lam, T.T.; Abler, A.S.; Kwong, J.M.; Tso, M.O. N-methyl-D-aspartate (NMDA)-induced apoptosis in rat retina. Invest Ophthalmol Vis Sci. 40(10):2391-7 (1999)

123. Lassmann, H.; Bartsch, U.; Montag, D.; Schachner, M. Dying-back oligodendrogliopathy: a late sequel of myelin-associated glycoprotein deficiency Glia. 19(2):104-10 (1997)

124. Latov, N.; Nilaver, G.; Zimmerman, E.A.; Johnson. W.G.; Silverman. A.J.; Defendini. R.; Cote. L. Fibrillary astrocytes proliferate in response to brain injury: a study combining immunoperoxidase technique for glial fibrillary acidic protein and radioautography of tritiated thymidine Dev Biol. 72(2):381-4 (1979)

125. Lee KS, Frank S, Vanderklish P, Arai A, Lynch G. Inhibition of proteolysis protects hippocampal neurons from ischemia. Proc Natl Acad Sci U S A 88(16): 7233–7237 (1991)

126. Lev, N.; Barhum, Y.; Melamed, E.; Offen, D. Bax-ablation attenuates experimental autoimmune encephalomyelitis in mice Neurosci Lett. 359(3):139-42 (2004)

127. Li, S; Jiang, Q.; Stys, P. Important Role of Reverse Na^+-Ca^{2+} Exchange in Spinal Cord White Matter Injury at Physiological Temperature The Journal of Neurophysiology Vol. 84 No. 2:1116-1119 (2000)

128. Liedtke W.; Malessa R.; Faustmann P.M.; Eis-Hübinger A.M. Human herpesvirus 6 polymerase chain reaction findings in human immunodeficiency virus associated neurological disease and multiple sclerosis. J Neurovirol. 1(3-4):253-8 (1995)

129. Lin, Y.J.; Koretsky, A.P. Manganese ion enhances T1-weighted MRI during brain activation: an approach to direct imaging of brain function Magn Reson Med. 38(3): 378-88 (1997)

130. Lingor, P.; Koeberle, P.; Kügler, S.; Bähr, M. Down-regulation of apoptosis mediators by RNAi inhibits axotomy-induced retinal ganglion cell death in vivo Brain 128(Pt 3):550-8 (2005)

131. Liu, M.C.; Akle, V.; Zheng, W.; Kitlen, J.; O'Steen, B.; Larner, S.F.; Dave, J.R.; Tortella, F.C.; Hayes, R.L.; Wang, K.K. Extensive degradation of myelin basic protein isoforms by calpain following traumatic brain injury : J Neurochem.;98(3):700-12(2006)

132. Lloyd, K.G. CNS compensation to dopamine neuron loss in Parkinson's disease Adv Exp Med Biol. 90:255-66 (1977)

133. Löfvenberg, L.; Backman, L. Calpain-induced proteolysis of beta-spectrins FEBS Lett. 443(2):89-92 (1999)

134. Lucchinetti, C.; Brück, W.; Parisi, J.; Scheithauer, B.; Rodriguez, M.; Lassmann, H. Heterogeneity of multiple sclerosis lesions: implications for the pathogenesis of demyelination. Annals of neurology 47(6):707-17 (2000)

135. Ludwin S.K.; Johnson E.S. Evidence for a "dying-back" gliopathy in demyelinating disease Ann Neurol. 9(3):301-5 (1981)

136. Lucas, D.R.; Newhouse, J.P. The toxic effect of sodium L-glutamate on the inner layers of the retina AMA Arch Ophthalmol. 58(2):193-201 (1957)

137. Lyons, S.A.; Pastor, A; Ohlemeyer, C.; Kann, O.; Wiegand, F.; Prass, K.; Knapp, F.; Kettenmann, H.; Dirnagl, U. Distinct Physiologic Properties of Microglia and Blood-Borne Cells in Rat Brain Slices After Permanent Middle Cerebral Artery Occlusion Journal of Cerebral Blood Flow & Metabolism 20, 1537–1549 (2000)

138. Maier, K.; Merkler, D.; Gerber, J.; Taheri, N.; Kuhnert, A.V.; Williams, S.K.; Neusch, C.; Bähr, M.; Diem R. Multiple neuroprotective mechanisms of minocycline in autoimmune CNS inflammation. Neurobiol Dis. 25(3):514-25 (2007)

139. Marik, C.; Felts, PA.; Bauer, J.; Lassmann, H.; Smith, K.J. Lesion genesis in a subset of patients with multiple sclerosis: a role for innate immunity? Brain 130(Pt 11):2800-15 (2007)

140. Martinou, J.C.; Dubois-Dauphin, M.; Staple, J.K.; Rodriguez, I.; Frankowski, H.; Missotten, M.; Albertini, P.; Talabot, D.; Catsicas, S.; Pietra, C. Overexpression of BCL-2 in transgenic mice protects neurons from naturally occurring cell death and experimental ischemia Neuron. 13(4):1017-30 (1994)

141. Matute, C.; Sánchez-Gómez, M.V.; Martínez-Millán, L.; Miledi, R. Glutamate receptor-mediated toxicity in optic nerve oligodendrocytes Proc Natl Acad Sci U S A. 94(16):8830-5 (1997)

142. Mayer, M.L.; Westbrook, G.L. The physiology of excitatory amino acids in the vertebrate central nervous system Prog Neurobiol. 28(3):197-276 (1987)

143. McDonald, J.W.; Althomsons, S.P.; Hyrc, K.L.; Choi, D.W.; Goldberg, M.P. Oligodendrocytes from forebrain are highly vulnerable to AMPA/kainate receptor-mediated excitotoxicity Nat Med. (3):291-7 (1998)

144. McDonald, W.I.; Compston, A.; Edan, G.; Goodkin, D.; Hartung, H.P.; Lublin, F.D.; McFarland, H.F.; Paty, D.W.; Polman, C.H.; Reingold, S.C.; Sandberg-Wollheim, M.; Sibley, W.; Thompson, A.; van den Noort, S.; Weinshenker, B.Y.; Wolinsky, J.S. Recommended diagnostic criteria for multiple sclerosis: guidelines from the International Panel on the diagnosis of multiple sclerosis Ann Neurol.;50(1):121-7 (2001)

145. McKernan. D.P.; Guerin, M.B.; O'Brien, C.J.; Cotter, T.G. A key role for calpains in retinal ganglion cell death Invest Ophthalmol Vis Sci.;48(12):5420-30 (2007)

146. Meyer, R.; Weissert, R.; Diem, R.; Storch, M.K.; de Graaf, K.L.; Kramer, B.; Bahr, M. Acute neuronal apoptosis in a rat model of multiple sclerosis J Neurosci. 21(16):6214-20 (2001)

147. Michel, L.; Berthelot, L.; Pettré, S.; Wiertlewski, S.; Lefrère, F.; Braudeau, C.; Brouard, S.; Soulillou, J.P.; Laplaud, D.A. Patients with relapsing-remitting multiple sclerosis have normal Treg function when cells expressing IL-7 receptor α-chain are excluded from the analysis J Clin Invest. 118(10): 3411–3419 (2008)

148. Mirandola, P.; Stefan, A.; Brambilla, E.; Campadelli-Fiume, G.; Grimaldi, L.M. Absence of human herpesvirus 6 and 7 from spinal fluid and serum of multiple sclerosis patients. Neurology 53(6):1367-8 (1999)

149. Morgan, J.; Caprioli, J.; Koseki, Y. Nitric oxide mediates excitotoxic and anoxic damage in rat retinal ganglion cells cocultured with astroglia Arch Ophthalmol.117(11):1524-9 (1999)

150. Nair, A.; Frederick, T.J.; Miller, S.D. Astrocytes in multiple sclerosis: a product of their environment Cell Mol Life Sci. 65(17):2702-20 (2008)

151. Nath, R.; Davis, M.; Probert, A.W.; Kupina, N.C.; Ren, X.; Schielke, G.P.; Wang, K.K. Processing of cdk5 activator p35 to its truncated form (p25) by

calpain in acutely injured neuronal cells Biochem Biophys Res Commun. 274(1):16-21 (2000)

152. Niller, H.H.; Wolf, H.; Minarovits, J. Regulation and dysregulation of Epstein-Barr virus latency: implications for the development of autoimmune diseases. Autoimmunity 41(4):298-328 (2008)

153. Norton, W.T.; Aquino, D.A.; Hozumi, I.; Chiu, F.C.; Brosnan, C.F. Quantitative aspects of reactive gliosis: a review Neurochem Res. 17(9):877-85 (1992)

154. Offen, D.; Kaye, J.F.; Bernard, O.; Merims, D.; Coire, C.I.; Panet, H.; Melamed, E.; Ben-Nun, A. Mice overexpressing Bcl-2 in their neurons are resistant to myelin oligodendrocyte glycoprotein (MOG)-induced experimental autoimmune encephalomyelitis (EAE) J Mol Neurosci. 15(3):167-76 (2000)

155. Ohgoh, M.; Hanada, T.; Smith, T.; Hashimoto, T.; Ueno, M.; Yamanishi, Y.; Watanabe, M.; Nishizawa, Y. Altered expression of glutamate transporters in experimental autoimmune encephalomyelitis J Neuroimmunol. 125(1-2):170-8 (2002)

156. Oka, T.; Walkup, R.D.; Tamada, Y.; Nakajima, E.; Tochigi, A.; Shearer, T.R.; Azuma, M. Amelioration of retinal degeneration and proteolysis in acute ocular hypertensive rats by calpain inhibitor ((1S)-1-((((1S)-1-benzyl-3-cyclopropylamino-2,3-di-oxopropyl)amino)carbonyl)-3-methylbutyl)carbamic acid 5-methoxy-3-oxapentyl ester. Neuroscience.;141(4):2139-45 (2006)

157. Oka, T.; Tamada, Y.; Nakajima, E.; Shearer, T.R.; Azuma, M. Presence of calpain-induced proteolysis in retinal degeneration and dysfunction in a rat model of acute ocular hypertension J Neurosci Res. 83(7):1342-51 (2006)

158. Oksenberg, J.R.; Hauser, S.L. Genetic of multiple sclerosis. In: Raine, C.S.; McFarland, H.F.; Hohlfeld, R. Multiple Sclerosis A Comprehensive Text Saunders Elsevier s. 214-222 (2008)

159. Olney, J.W. Glutamate-induced retinal degeneration in neonatal mice. Electron-microscopy of the acutely evolving lesion. J Neuropathol Exp Neurol 28: 455-474 (1969)

160. Osborne, N.N.; Block, F.; Sontag, K.H. Reduction of ocular blood flow results in glial fibrillary acidic protein (GFAP) expression in rat retinal Müller cells Vis Neurosci. 7(6):637-9 (1991)

161. Ost, M.; Nylén, K.; Csajbok, L.; Ohrfelt, A.O.; Tullberg, M.; Wikkelsö, C.; Nellgård, P.; Rosengren, L.; Blennow, K.; Nellgård, B. Initial CSF total tau correlates with 1-year outcome in patients with traumatic brain injury Neurology 67(9):1600-4 (2006)

162. Padgett, B.L.; Walker, D.L.; ZuRhein, G.M.; Eckroade, R.J.; Dessel, B.H. Cultivation of papova-like virus from human brain with progressive multifocal leucoencephalopathy Lancet. 1(7712):1257-60 (1971)

163. Paterson, P.Y. Transfer of allergic encephalomyelitis in rats by means of lymph node cells J Exp Med. 111:119-36 (1960)

164. Patrikios ,P.; Stadelmann, C.; Kutzelnigg, A.; Rauschka, H.; Schmidbauer, M.; Laursen, H.; Sorensen, P.S.; Brück, W.; Lucchinetti, C.; Lassmann, H. Remyelination is extensive in a subset of multiple sclerosis patients Brain. 129(Pt 12):3165-72 (2006)

165. Payne, F.E.; Baublis, J.V.; Itabashi, H.H. Isolation of measles virus from cell cultures of brain from a patient with subacute sclerosing panencephalitis N Engl J Med. (11):585-9 (1969)

166. Peng, S.; Kuang, Z.; Zhang, Y.; Xu, H.; Cheng, Q. The protective effects and potential mechanism of Calpain inhibitor Calpeptin against focal cerebral ischemia-reperfusion injury in rats Mol. Biol Rep. 38(2):905-12 (2011)

167. Piani, D.; Frei, K.; Do, K.Q.; Cuénod, M.; Fontana, A. Murine brain macrophages induced NMDA receptor mediated neurotoxicity in vitro by secreting glutamate Neurosci Lett. 133(2):159-62 (1991)

168. Polman, C.H.; Dijkstra, C.D.; Sminia, T.; Koetsier, J.C. Immunohistological analysis of macrophages in the central nervous system of Lewis rats with acute experimental allergic encephalomyelitis J Neuroimmunol. 11(3):215-22 (1986)

169. Pottorf, W.J.; Johanns, T.M.; Derrington, S.M.; Strehler, E.E.; Enyedi, A.; Thayer, S.A. Glutamate-induced protease-mediated loss of plasma membrane Ca2+ pump activity in rat hippocampal neurons Journal of neurochemistry 98(5): 1646-1656 (2006)

170. Prayoonwiwat, N.; Rodriguez, M. The potential for oligodendrocyte proliferation during demyelinating disease J Neuropathol Exp Neurol. 52(1):55-63 (1993)

171. Pulicken, M.; Gordon-Lipkin, E.; Balcer, L.J.; Frohman, E.; Cutter, G.; Calabresi, P.A. Optical coherence tomography and disease subtype in mutliple sclerosis. Neurology 69:2085-92 (2007)

172. Quigley, H.A.; Nickells, R.W.; Kerrigan, L.A.; Pease, M.E.; Thibault, D.J.; Zack, D.J. Retinal ganglion cell death in experimental glaucoma and after axotomy occurs by apoptosis Invest Ophthalmol Vis Sci. 36(5):774-86 (1995)

173. Quigley, H.A.; McKinnon, S.J.; Zack, D.J.; Pease, M.E.; Kerrigan-Baumrind, L.A.; Kerrigan, D.F.; Mitchel, R.S. Retrograde axonal transport of BDNF in retinal ganglion cells is blocked by acute IOP elevation in rats Invest Ophthalmol Vis Sci. 41(11):3460-6 (2000)

174. Reichenbach, A.; Schneider, H.; Leibnitz, L.; Reichelt, W.; Schaaf, P.; Schümann, R. The structure of rabbit retinal Müller (glial) cells is adapted to the surrounding retinal layers Anat Embryol (Berl). 180(1):71-9 (1989)

175. Ridge, S.C.; Sloboda, A.E.; McReynolds, R.A.; Levine, S.; Oronsky, A.L.; Kerwar, S.S. Suppression of experimental allergic encephalomyelitis by mitoxantrone Clin Immunol Immunopathol. 35(1):35-42 (1985)

176. Sadovnick, A.D.; Ebers, G.C. Epidemiology of multiple sclerosis: a critical overview Can J Neurol Sci. 20(1):17-29 (1993)

177. Sadovnick, A.D.; Armstrong, H.; Rice, G.P.; Bulman, D.; Hashimoto, L.; Paty, D.W.; Hashimoto, S.A.; Warren, S.; Hader, W.; Murray, T.J. A population-based study of multiple sclerosis in twins: update Ann Neurol. 33(3):281-5 (1993)

178. Saidha, S.; Syc, S.B.; Ibrahim, M.A.; Eckstein, C.; Warner, C.V.; Farrell, S.K.; Oakley, JD.; Durbin, M.K.; Meyer, S.A.; Balcer, L.J.; Frohman, E.M.; Rosenzweig, J.M.; Newsome, S.D.; Ratchford, J.N.; Nguyen, Q.D.; Calabresi, P.A. Primary retinal pathology in multiple sclerosis as detected by optical coherence tomography Brain 134:518-33 (2011)

179. Sattler, R.; Tymianski, M. Molecular mechanisms of calcium-dependent excitotoxicity J Mol Med 78(1):3-13 (2000)

180. Sättler, M.B.; Merkler, D.; Maier, K.; Stadelmann, C.; Ehrenreich, H.; Bähr, M, Diem, R. Neuroprotective effects and intracellular signaling pathways of erythropoietin in a rat model of multiple sclerosis 1: Cell Death Differ. 11 Suppl 2:S181-92 (2004)

181. Schaecher, K.E.; Shields, D.C.; Banik, N.L. Mechanism of myelin breakdown in experimental demyelination: a putative role for calpain Neurochem Res.;26(6):731-7 (2001)

182. Schafer, D.P.; Jha, S.; Liu, F.; Akella, T.; McCullough, L.D.; Rasband, M.N. Disruption of the axon initial segment cytoskeleton is a new mechanism for neuronal injury J Neurosci. 29(42):13242-54 (2009)

183. Schirmer, L.; Albert, M.; Buss, A.; Schulz-Schaeffer, W.J.; Antel, J.P.; Brück, W.; Stadelmann, C. Substantial early.; but nonprogressive neuronal loss in multiple sclerosis (MS) spinal cord Ann Neurol. 66(5):698-704 (2009)

184. Schirmer, L.; Antel, J.P.; Brück, W.; Stadelmann, C. Axonal loss and neurofilament phosphorylation changes accompany lesion development and clinical progression in multiple sclerosis Brain Pathol. (4):428-40 (2011)

185. Seubert, P.; Larson, J.; Oliver, M.; Jung, M.W.; Baudry, M.; Lynch, G. Stimulation of NMDA receptors induces proteolysis of spectrin in hippocampus. Brain Res.;460(1):189–194 (1988)

186. Shijie, J.; Takeuchi, H.; Yawata. I.; Harada, Y.; Sonobe, Y.; Doi, Y.; Liang, J.; Hua, L.; Yasuoka, S.; Zhou, Y.; Noda, M.; Kawanokuchi, J.; Mizuno, T.; Suzumura, A. Blockade of glutamate release from microglia attenuates experimental autoimmune encephalomyelitis in mice Tohoku J Exp Med. 217(2):87-92 (2009)

187. Shields, D.C, Banik, N.L. Pathophysiological role of calpain in experimental demyelination J Neurosci Res. 55(5):533-41 (1999)

188. Siliprandi, R.; Canella, R.; Carmignoto, G.; Schiavo, N.; Zanellato, A.; Zanoni, R.; Vantini, G. N-methyl-D-aspartate-induced neurotoxicity in the adult rat retina Vis Neurosci 8(6):567-73 (1992)

189. Siman, R.; Baudry, M.; Lynch, G. Brain fodrin: substrate for calpain I, an endogenous calcium-activated protease Proc Natl Acad Sci U S A. 81(11):3572-6 (1984)

190. Simon, P.; Thanos, S. Combined methods of retrograde staining, layer-separation and viscoelastic cell stabilization to isolate retinal ganglion cells in adult rats J Neurosci Methods. 83(2):113-24 (1998)

191. Simpson, J.E.; Newcombe, J.; Cuzner, M.L.; Woodroofe, M.N. Expression of monocyte chemoattractant protein-1 and other beta-chemokines by resident glia and inflammatory cells in multiple sclerosis lesions J Neuroimmunol. 84(2):238-49 (1998)

192. Sindern, E.; Niederkinkhaus, Y.; Henschel, M.; Ossege, L.M.; Patzold, T.; Malin, J.P. Differential release of beta-chemokines in serum and CSF of patients with relapsing-remitting multiple sclerosis Acta Neurol Scand. 104(2):88-91 (2001)

193. Sisk, D.R.; Kuwabara, T. Histologic changes in the inner retina of albino rats following intravitreal injection of monosodium L-glutamate Graefes Arch Clin Exp Ophthalmol. 223(5):250-8 (1985)

194. Smith, K.J.; Kapoor, R.; Hall, S.M.; Davies, M. Electrically active axons degenerate when exposed to nitric oxide Ann Neurol. 49(4):470-6 (2001)

195. Smith, A.W.; Das, A.; Guyton, M.K.; Ray, S.K.; Rohrer, B.; Banik, N.L. Calpain inhibition attenuates apoptosis of retinal ganglion cells in acute optic neuritis. Invest Ophthalmol Vis Sci. 52(7):4935-41 (2011)

196. Sørensen, T.L.; Tani, M.; Jensen, J.; Pierce, V.; Lucchinetti, C.; Folcik, V.A.; Qin, S.; Rottman, J.; Sellebjerg, F.; Strieter, R.M.; Frederiksen, J.L.; Ransohoff, R.M. Expression of specific chemokines and chemokine receptors in the central nervous system of multiple sclerosis patients J Clin Invest. 103(6):807-15 (1999)

197. Sommer, B.; Köhler, M.; Sprengel, R.; Seeburg, P.H. RNA editing in brain controls a determinant of ion flow in glutamate-gated channels Cell. 67(1):11-9 (1991)

198. Sospedra, M.; Martin, R. Immunology of multiple sclerosis. In: Raine, C.S.; McFarland, H.; Hohlfeld, R, eds. Multiple Sclerosis: A Comprehensive Test. 1st ed. Philadelphia, PA: Saunders Elsevier:192-213 (2008)

199. Stefferl, A.; Brehm.; U, Storch, M.; Lambracht-Washington, D.; Bourquin, C.; Wonigeit, K.; Lassmann, H.; Linington, C. Myelin oligodendrocyte glycoprotein induces experimental autoimmune encephalomyelitis in the "resistant" Brown Norway rat: disease susceptibility is determined by MHC and MHC-linked effects on the B cell response J Immunol.;163(1):40-9 (1999)

200. Steinman, L. Blocking adhesion molecules as therapy for multiple sclerosis: natalizumab Nat Rev Drug Discov. 4(6):510-8 (2005)

201. Stichel, C.C.; Müller, H.W. The CNS lesion scar: new vistas on an old regeneration barrier Cell Tissue Res. 294(1):1-9 (1998)

202. Stys, P.K.; Jiang, Q. Calpain-dependent neurofilament breakdown in anoxic and ischemic rat central axons Neurosci Lett. 9;328(2):150-4 (2002)

203. Stys, P. K. General mechanisms of axonal damage and its prevention J Neurol Sci. 15;233(1-2):3-13 (2005)

204. Sucher, N.J.; Lipton, S.A.; Dreyer, E.B. Molecular basis of glutamate toxicity in retinal ganglion cells Vision Res. 37(24):3483-93 (1997)

205. Syc, S.B.; Saidha, S.; Newsome, S.D.; Ratchford, J.N.; Levy, M.; Ford, E.; Crainiceanu, C.M.; Durbin, M.K.; Oakley, J.D.; Meyer, S.A.; Frohman, E.M.; Calabresi, P.A. Optical coherence tomography segmentation reveals ganglion cell layer pathology after optic neuritis Brain. [Epub ahead of print] (2011)

206. Takeda, A. Manganese action in brain function Brain Research Reviews 41(1): 79-87 (2003)

207. Takeuchi, H.; Mizuno, T.; Zhang, G.; Wang, J.; Kawanokuchi, J.; Kuno, R.; Suzumura, A. Neuritic beading induced by activated microglia is an early feature of neuronal dysfunction toward neuronal death by inhibition of

mitochondrial respiration and axonal transport J Biol Chem. 280(11):10444-54 (2005)

208. Takeuchi, H.; Jin, S.; Wang, J.; Zhang, G.; Kawanokuchi, J.; Kuno, R.; Sonobe, Y.; Mizuno, T.; Suzumura, A. Tumor necrosis factor-alpha induces neurotoxicity via glutamate release from hemichannels of activated microglia in an autocrine manner J Biol Chem. 281(30):21362-8 (2006)

209. Tamada, Y., Nakajima, E., Nakajima, T., Shearer, T. R.; Azuma, M. Proteolysis of neuronal cytoskeletal proteins by calpain contributes to rat retinal cell death induced by hypoxia. Brain Res. 1050: 148–155 (2005)

210. Tanuma, N.; Sakuma, H.; Sasaki, A.; Matsumoto, Y. Chemokine expression by astrocytes plays a role in microglia/macrophage activation and subsequent neurodegeneration in secondary progressive multiple sclerosis Acta Neuropathol. 112(2):195-204 (2006)

211. Targett, M.P.; Sussman, J.; Scolding, N.; O'Leary, M.T.; Compston, D.A.S.; Blakemore, W. F. Failure to achieve remyelination of demyelinated rat axons following transplantation of glial cells obtained from the adult human brain Neuropathol Appl Neurobiol. 22(3):199-206 (1996)

212. Taschenberger, H.; Engert, F.; Grantyn, R. Synaptic current kinetics in a solely AMPA-receptor-operated glutamatergic synapse formed by rat retinal ganglion neurons J Neurophysiol. 74(3):1123-36 (1995)

213. Teitelbaum, D.; Meshorer, A.; Hirshfeld, T.; Arnon, R.; Sela, M. Suppression of experimental allergic encephalomyelitis by a synthetic polypeptide. Eur J Immunol. 1(4):242–248 (1971)

214. The International Multiple Sclerosis Genetics Consortium, Risk allels for multiple sclerosis identified in a genomewide study N Engl J Med. 357(9):851-62 (2007)

215. The Optic Neuritis Study Group Multiple Sclerosis Risk after Optic Neuritis: Final Optic Neuritis Treatment Trial Follow-Up Arch. Neurol. 65 (6): 727–32. (2008)

216. Tikka, T.M.; Vartiainen, N.E.; Goldsteins, G.; Oja, S.S.; Andersen, P.M.; Marklund, S.L.; Koistinaho, J. Minocycline prevents neurotoxicity induced by cerebrospinal fluid from patients with motor neurone disease Brain. 125(Pt 4):722-31 (2002)

217. Toft-Hansen, H.; Füchtbauer, L.; Owens, T. Inhibition of reactive astrocytosis in established experimental autoimmune encephalomyelitis favors infiltration by myeloid cells over T cells and enhances severity of disease Glia. 59(1):166-76 (2011)

218. Trapp, B.D.; Peterson, J.; Ransohoff, R.M.; Rudick, R.; Mork, S.; Bo, L. Axonal transection in the lesions of multiple sclerosis. N Engl J Med 338: 278–85 (1998)

219. Trapp, B.D.; Ransohoff, R.M.; Fisher, E.; Rudick, R.A. Neurodegeneration in multiple sclerosis: relationship to neurological disability. The Neuroscientist 5:48-57 (1999)

220. Trapp, B.D.; Nave, K. A. Multiple sclerosis: an immune or neurodegenerative disorder? Annu Rev Neurosci. 31:247-69 (2008)

221. Trip S.A.; Schlottmann P.G.; Jones S.J.; Altmann D.R.; Garway-Heath D.F.; Thompson A.J.; Plant, G.T.; Miller, D.H. Retinal nerve fiber layer axonal loss and visual dysfunction in optic neuritis Ann Neurol 58:383-91 (2005)

222. Tsai J.C.; Gilden D.H. Chlamydia pneumoniae and multiple sclerosis: no significant association. Trends Microbiol. 9(4):152-4 (2001)

223. Tso, M.O.; Shih, C.Y.; McLean, I.W. Is there a blood-brain barrier at the optic nerve head? Arch Ophthalmol 93:815-25 (1975)

224. Tumani, H.; Hartung, H.P.; Hemmer, B.; Teunissen, C.; Deisenhammer, F.; Giovannoni, G.; Zettl ,U.K.; BioMS Study Group Cerebrospinal fluid biomarkers in multiple sclerosis Neurobiol Dis. 35(2):117-27 (2009)

225. van der Valk, P.; Amor, S. Preactive lesions in multiple sclerosis Curr Opin Neurol. 22(3):207-13 (2009)

226. van Damme, J.; Wuyts, A.; Froyen, G.; Van, Coillie E.; Struyf, S.; Billiau, A.; Proost, P.; Wang, J.M.; Opdenakker, G. Granulocyte chemotactic protein-2 and related CXC chemokines: from gene regulation to receptor usage J Leukoc Biol. 62(5):563-9 (1997)

227. Vandvik, B.; Norrby, E.; Nordal, H.J.; Degré, M. Oligoclonal measles virus-specific IgG antibodies isolated from cerebrospinal fluids, brain extracts, and sera from patients with subacute sclerosing panencephalitis and multiple sclerosis Scand J Immunol. 5(8):979-92 (1976)

228. Verdaguer, E.; Alvira, D.; Jimenez, A.; Rimbau, V.; Camins, A.; Pallas, M. Inhibition of the cdk5/MEF2 pathway is involved in the antiapoptotic properties of calpain inhibitors in cerebellar neurons. Br J Pharmacol. 145(8):1103-11(2005)

229. Villarroya, H.; Violleau, K.; Ben Younes-Chennoufi, A.; Baumann, N. Myelin-induced experimental allergic encephalomyelitis in Lewis rats: tumor necrosis factor alpha levels in serum and cerebrospinal fluid immunohistochemical expression in glial cells and macrophages of optic nerve and spinal cord J Neuroimmunol. 64(1):55-61 (1996)

230. Voskuhl, R.R.; Peterson, R.S.; Song, B.; Ao, Y.; Morales, L.B.; Tiwari-Woodruff, S.; Sofroniew, M.V. Reactive astrocytes form scar-like perivascular barriers to leukocytes during adaptive immune inflammation of the CNS.J Neurosci. 29(37):11511-22 (2009)

231. Wang, X.; Tay S.S.; Ng, Y.K. An immunohistochemical study of neuronal and glial cell reactions in retinae of rats with experimental glaucoma Exp Brain Res. 132(4):476-84 (2000)

232. Waxman, S.G.; Craner, M.; Black, J.A., Sodium channel expression along axons in MS and its models Trends in Pharmacological Sciences, 25: 584-592 (2004)

233. Weber, T.; Trebst, C.; Frye, S.; Cinque, P.; Vago, L.; Sindic, C.J.; Schulz-Schaeffer, W.J.; Kretzschmar, H.A.; Enzensberger, W.; Hunsmann, G.; Lüke, W. Analysis of the systemic and intrathecal humoral immune response in progressive multifocal leukoencephalopathy J Infect Dis. 176(1):250-4 (1997)

234. Weishaupt, J.H.; Rohde, G.; Pölking, E.; Siren, A.L.; Ehrenreich, H.; Bähr, M. Effect of erythropoietin axotomy-induced apoptosis in rat retinal ganglion cells Invest Ophthalmol Vis Sci. 45(5):1514-22 (2004)

235. Wekerle, H. Lessons from multiple sclerosis: models, concepts, observations Ann Rheum Dis. 67 Suppl 3:iii56-60 (2008)

236. Wilkins, A.; Scolding, N. Protecting axons in multiple sclerosis Mult Scler. 2008 14(8):1013-25 (2008)

237. Willenborg, D.O.; Fordham, S.A.; Cowden, WB.; Ramshaw, I.A. Cytokines and murine autoimmune encephalomyelitis: inhibition or enhancement of disease with antibodies to select cytokines.; or by delivery of exogenous cytokines using a recombinant vaccinia virus system Scand J Immunol..; 41(1):31-41 (1995)

238. Wolswijk, G.; Balesar, R Changes in the expression and localization of the paranodal protein Caspr on axons in chronic multiple sclerosis Brain. 126(Pt 7):1638-49 (2003)

239. Wujek, J.R.; Bjartmar, C.; Richer, E.; Ransohoff, R.M.; Yu, M.; Tuohy, V.K.; Trapp, B.D. Axon loss in the spinal cord determines permanent neurological disability in an animal model of multiple sclerosis J Neuropathol Exp Neurol. 61(1):23-32 (2002)

240. Yawata, I.; Takeuchi, H.; Doi, Y.; Liang, J.; Mizuno, T.; Suzumura A. Macrophage-induced neurotoxicity is mediated by glutamate and attenuated by glutaminase inhibitors and gap junction inhibitors Life Sci. 82(21-22):1111-6 (2008)

241. Yednock, T.A.; Cannon, C.; Fritz, L.C.; Sanchez-Madrid, F.; Steinman, L.; Karin, N. Prevention of experimental autoimmune encephalomyelitis by antibodies against alpha 4 beta 1 integrin Nature. 356(6364):63-6 (1992)

242. Yong, V.W.; Wells, J.; Giuliani, F.; Casha, S.; Power, C.; Metz, L.M. The promise of minocycline in neurology Lancet Neurol. 3(12):744-51 (2004)

243. Yoshida, S.; Sotozono, C.; Ikeda, T.; Kinoshita, S. Interleukin-6 (IL-6) production by cytokine-stimulated human Müller cells Curr Eye Res. 22(5):341-7 (2001)

244. Yrjänheikki, J.; Keinänen, R.; Pellikka, M.; Hökfelt, T.; Koistinaho, J. Tetracyclines inhibit microglial activation and are neuroprotective in global brain ischemia Proc Natl Acad Sci U S A.;95(26):15769-74 (1998)

245. Yu, S.P; Choi, D.W Na+-Ca2+ Exchange currents in cortical neurons: concomitant forward and reverse operation and effect of glutamate

246. Zemlan, F.P.; Rosenberg, W.S.; Luebbe, P.A.; Campbell, T.A.; Dean, G.E.; Weiner, N.E.; Cohen, J.A.; Rudick ,R.A.; Woo, D. Quantification of axonal damage in traumatic brain injury: affinity purification and characterization of cerebrospinal fluid tau proteins J Neurochem. 72(2):741-50 (1999)

247. Zemlan, F.P.; Jauch ,E.C.; Mulchahey, J.J.; Gabbita, S.P.; Rosenberg, W.S.; Speciale, S.G.; Zuccarello, M. C-tau biomarker of neuronal damage in severe brain injured patients: association with elevated intracranial pressure and clinical outcome Brain Res. (1):131-9 (2002)

248. Zhu, B.; Moore, G.R.; Zwimpfer, T.J.; Kastrukoff, L.F.; Dyer, J.K.; Steeves, J.D.; Paty, D.W.; Cynader, M.S. Axonal cytoskeleton changes in experimental optic neuritis Brain Res. 824(2):204-17 (1999)

List of Figures and Tables

Abbreviations

AMPA   amino-3-hydroxy-5-methyl-4-isoxazolepropionic acid

Apaf1   Apoptosis protease activated factor

APC   Antigen Presenting Cell

APP   β-Amyloid Precursor Protein

ATP   Adenosine Triphosphate

BBB   Blood-Brain-Barrier

BDNF   Brain-derived neurotrophic factor

BN   Brown Norway rat strain

BCA   Bicinchonic Acid

BSA   Bovine Serum Albumine

Caspase cysteine-aspartic acid proteases

Caspr   glycoprotein contactin-associated protein

CNPase   2', 3'-cyclic nucleotide 3'-phosphodiesterase

CNQX   6-cyano-7-nitroquinoxaline-2,3-dione

CNTF   Cliliary Neurotrophic Factor

CD   Cluster of Differentiation

CDK5   Cyclin-Dependent Protein Kinase 5

CNS   Central Nervous System

CBX   Carbenoxolone

CSF   Cerebrospinal Fluid

DAB   Diaminobenzidin

DAPI   4', 6-diamidino-2-phenylindole

EAE   Experimental Autoimmune Encephalomyelitis

EMAP   Endothelial monocyte-activating polypeptide

EtOH   Ethanol

Epo   Erythropoietin

FLASH Fast Low Angle Shot

GA   Glatiramer Acetate

GAPDH Glyceraldehyde-3-Phosphate Dehydrogenase

GFAP   Glial Fibrillary Acidic Protein

HLA   Human Leukocyte Antigen

HRP   Horseradish Peroxidase

Ig Immune globuline

IGF-I Insulin-like growth factor-I

iNOS   inducible Nitric Oxide Synthase

LFB Luxol Fast Blue

MAPK   Mitogen-activated protein kinase

MBP   Myelin Basic Protein

MHC   Major Histocompatibility Complex

MEMRI Manganese Enhanced Magnetic Resonance Imaging

MK-801 (+)-5-methyl-10,11-dihydro-5H-dibenzo[a, d]cyclohepten-5, 10-imine

MOG   Myelin Oligodendrocyte Glycoprotein

MRI Magnet Resonance Imaging

MS   Multiple Sclerosis

MSME Multi-Slice Multi Echo

NBQX   2,3-dihydroxy-6-nitro-7-sulfamoyl-benzo[f]quinoxaline-2,3-dione

NCX Na^+/Ca^{2+} exchanger

NMDA   N-methyl-D-aspartic acid

NO   Nitric Oxide

OGB Oligoclonal IgG Bands

ON   Optic Nerve

OPC Oligodendrocyte Progenitor Cells

PBS   Phosphate Buffered Saline

PBS-T   Phosphate Buffered Saline with Tween

PCNA Proliferating Cell Nuclear Antigen

PFA   Paraformaldehyde

p.i. post immunisation

PI3K Phosphoinositide 3-kinase

PLP   Proteolipid Protein

PMCA   Plasma Membrane Ca^{2+} ATPase

PML   Progressice Multofocal Leukoencephalopathy

PPMS   Primary-Progressive Multiple Sclerosis

PRMS   Progressive-Relapsing Multiple Sclerosis

RARE Rapide Acquisition with Relaxation Enhancement

RGC   Retinal Ganglion Cell

RNFL   Retinal Nerve Fiber Layer

RRMS   Relapsing-Remitting Multiple Sclerosis

RT   Room Temperature

SBDP Spectrin Breakdown Products

SEM   Standard Error of the Mean

SDS-PAGE Sodium-Dodecyl Sulfate –Poly Acrylamide Gel Electrophoresis

SJA6017 N-(4-fluorophenylsulfonyl)-L-valyl-L-leucinal

SNJ-1945   ((1S)-1((((1S)-1-benzyl-3-cyclopropylamino-2,3-dioxopropyl)   amino)
              carbonyl)-3-methylbutyl) carbamic acid 5-methoxy-3-oxapentyl ester

SPMS   Secondary-Progressive Multiple Sclerosis

SSPE Subacute Sclerosing Panencephalitis

TUNEL TdT-mediated dUTP-biotin Nick End Labeling

Treg   regulatory T-cells

VDCC   Voltage Dependent Calcium Channels

Acknowledgements

I would like to thank the following people for their contribution to my thesis:

Prof Dr. Ricarda Diem for giving me the opportunity to work in her lab, constructive critism and encouragement and being all one can wish for in a group leader.

Prof. Dr. Tobias Hartmann for being my PhD supervisor and his insightful comments on my work.

Dr. Sarah Williams and Dr. Richard Fairless for patiently explaining me all the techniques, invaluable advice concerning my experiments, great discussions about my work and linguistic improvement of my thesis

My fellow PhD student, Aleksandar Stojic, for being a great friend, for interesting discussions about lab-related and unrelated topics, cheering me up so many times and for participating in monopoly marathons.

Jovana Bojcevski for helping me with my MRI experiments, explaining the physics behind it, for being a great companion in the long hours of MRI scans and for the crazy cycling tours.

Andreas Müller for explaining me how to use the MRI and his willingness to try and make time for me to use it as often as possible.

Marika Dienes, who has been a great help in the lab. Thanks for the smiley in my tip box.

Verena Burg for being a good friend inside and outside the lab and as an inspiration how to stay in a good mood if things don´t work out as planned.

Also the rest of Prof. Hartmanns group for nice barbecues and chats and for just being a very pleasant group to work next to.

Dr. Wolfram Sühs for bringing so much life and fun into the lab.

Prof. Dr. Markus Otto and his group for their help with the Multi-Spot assays.

Prof Ben Bahr for providing the antibody against calpain-mediated spectrin breakdown product.

My parents for their love and support and willingness to try to understand as much of my work as possible.

Curriculum vitae

Personal data

Name: Dorit Hoffmann

Date of Birth: 14.08.1982

Place of Birth: Bremen

Contact: Dorit.Hoffmann@gmx.de

Nationality: German

Education

1988-1992	Primary School, Rönnebeck
1992-1998	Secondary school, Blumenthal
1998-2001	University entrance diploma, Blumenthal
2002-2008	Study of biology, University of Osnabrück
2008-03	Diploma thesis, University of Osnabrück, Department of Animal Physiology.
	Title: The purinereceptor-signalin pathway of the marine ciliate Euplotes vannus: Pharmacological influence on membrane potential and ion currents
2008-present	Doctoral studies, Saarland University, Homburg.
	Focus on neurodegenerative changes in the retina and optic nerve during the induction phase of EAE in Brown Norway rats

Publications:

Fairless, R.; Williams, S.K.; Hoffmann, D.B.; Hochmeister, S.; Stojic, A.; Schmitz, F.; Storch, M.K.; Ricarda Diem, R. Preclinical retinal neurodegeneration in a model of multiple sclerosis The Journal of Neuroscience *accepted*

Hoffmann, D.B.; Williams, S.K.; Bojcevski, J.; Müller, A.; Stadelmann, C.; Naidoo, V.; Bahr, B.A.; Diem, R.; Fairless, R. Calpain activation mediates preclinical neurodegeneration in autoimmune optic neuritis *submitted*

Poster presentations:

Poster presentation at Ectrims 2009 Duesseldorf, Germany

- Early neurodegenerative changes in a rat model of multiple sclerosis

Poster presentation at SfN 2010 San Diego, USA

- Magnetic Resonance Imaging of early calcium influx into optic nerves during autoimmune optic neuritis

List of Contributors to this work

Die nachstehend aufgeführten Personen haben in der jeweils beschriebenen Weise an dieser Arbeit mitgewirkt:

Dr. Sarah Williams	Zweite Person bei der Auszählung der Fluorogold-gelabelten retinalen Ganglienzellen (Abschnitt 4.13)
Dr. Richard Fairless	Bereitstellung der Daten über den Verlauf der Degeneration von retinalen Ganglienzellen (Abschnitt 4.2)
Alice Pabst Dr. Stefan Lehnert Arbeitsgruppe Prof. Markus Otto	Bedienung des Sector Imager 6000 für die Messung der Multi-Spot ELISAs durchgeführt in Ulm (Abschnitt 4.3.2 und 4.10)
Andreas Müller	Einarbeitung in die Benutzung des MRT Gerätes und Unterstützung bei der Positionierung und Überwachung der Versuchstiere und Scans
Jovana Bojcevski	Unterstützung bei der Positionierung und Überwachung der Versuchstiere und Scans beim MRT

Declaration of academic honesty / Eidesstattliche Erklärung

Erklärung gemäß § 7 Abs. 1 Nr. 4

Ich erkläre hiermit an Eides statt, dass ich die vorliegende Arbeit ohne unzulässige Hilfe Dritter und ohne Benutzung anderer als der angegebenen Hilfsmittel angefertigt habe. Die aus anderen Quellen direkt oder indirekt übernommenen Daten und Konzepte sind unter Angabe der Quelle gekennzeichnet.

Bei der Auswahl und Auswertung des Materials sowie bei der Herstellung des Manuskripts habe ich keine Unterstützungsleistungen erhalten. Weitere Personen waren an der inhaltlich-materiellen Erstellung der vorliegenden Arbeit nicht beteiligt. Insbesondere habe ich nicht die entgeltliche Hilfe von Vermittlungs- bzw. Beratungsdiensten (Promotionsberaterinnen/Promotionsberater oder anderer Personen) in Anspruch genommen. Dritte haben von mir weder unmittelbar noch mittelbar geldwerte Leistungen für Arbeiten erhalten, die im Zusammenhang mit dem Inhalt der vorgelegten Dissertation stehen.

Die Arbeit wurde von mir bisher weder im Inland noch im Ausland in gleicher oder ähnlicher Form einer anderen Prüfungsbehörde vorgelegt und ist auch noch nicht veröffentlicht.

Ich versichere an Eides statt, dass ich nach bestem Wissen die Wahrheit gesagt und nichts verschwiegen habe.

Vor Aufnahme der vorstehenden Versicherung an Eides statt wurde ich über die Bedeutung einer eidesstattlichen Versicherung und die strafrechtlichen Folgen einer unrichtigen oder unvollständigen eidesstattlichen Versicherung belehrt.

Homburg, 30.05.2012

_____

Dorit Hoffmann